DEVELOPMENT OF NANOCOMPOSITES FOR THE PLY-DROP REGIONS OF GLASS FIBER REINFORCED POLYMER (GFRP) COMPOSITE STRUCTURES

A THESIS SUBMITTED TO
THE GRADUATE SCHOOL OF NATURAL AND APPLIED SCIENCES
OF
MIDDLE EAST TECHNICAL UNIVERSITY

BY

DOĞA SAVAŞ

IN PARTIAL FULFILLMENT OF THE REQUIREMENTS
FOR
THE DEGREE OF MASTER OF SCIENCE
IN
METALLURGICAL AND MATERIALS ENGINEERING

DECEMBER 2023

Approval of the thesis:

DEVELOPMENT OF NANOCOMPOSITES FOR THE PLY-DROP REGIONS OF GLASS FIBER REINFORCED POLYMER (GFRP) COMPOSITE STRUCTURES

submitted by **DOĞA SAVAŞ** in partial fulfillment of the requirements for the degree of **Master of Science** i**n Metallurgical and Materials Engineering, Middle East Technical University** by,

Prof. Dr. Halil Kalıpçılar
Dean, Graduate School of **Natural and Applied Sciences** _____

Prof. Dr. Ali Kalkanlı
Head of the Department, **Metallurgical and Material Eng.** _____

Prof. Dr. Arcan F. Dericioğlu
Supervisor, **Metallurgical and Materials Eng., METU** _____

Examining Committee Members:

Prof. Dr. Cevdet Kaynak
Metallurgical and Materials Eng, METU _____

Prof. Dr. Arcan F. Dericioğlu
Metallurgical and Materials Eng, METU _____

Prof. Dr. Ziya Esen
Mechanical Eng., Çankaya University _____

Prof. Dr. Altan Kayran
Aerospace Eng., METU _____

Assist. Prof. Dr. Irmak Sargın
Metallurgical and Materials Eng., METU _____

Date: 11.12.2023

I hereby declare that all information in this document has been obtained and presented in accordance with academic rules and ethical conduct. I also declare that, as required by these rules and conduct, I have fully cited and referenced all material and results that are not original to this work.

Name, Last name: Doğa Savaş

Signature:

ABSTRACT

DEVELOPMENT OF NANOCOMPOSITES FOR THE PLY-DROP REGIONS OF GLASS FIBER REINFORCED POLYMER (GFRP) COMPOSITE STRUCTURES

Savaş, Doğa
Master of Science, Metallurgical and Materials Engineering
Supervisor: Prof. Dr. Arcan F. Dericioğlu

December 2023, 110 pages

In the current study, incorporation of nanoparticle reinforcement in the matrix of glass fiber reinforced polymer (GFRP) composite structures, and its effect on the structural integrity of the ply-drop regions has been studied. In the GFRP composites used in applications such as wind turbines, ply-drop regions are created along the wind axis to adjust the thickness and, thus, the weight of the components. Damage formation in such composite structures usually occurs in these regions due to structural discontinuity caused by the ply-drop. Therefore, this study aims to improve the mechanical properties of the ply-drop regions in the composites by reinforcing their matrix (resin) with nanoparticles. In the scope of the experimental studies, nanoparticles such as functionalized carbon nanotubes (fCNT), cellulose nanofibers, and nanoclay have been used in different quantities to reinforce the matrix of the GFRP composite. Various combinations of GFRP composites with pristine epoxy matrix or nanocomposite matrix have been produced and compared. The best results were obtained by 0.35 wt% fCNT containing nanocomposite matrix with a ~28% increase in fracture toughness while the strength remains constant. Moreover, mode I and mode II interlaminar fracture toughnesses of glass fiber reinforced composites with nanocomposite matrix were increased by ~8% and ~35%, respectively.

Consequently, test specimens representing the ply-drop regions were manufactured using the developed nanocomposite with improved fracture toughness, and delamination tests were carried out to study the crack formation mechanisms in detail. As a result of these tests, although there was a decrease in tensile and delamination strength, work of fracture and failure strain were increased by ~6% and ~9%, respectively. Observed slight deterioration in tensile properties may be acceptable considering the advantages that the fCNT incorporation provides in the fracture behavior of the ply-drop regions.

Keywords: Glass Fiber Reinforced Polymer (GFRP), Nanocomposites, Carbon Nanotube, Ply-Drop Regions, Ultrasonication

ÖZ

CAM ELYAF TAKVİYELİ POLİMER (CTP) KOMPOZİT YAPILARIN KATMAN DÜŞÜŞ BÖLGELERİ İÇİN NANOKOMPOZİTLERİN GELİŞTİRİLMESİ

Savaş, Doğa
Yüksek Lisans, Metalurji ve Malzeme Mühendisliği
Tez Yöneticisi: Prof. Dr. Arcan F. Dericioğlu

Aralık 2023, 110 sayfa

Bu çalışmada, cam elyaf takviyeli polimer (CTP) kompozit yapıların matrisine nanopartikül takviyesinin dahil edilmesi ve bunun katman düşüş bölgelerinin yapısal bütünlüğü üzerindeki etkisi incelenmiştir. Rüzgar türbinleri gibi uygulamalarda kullanılan CTP kompozitlerde, bileşenlerin kalınlığını ve dolayısıyla ağırlığını ayarlamak için rüzgar ekseni boyunca katman düşüş bölgeleri oluşturulmaktadır. Bu tür kompozit yapılarda hasar oluşumu genellikle bu bölgelerde tabaka düşmesinden kaynaklanan yapısal süreksizlik nedeniyle meydana gelir. Bu nedenle, bu çalışma kompozitlerdeki katman düşüş bölgelerinin matrislerini (reçine) nanopartiküllerle güçlendirerek mekanik özelliklerini geliştirmeyi amaçlamaktadır. Deneysel çalışmalar kapsamında, CTP kompozitin matrisini güçlendirmek için fonksiyonelleştirilmiş karbon nanotüpler (fCNT), selüloz nanolifler ve nanokil gibi nanopartiküller farklı miktarlarda kullanılmıştır. GFRP kompozitlerinin saf epoksi matris veya nanokompozit matris ile çeşitli kombinasyonları üretilmiş ve karşılaştırılmıştır. En iyi sonuçlar, mukavemet sabit kalırken kırılma tokluğunda ~%28 artış sağlayan ağırlıkça %0,35 fCNT içeren nanokompozit matris ile elde edildi. Ayrıca, nanokompozit matrisli cam elyaf takviyeli kompozitlerin, mod I ve

mod II tabakalar arası kırılma toklukları sırasıyla ~%8 ve ~%35 oranında arttırılmıştır. Sonuç olarak, geliştirilen kırılma tokluğuna sahip nanokompozit kullanılarak katman düşüş bölgelerini temsil eden test numuneleri üretildi ve çatlak oluşum mekanizmalarını detaylı olarak incelemek için delaminasyon testleri yapıldı. Bu testler sonucunda çekme ve delaminasyon mukavemetinde azalma olmasına rağmen kırılma işinde ~%6 ve kopma geriniminde ~%9 oranında artış görülmüştür. Çekme özelliklerinde gözlenen hafif bozulma, fCNT eklenmesinin katman düşüş bölgelerinin kırılma davranışında sağladığı avantajlar dikkate alındığında kabul edilebilir olabilir.

Anahtar Kelimeler: Cam Elyaf Takviyeli Polimer (CTP), Nanokompozit, Karbon Nanotüp, Katman Düşüş Bölgesi, Ultrasonik Karıştırma

To my lovely girlfriend…

ACKNOWLEDGMENTS

First of all, I would like to express my gratitude to my dear supervisor, Prof. Dr. Arcan F. Dericioğlu, who supported and motivated me with his great communication skills throughout the study. I thank him for helping me solve every problem with his comments and efforts.

I thank Prof. Dr. Altan Kayran from the METU Aerospace Engineering Department for his support. Also, from the METU Aerospace Engineering Department, I would like to thank Özgün Şener and Fırat Ergin, who took part in the joint project. It is so much fun working together.

The supportive attitude of Turkish Aerospace Inc. is essential for the continuation of this work. I thank my dear manager Kenan Baştimur and my dear chiefs Emre Ertürk and Onur Kemerli for their continuous positive and understanding attitude. It would have been impossible for me to continue this work without their support. Also, I thank my colleagues who filled my void during my absence.

I am grateful to my dear girlfriend Zeynep Emir, who raised me when I fell and increased my motivation with her energy and love.

I want to express my gratitude to my mother Ayşen Sayın, and my father Hüseyin Savaş, who have given me constant support and love since my birth.

I would like to thank the dear committee members in my defense jury, Prof. Dr. Cevdet Kaynak, Prof. Dr. Ziya Esen, Prof. Dr. Altan Kayran and Assist. Prof. Dr. Irmak Sargın.

TABLE OF CONTENTS

LIST OF TABLES

TABLES

LIST OF FIGURES

FIGURES

LIST OF ABBREVIATIONS

ABBREVIATIONS

FRP: Fiber Reinforced Polymer

GFRP: Glass Fiber Reinforced Polymer

CFRP: Carbon Fiber Reinforced Polymer

NP-FRP: Nanoparticle Reinforced Fiber Reinforced Polymers

CNT: Carbon Nanotube

fCNT: Functionalized Carbon Nanotube

DWCNT: Double-Walled Carbon Nanotube

MWCNT: Multi-Walled Carbon Nanotube

SWCNT: Single-Walled Carbon Nanotube

CNF: Cellulose Nanofibril

CNC: Cellulose Nanocrystal

DC: Direct Current

AC: Alternating Current

RTM: Resin Transfer Molding

VARTM: Vacuum Assisted Resin Transfer Molding

SCRIMP: Seemann Composite Resin Infusion Process

ILSS: Interlaminar Shear Strength

SENB: Single-Edge Notch Bending

DCB: Double Cantilever Beam

ENF: End Notched Flexure

CV%: Coefficient of Variation

LIST OF SYMBOLS

SYMBOLS

%: Percent

wt%: Weight Percent

GW: Gigawatt

W: Watt

nm: Nanometer

mm: Micrometer

μm: Micron

MPa: Megapascal

GPa: Gigapascal

TPa: Terapascal

kHz: Kilohertz

MHz: Megahertz

°C: Degree Celcius

ml: Mililiter

G: Energy Required for Fracture

K: Resistance of the Material to Fracture

σ: Tensile Strength

η: Viscosity

E: Elastic Modulus

CHAPTER 1

INTRODUCTION

The rapid growth of technology and global economy has increased the need for electric energy. In addition, acquiring this electricity for an affordable price and with a low carbon footprint is demanded. In response to these demands, the wind turbine generator industry has increased its research efforts to reduce the cost, extend the life, and enhance the reliability of the wind generator systems. The long and slender rotating blades are essential parts of the turbines. The high density of conventional metallic materials for wind turbine blade construction limits their use and reduces payload. Therefore, fiber reinforced composites are frequently utilized in the manufacture of high-load blades to save weight and extend fatigue life [1].

Fiber reinforced polymer (FRP) has been used in many of structural applications, such as aerospace, automotive, marine, and wind power industries since the 1930s., because they have high specific strength and specific modulus. Layered construction is a distinctive feature of laminated composites. A polymer resin surrounds the fibers in FRP composites. Carbon, glass, or aramid fibers are usually embedded in resins such as epoxy, vinyl ester, or polyester for structural use. While the fibers provide strength and stiffness, the resin holds the fibers together and spreads the loads [2]. As the fiber/resin ratio increases, the mechanical properties of the composite, such as strength and stiffness, increase. However, if this ratio increases extremely the fibers cannot be wetted by the resin causing reduction in fatigue resistance. The ideal fiber-resin ration is 35-65% by weight [3].

The main advantages of FRPs are their lightweight, high strength, resistance to corrosion, and expected durability over their lifetime. In structural applications, shapes made of glass or carbon fiber reinforced polymer (GFRP or CFRP) are employed. Due to its electrical insulation and electromagnetic transparency, GFRP

is more widely used in structural applcations than CFRP which is electro-conductive. Moreover, GFRP requires less energy to manufacture than CFRP. Hence, glass fiber is the most frequently utilized reinforcing material in wind turbine blades due to its high strength and reasonable cost compared to other composite reinforcing fibers [2].

The payload is increased by the weight reduction provided by layered composites. These composites are helpful thanks to their inplane and fiber-dominant features. However, through the thickness properties may be constrained by poor matrix-resin interaction and frail fiber-matrix interfacial bonding. FRPs must undergo major through-the-thickness property improvements to compete favorably with monolithic metallic constructions without delamination issues for aerospace and military components [4].

The structural elements of wind turbine blades are created by layering plies on top of one another to achieve the required laminate thickness. They are flat due to the uniform thickness of each ply used to create the laminate. In practice, however, many structural components require the tapering of laminates. Plies are terminated at various points to make the thickness adjustment. This is referred to as ply drop-off (Fig. 1.1) [5].

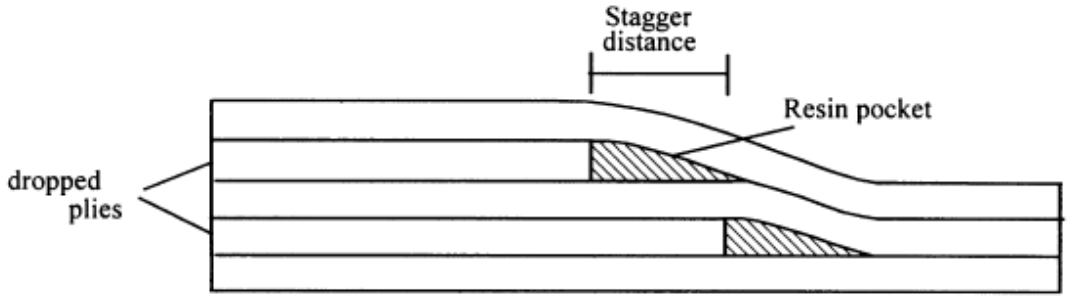

Figure 1.1. Characteristic feature of ply drop-off.

The use of ply drop-off in all of these applications results in critical material savings and makes it a cost-effective solution. On the other hand, ply drop-off zones can create discontinuity in the structure resulting in stress concentration sites. As a result, the components fail due to delamination or resin failure around these critical regions.

Long before the laminate reaches its maximum load-carrying capability, interlaminar stresses that build near the drop-off may cause it to break. Hence, a decreased laminate strength could negate any potential benefits of reducing plies. Therefore, ply drop zones should be created appropriately by weighing the pros and cons.

Numerous investigations have been conducted on ply drops in aerospace composite applications and wind turbine blades. The resistance to ply delamination, G_{Ic}, and G_{IIc} for pure opening and shearing modes, respectively, is a significant function of the resin's toughness, as determined by standard experiments [6]. In other words, delamination resistance is a resin-dominated feature related to the resin's toughness [7]. In this thesis, the effect of nanoparticle incorporation, applied to the resin pockets (Fig. 1.1), on the structural integrity of ply-drop regions in the wind blades has been studied. The main purpose was to increase the fracture toughness of the FRP without negatively affecting its tensile properties. Three different nanoparticles were candidates to provide the best contribution to mechanical properties in the ply-drop regions; namely functionalized multi-walled carbon nanotube, nanoclay, and cellulose nanofiber.

Fig. 1.2 shows the road map of the composites to be produced within the scope of the study. First, polymer nanocomposites have been produced with three different nanoparticles. After the selection of the most effective nanoparticle type and amount based on the preliminary studies, GFRP composites have been produced by adding this nanoparticle to the resin to transform their matrix to nanocomposite structure. Finally, GFRP composites with nanocomposite matrix have been constructed with the ply drop-off zone configuration.

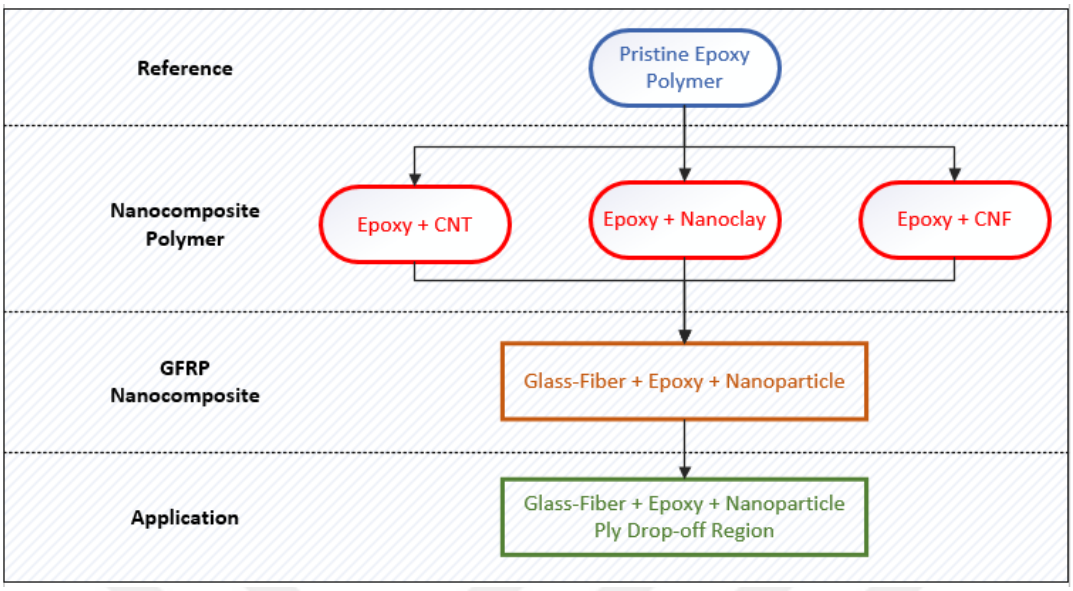

Figure 1.2. Road map of the composites to be produced in the study.

FRP's resistance to crack propagation through various modes is essential for its mechanical and structural performance. FRP's ability to absorb fracture energy plays a critical role in designs. Many efforts have been made over the years to improve fracture toughness. In these studies, the addition of carbon nanotubes (CNTs) has been extensively tested, and it was observed to have a significant effect on the interlayer properties of composite structures. Based on these pieces of information, this thesis focuses on improving the fracture toughness of glass fiber reinforced epoxy composite used in wind turbine blades by adding nanoparticles to epoxy resin.

Polymer composites are the fundamental structures for wind blades. The fibers are introduced to the polymer matrices to improve mechanical and fractural properties. Moreover, microscopic voids and defects occurring due to the high reinforcement content cause the composites to fail prematurely. Introducing nano-scale fillers can change the properties of composites significantly, even at a very low filler content. Several studies have demonstrated that introducing CNTs into a polymer matrix can enhance the bulk matrix's toughness and the interface properties of CNT-polymer nanocomposites. For instance, Gojny et al. show that amine-functionalized double-walled CNTs (DWCNTs) increase the fracture toughness of epoxy resin by 26% and

proved that enhanced properties of wind blades can be achieved by introducing nanoparticles [4].

As a result of the current study, it was seen that the most significant contribution to the fracture toughness values of polymer resin is obtained by nanoclay. The addition of 1.00 wt% nanoclay increased the toughness properties of the resin by ~34%. However, this addition reduced tensile strength by ~30%. Therefore, in choosing the nanoparticle type and amount, 0.35 wt% fCNT was determined to be the most optimal choice, as the priority was to increase the fracture toughness of the composites without considerably decreasing their strength. 0.35 wt% fCNT incorporation increased the fracture toughness by ~28%, while tensile strength remained at the same level with that of the pure resin. For the GFRP composites with 0.35 wt% fCNT incorporated nanocomposite matrix, the mode I fracture toughness, G_{Ic}, was improved by ~8% compared to the pristine matrix GFRP composite. Similarly, an increase of ~35% in mode II fracture toughness, G_{IIc}, was observed in GFRP composites with nanocomposite matrix. Finally, GFRP nanocomposites with ply drop-off zones were produced and tested. As a result of these tests, tensile and delamination strengths decreased by ~3% and ~10%, respectively. On the other hand, ~6% and ~9% increase in work of fracture and failure strain, were observed, respectively, which are quantitative values related with the fracture behavior of the composites.

Following this introductory chapter, Chapter 1, Literature Review is covered in Chapter 2 briefly explaining the ply drop-off zones in wind turbines. Chapter 2 also covers literature information regarding GFRP composites and nanoparticles as well as their production methods and mechanical properties. In Chapter 3, all materials and production methods used throughout this study are explained along with the details of the testing applied. Chapter 4 presents the results of the tests performed in this thesis together with the pertaining discussions. In Chapter 5, Conclusions, key findings of this study are briefly summarized.

CHAPTER 2

LITERATURE REVIEW

2.1 Wind Turbine

To reduce the use of fossil fuels, it is necessary to turn to renewable energy sources. One of the renewable energy sources with the quickest development is wind energy. The operational wind energy generation capacity has dramatically expanded over the past few decades. While it was around 7.5 GW in 1997, it increased to 564 GW in 2018. According to the data, 60 GW of additional capacity was established in 2019 and 93 GW in 2020, and significant growth in wind energy is projected over the coming decades [8].

The history of wind turbines for electricity production began in 1888 in Cleveland, Ohio, United States, with Charles F. Brush, and in 1889 in Askov, Denmark, with Poul La Cour. S. Morgan-Smith constructed steel-bladed wind turbines at Grandpa's Knob in Vermont, United States, in 1941 to produce wind-generated electricity. After only a few hundred hours of intermittent operation, one of the blades failed (Fig. 2.1a). The importance of material selection in wind turbines was understood after the use of metal materials and failures. In 1956, the Gedser turbine blade, constructed with composite blades and steel spars supported by wooden ribs, was designed in Denmark. Following these developments, composite materials have become the primary materials for wind turbines [3].

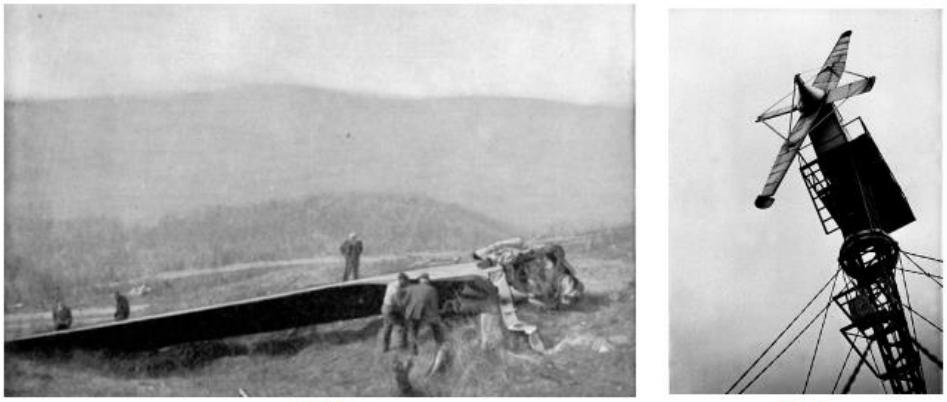

(a) (b)

Figure 2.1. (a) S. Morgan-Smith's failed wind turbine blade in 1941; (b) Gedser wind turbine [3].

2.1.1 Wind Turbine Blade Structure

Wind turbine blades consist of two opposing faces. A group of shear webs connects these faces. Load-carrying laminate flapwises are attached to shear webs as part of the sandwich structure. This structure is usually made of thick GFRM (glass fiber reinforced materials) or CFRM (carbon fiber reinforced materials) for additional structural rigidity (Fig. 2.2) [3].

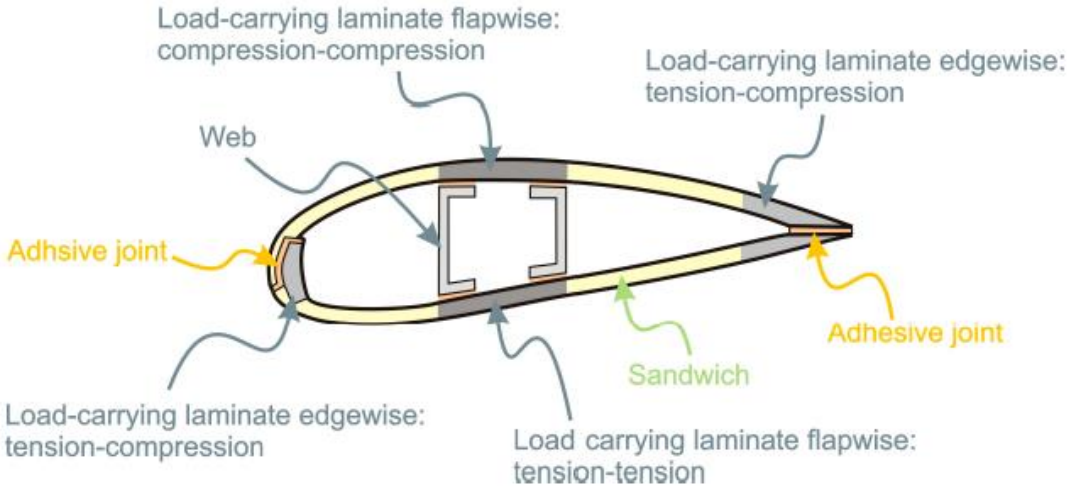

Figure 2.2. Schematic diagram of wind turbine blade.

2.1.2 Wind Turbine Blade Materials

The wind turbine industry continues its search for new and improved materials. The features needed in turbine blade design can be achieved with advanced materials. These materials are studied to provide structures with superior performance properties, extended product life, easy manufacturability, reduced density and easy recyclability. With the use of these material systems, high aerodynamic performance, reduced material deposition and extended life cycle are aimed. In addition, superior mechanical properties such as strength, fracture toughness and stiffness are desired [9].

In today's technologies, wind turbine blades are produced from composite materials consisting of multiple components with very different properties. Composite materials consist of reinforcing materials encapsulated in matrix resin, and the strength of the reinforcing material is combined with the binding properties of the resin. This combination gains properties that cannot be obtained from a single material. In most structural designs, glass, carbon, and aramid are used as reinforcing fibers, and epoxy and polyester are used as matrices.

Most wind turbine blades are created from glass fiber reinforced epoxy. In some structures, wood-epoxy composites or polyester are used as resin. Aluminum or steel can also be used in some small turbine blades, but these are heavier. Long blades may require different structural solutions, such as carbon-epoxy. For example, using carbon fiber means 2 tonnes less weight for a 61-meter-long blade [10]. However, the use of carbon fiber requires more precise production and higher production costs. As a result, glass-epoxy composites are always the first choice in wind turbine blade production due to the advantages they provide compared to their cost.

2.1.3 Wind Turbine Blade Production

In the early stages of wind energy development, wind turbine blades were typically crafted using a wet hand lay-up method in open molds. This process involved using paint brushes and rollers to saturate the glass fiber reinforcement with adhesive and bonding the shells to the spars. This technique was primarily employed for producing small and medium-sized blades. However, open-mold technology had its drawbacks, including high labor costs, relatively lower product quality, and environmental concerns [3].

The advent of vacuum infusion and prepreg technologies significantly improved manufacturing quality. Prepreg technology involved composite fibers pre-impregnated with a portion of the matrix material. For instance, the Danish wind turbine manufacturer Vestas extensively employed prepreg technology, allowing for industrial impregnation of fibers and their formation into intricate structures [11].

Resin infusion technology is one of the most widely used methods for crafting wind turbine blades, particularly for longer ones. In this method, fibers are placed within a sealed mold, and resin is introduced under pressure into the mold cavity. After the resin fills the space between the fibers, the part is heated to cure it. Resin infusion technology can be categorized into two types: Resin Transfer Molding (RTM) and Vacuum Assisted Resin Transfer Molding (VARTM), or Vacuum Infusion Process. RTM involves injecting resin at a pressure higher than atmospheric, while VARTM typically introduces resin under a vacuum bag or at a pressure lower than atmospheric [12]. SCRIMP, known as the Seemann Composite Resin Infusion Process, emerged in the late 1980s as a variation of VARTM, particularly suited for producing large and bulky components. Nowadays, vacuum-assisted resin transfer molding (VARTM) is the prevailing method for crafting rotor blades for wind turbines.

2.2 Ply Drop-off Region in Wind Turbine Blade

Adjusting the number of layers in composite materials, known as ply drops, is a crucial factor in designing various structures, including wind turbine blades, wing and fin skin structures, and helicopter rotor blades. To optimize the design of modern laminated composite wind turbine blades, it becomes necessary to incorporate thickness variations. These alterations in thickness are achieved by reducing the number of plies along the length of the structure (Fig. 2.3) [13].

Blades on wind turbines and aircraft wings typically feature thickness variations, with thicker portions near the base and thinner parts towards the tips, thanks to how plies are arranged. This design also includes adding extra plies in certain areas to enhance strength, resulting in cost-effective material savings and a lighter weight that allows for greater payload capacity. The process of terminating internal plies serves as an efficient means to tailor stiffness, enabling the attainment of the desired aerodynamic blade shape [14].

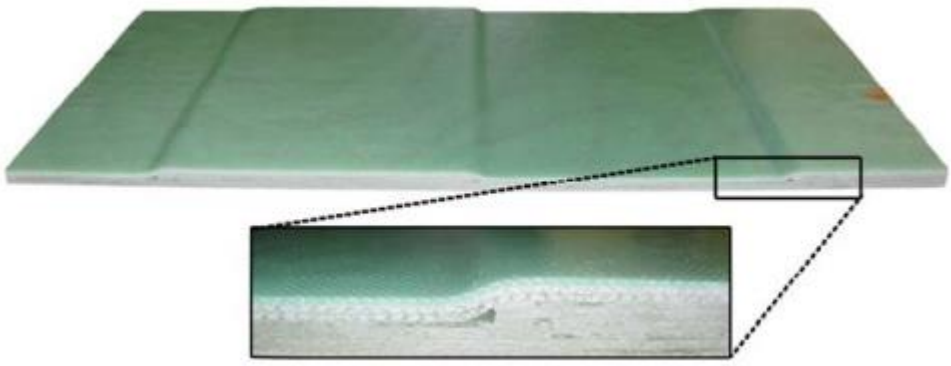

Figure 2.3. Ply drop-off design of a composite material.

The tapered structures generate local stress concentrations, especially interlaminar stresses, near the ply drop-off. These stresses may result in the delamination of plies and the failure of these regions. Fig. 2.4 illustrates a schematic of a delamination fracture originating from a resin pocket in the ply drop region [8].

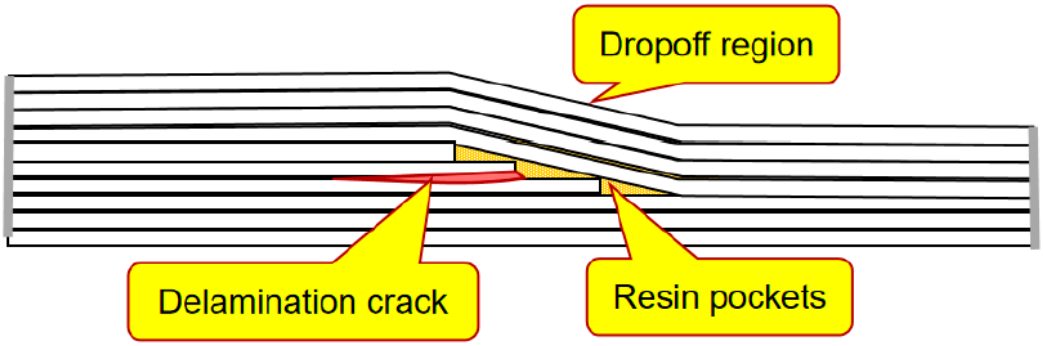

Figure 2.4. Schematic of ply drop-off region with crack delamination [8].

Ply drop-off, a disruption within composite structures, can lead to issues like concentrated stress at the drop-off point, resulting in potential component failure due to delamination or resin problems. This stress concentration can cause failure before the composite reaches its full load-bearing capacity. To maintain composite strength while reducing plies, it's important to explore factors such as drop thickness, transition slope, and ply arrangement and establish design guidelines for tapered composites [14]. This study focuses on improving the resin matrix to address delamination concerns in the drop-off areas of wind turbine blades rather than concentrating on design parameters.

2.3 Glass Fiber Reinforced Polymer (GFRP) Composites

Composite materials have found increasing use across various fields in recent decades. They play a vital role when it's crucial to reduce the weight of a structure that doesn't contribute to its function, thereby enhancing the payload-to-weight ratio. Fiber reinforced polymer composites (FRPs) possess excellent specific moduli and strengths, making them valuable in numerous structural applications, including aircraft components like wings and fins, helicopter parts such as yokes and rotor blades, wind turbine blades, mechanical prosthetic limbs, and satellites. Composite structures also meet the requirement of adjusting the structure's thickness from one point to another, known as ply drop-off [15].

A significant portion of wind turbine blades is made from glass fiber reinforced polymer (GFRP) composites, known for their high strength-to-weight ratio, resistance to corrosion and fatigue, and suitability for economical production of long and lightweight blades. They can also be integrated with additional components for improved performance. However, GFRP composites undergo irreversible cross-linking during curing, making recycling difficult. Carbon fiber, which is stronger and stiffer, is used less due to its higher cost [16].

Epoxy is a widely used thermosetting polymer in various industries, including aerospace, adhesives, coatings, and electronics. Its popularity stems from its exceptional mechanical and chemical properties and resistance to high temperatures without warping. The impressive qualities of epoxy polymers arise from the curing process, which involves converting a low molecular-weight resin into a high molecular-weight polymer with a three-dimensional network structure through chemical reactions and, occasionally, physical interlocking [17].

Blade material challenges in wind turbine design include improving fatigue life, stiffness, and achieving lightweight structures. Design requirements, harsh environmental conditions, and the demand for longer blades influence material selection. Current material research involves incorporating nanoparticles for reinforcement, exploring hybrid fiber architectures, and studying recyclable alternatives such as thermoplastics, cellulosic fibers, and bio-resins [16].

2.4 Nanoparticles

Nano-size particles have a vast potential for various applications due to their exceptional mechanical, thermal, and electrical properties. Since the beginning of the twenty-first century, the scientific community and industry have shown great interest in mechanically reinforcing polymers with nanoparticles. Even with a relatively low level of adding (0.1–1 %wt), improvements in the mechanical properties of polymers have been reported, making nanoparticles very intriguing for

composites [18]. In this study, three different nanoparticles have been used to reinforce the GFRP composite: functionalized carbon nanotube (fCNT), nanoclay, and cellulose nanofiber.

2.4.1 Functionalized Carbon Nanotube (fCNT)

Using nanoparticles to reinforce polymer composites is a promising engineering technique, particularly with carbon nanotubes (CNTs). CNTs exhibit exceptional thermal, mechanical, and electrical properties, making them valuable for enhancing polymers. They have a high specific surface area and efficient stress transfer capacity, making them suitable for high-performance composites in structural applications. CNTs also improve electrical conductivity and mechanical properties even at low concentrations. In summary, CNTs are a strong contender for strengthening polymeric materials due to their outstanding aspect ratio, low density, and impressive stiffness and strength [19].

CNTs are unique one-dimensional carbon materials with an extraordinary aspect ratio exceeding 1000, setting them apart from substances like diamond, graphite, and fullerenes (like C60 and C70). They can be visualized as tiny cylinders made of nanometer-sized graphite layers. These CNTs come in two main varieties, namely single-walled CNTs (SWCNTs) and multi-walled CNTs (MWCNTs). (Fig. 2.5) MWCNTs are constructed with multiple concentric cylindrical layers of graphene, organized around a central hollow core, and can reach diameters up to 100 nm. In contrast, SWCNTs are simpler, consisting of a single graphene layer seamlessly folded into a cylinder, with diameters ranging from 0.4 to 3 nm [20].

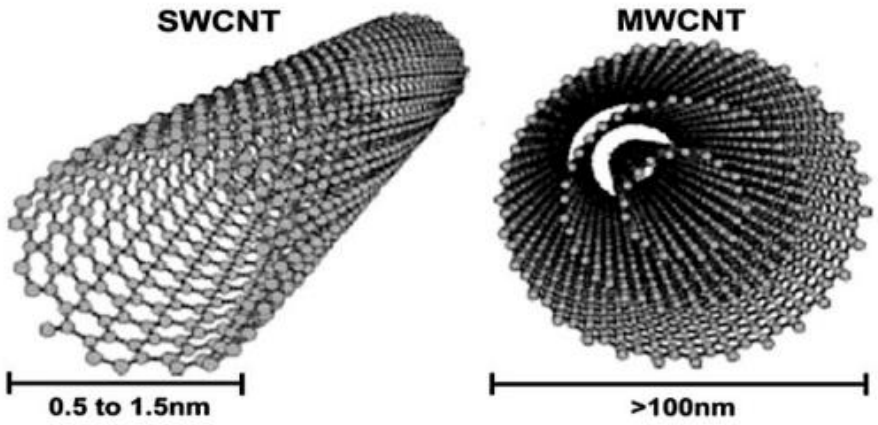

Figure 2.5. Schematic of single-walled carbon nanotube (SWCNT) and multi-walled carbon nanotube (MWCNT) [21].

The chemical bonding within CNTs primarily consists of sp2 carbon-carbon bonds. This unique bonding structure, stronger than the sp3 bonds found in diamond, is responsible for the remarkably high mechanical properties of CNTs. It's well-known that CNTs possess mechanical properties surpassing any known material. Although precise values for CNTs' mechanical properties may need to be firmly established, theoretical and experimental evidence supports their extraordinary mechanical attributes. For example, CNTs can exhibit Young's modulus, reaching as high as 1.2 TPa, and tensile strength ranging from 50 to 200 GPa. These remarkable figures position CNTs as the strongest and most rigid materials on our planet [22].

Epoxy composites strengthened with carbon nanotubes (CNTs) have exhibited enhanced mechanical properties, although the degree of improvement varies between different research studies. For instance, Allaoui et al. achieved a remarkable 100% increase in Young's modulus with just one wt% CNTs. In contrast, Zhu et al. observed a more moderate enhancement with the same fCNTconcentration. Multiple factors contribute to this variability, and addressing these challenges is crucial to harness the potential of CNTs fully [17].

Achieving an effective dispersion of CNTs within the polymer matrix is a significant challenge due to their distinctive characteristics. CNTs are typically supplied in tightly entangled bundles, leading to difficulties in achieving even distribution, and

their small nanometer-scale diameter and high aspect ratio further complicate dispersion. Aggressive mixing techniques like ultrasonication are utilized to overcome these dispersion challenges. Moreover, because fCNTsurfaces are chemically inert, establishing a strong bond between CNTs and the polymer matrix is challenging. CNTs primarily interact with the matrix through van der Waals forces, limiting load transfer efficiency. Therefore, researchers focus on the chemical functionalization of CNTs, which involves covalently bonding molecules like carboxyl groups to the fCNTstructure. (Fig. 2.6). While this process modifies the fCNTstructure, it enhances their interaction with the matrix. In this particular study, carboxyl-functionalized CNTs are employed.

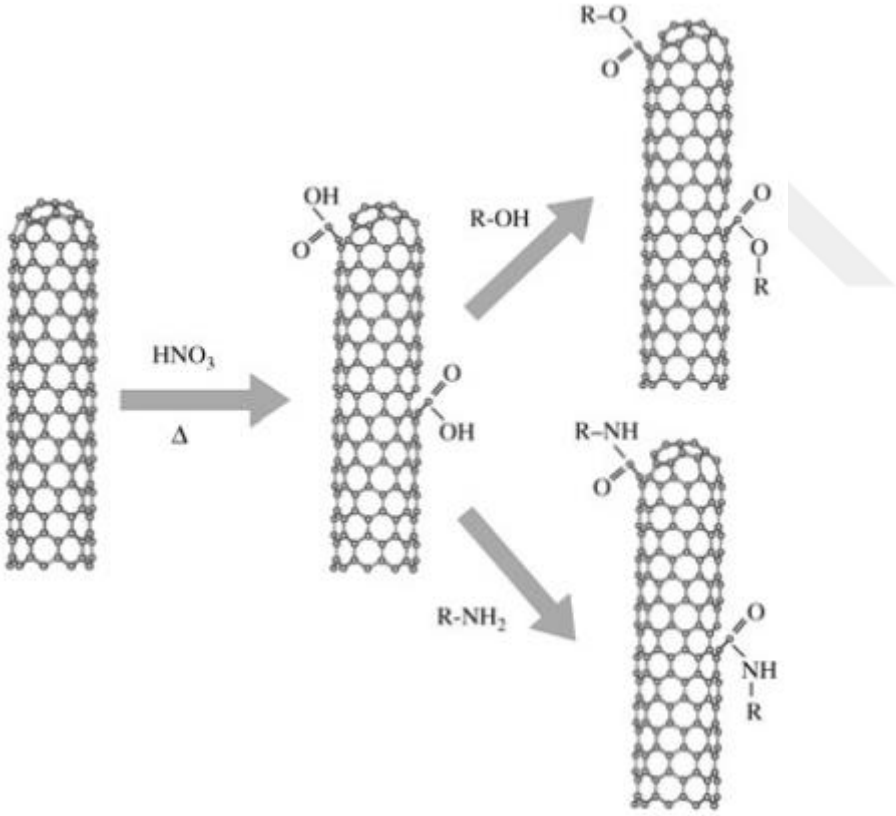

Figure 2.6. Schematic of chemical functionalization of fCNTby carboxyl groups [23].

2.4.2 Nanoclay

Nanoclay incorporated polymer nanocomposites are gaining a lot of attention due to the properties offered by the layered structure of nanoclay particles with exceptionally high aspect ratios. Since these composites exhibit significant benefits in thermal, mechanical, and barrier properties over unmodified polymers, they can be used in high-performance applications.

In nanotechnology applications, montmorillonite is one of the most commonly researched nanoclays. Montmorillonite is a clay material with a 2:1 sheet arrangement that involves the smectite group. In a 2:1 arrangement, each octahedral sheet is connected to two tetrahedral sheets (Fig. 2.7). Due to its abundance and non-invasive nature, montmorillonite is a material of interest in industrial applications and product development. This nanoclay has a flat morphology composed of clay layers. The width of montmorillonite particulates can range from 200 to 600 nm, whereas their thickness is typically no more than a few nanometers. Montmorillonite is naturally charged with a variety of metal ions, including Na+ and Ca+. In addition, cationic exchange capacity creates a negative charge during isomorphic substitution between layers. These properties significantly affect montmorillonite's dispersive nature and cause its hydrophilic behavior.

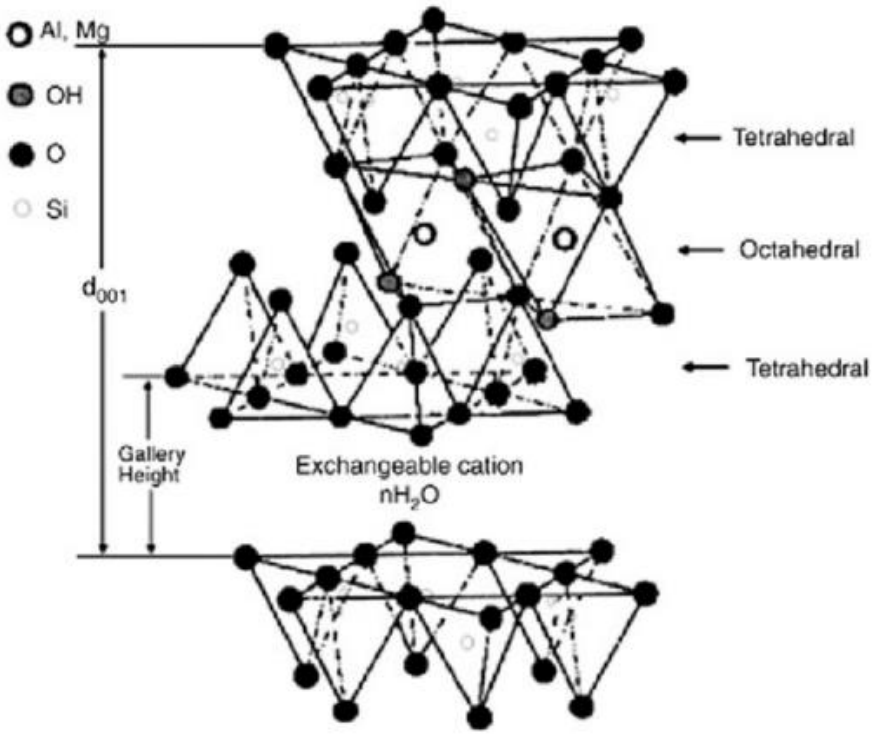

Figure 2.7. Schematic of 2:1 montmorillonite clay [24].

Various research groups have developed advanced techniques for preparing polymer-clay nanocomposites. These methods typically involve incorporating layered silicates, such as montmorillonite, at the molecular level within the polymer. The structure of polymer-clay nanocomposites can be categorized into two main types: intercalated and delaminated. Intercalated structures are well-ordered, with multiple layers where expanded polymer chains are inserted into the spaces between individual silicate layers. In contrast, delaminated or exfoliated structures occur when the separate silicate layers are no longer closely associated with the gallery cations of neighboring layers, resulting in the uniform distribution of silicate layers throughout the organic polymer. However, in a delaminated structure, the silicate layers may not exhibit the same level of orderliness as in an intercalated structure [25].

Okada et al. observed a significant enhancement in the modulus of clay-polyamide-6 composites, with a 90% increase resulting from the inclusion of 4 wt% of

exfoliated clay. However, regarding fracture behavior, research on brittle thermoset matrices has produced conflicting results. For instance, in the silane-treated clay-polyester system, quasi-static fracture toughness increased, but the exfoliated silicate layers had a minimal impact on the fracture properties of clay-glassy epoxy nanocomposites [26].

2.4.3 Cellulose Nanofiber

Cellulose, a fundamental component in plant structures, is commonly found in plant-based materials like wood, cotton, and hemp. Some microorganisms and marine organisms can also independently produce cellulose. Nano-scale cellulose fibers, known as cellulose nanofibrils (CNF), have garnered increasing interest in recent years due to their remarkable properties, including high strength and stiffness, low weight, biodegradability, renewability, and ease of functionalization. These fibers, typically ranging from 5 to 50 nanometers in diameter and several micrometers in length, can be derived from wood pulp or non-woody sources through chemical/enzymatic pre-treatments and mechanical processing. Transparent films can be produced from CNF after drying from its highly viscous aqueous gel state.

CNF's exceptional mechanical properties, with an elastic modulus of 79-220 GPa and tensile strength of 1.7-7.7 GPa, as well as its low density, have led to its extensive utilization in various industries [27]. Epoxy resins are increasingly being enhanced with nanocellulose fillers (CNFs and CNCs) at relatively low concentrations to develop high-performance engineering materials with improved mechanical, physical, wear, thermal, and electrical characteristics. Mechanical tests have demonstrated significant enhancements in the tensile modulus, tensile strength, elongation at break, flexural strength, and impact strength of epoxy composites when CNFs are added. Notably, the mechanical properties of CNF/epoxy nanocomposites at a 0.75% concentration exhibit substantial improvement, as the CNF filler is well-dispersed throughout the epoxy matrix without agglomerations or micro-voids [28].

2.5 Mixing Methods

In recent years, materials science and nanotechnology, in particular, have made incredible progress forward. Nanoparticles' high surface-to-volume ratio and distinct characteristics suggest they might significantly improve the mechanical, thermal, and electrical properties of a wide range of materials. Integrating nanoparticles into epoxy matrices to create nanocomposites with enhanced performance is one such potential use. However, getting a uniform nanoparticle dispersion throughout the epoxy matrix is challenging. Uniform dispersion of nanoparticles inside the epoxy matrix is necessary to achieve the intended improvements in the nanocomposite's characteristics. Agglomeration, resulting from insufficient dispersion, reduces the material's strength and consequently produces stress concentration areas. The use of efficient mixing methods further enhances the advantages of nanoparticle incorporation. Some of the main mixing techniques are discussed in the following chapters.

2.5.1 Calendering

The calender, also known as a three-roll mill, is a type of equipment used to disperse or homogenize materials with high viscosity by applying shear force in the form of rotating rollers. Typically, a calendering machine will have three concentric rollers rotating at different speeds, as shown in Fig. 2.8. The first and third rollers, known as the feeder and apron rollers, rotate in the same direction. In contrast, the central roller turns oppositely.

The mixing process begins when the ingredients are added to the hopper and dragged toward the center by the feed rollers. When the material has been pre-dispersed, it will adhere to the underside of the central roller and be carried through the second gap. The appropriate degree of fineness in dispersion is achieved in this space. The material still on the center roller is subjected to even greater shear stress as it passes through the second gap between the center roller and the apron roller, which is

moving faster. The finished product is transferred from the apron roller to the apron through a knife blade. This milling cycle can be repeated many times to get the best possible dispersion. The short residence time and solid shear forces are the results of the tight gaps (controllable between 500 to around 5 microns) between the rollers and the mismatch in the angular velocity of the neighboring rollers. The gap width between the rollers may be modified and maintained manually or hydraulically, making it simple to get a monitored and narrow size distribution of particles in viscous materials.

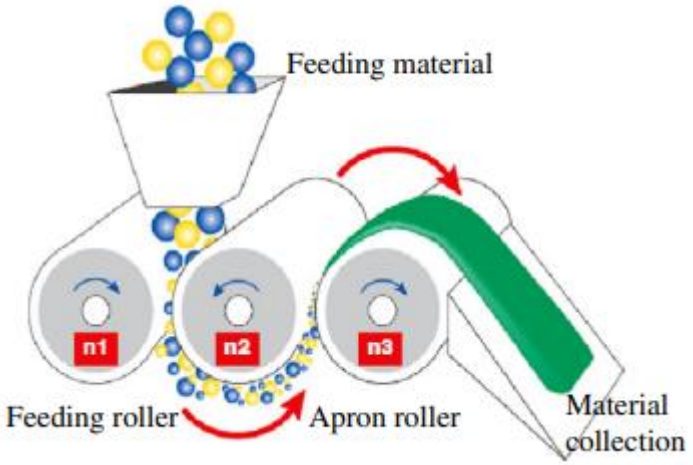

Figure 2.8. Schematic of three roll mill and its working principle [20].

2.5.2 Ultrasonication

Ultrasonication is the process of using ultrasonic radiation to agitate particles in a solution for a variety of reasons. To achieve this, an ultrasonic bath or sonicator (ultrasonic probe/horn) is commonly used in the lab (Fig. 2.9). It's the accepted standard for dispersing nanoparticles. Inducing cavitation in liquid suspensions is the goal of ultrasonication, which uses high-frequency sound waves (usually in the range of 20 kHz to several MHz). Cavitation creates significant localized shear stresses and disperses nanoparticles throughout the epoxy resin by splitting nanoparticle agglomerates. Ultrasonication's usefulness comes from its capacity to provide a mild

but powerful energy source, which allows for optimal nanoparticle dispersion without damaging the epoxy matrix.

Figure 2.9. Ultrasonicator used in the study.

The idea behind this method is that as ultrasound travels through a medium, it induces attenuated waves in the molecules due to a sequence of compressions. These shock waves facilitate the "peeling off" of individual nanoparticles located in the outer section of the nanoparticle bundles, or agglomerates, and lead to the breakup of individual nanoparticles from the bundles. Water bath sonicators used in laboratories typically operate at 20–23 kHz and generate less than 100 W of power. Most commercial probe sonicators can be adjusted from 100 W to 1500 W in power, with an amplitude of 20–70%. In this research, the nanoparticles in the epoxy matrix are mixed using a high-power ultrasonicator (up to 500 W).

Typically, titanium or another inert metal is used to make the probe. The tips of most probes have a diameter ranging from 1.6 to 12.7 mm and are linked to the probe through a base unit. 8. This implies that the energy from the broad base is concentrated on the tip, giving the probe a high intensity. As a result of this setup, sonication may immediately create excessive heat. Therefore, it's important to sonicate the samples for short periods and keep them cool (in an ice bath, for example). CNTs are quickly and severely destroyed if the sonication treatment is too strong and long-lasting, especially when a probe sonicator is used. The development of defects on the fCNTsurface was validated by Raman spectroscopy, which showed that continuous ultrasonication of CNTs led to a dramatic rise in the intensity of the D band (indicating disordered sp3 carbon on CNTs). CNTs can degrade into amorphous carbon nanofibers if their graphene layers are destroyed. Due to localized damage, the CNT/ polymer composites' electrical and mechanical characteristics degrade. Therefore, the working conditions of the sonicator must be carefully decided.

2.5.3 High-Shear Mixing

High-shear mixing techniques need the use of specialist equipment, such as high-speed mixers or rotor-stator devices (Fig. 2.10), to generate severe mechanical forces and turbulence. High shear rates and fluid velocity work together to disperse nanoparticles throughout the epoxy matrix by dispersing agglomerates of particles. Typically driven by an electric motor, a high-shear mixer's impeller or high-speed rotor is used to generate flow and shear. Shear occurs in a fluid when there is a velocity difference between neighboring fluid regions. In this process, shear results from a velocity differential between the fluid at the center and the outside diameter of the rotor, known as the tip velocity, which is greater.

Figure 2.10. High-Shear Mixer.

The mixing speed and the propeller's size and form determine the dispersion outcomes. A reasonably fine dispersion of CNTs in a polymer matrix may be produced after intense stirring. Although MWCNTs have a tendency to re-agglomerate, they may be distributed more easily than SWCNTs using this method. The frictional contacts and elastic interlocking processes identified in experiments are primarily responsible for this behavior. Using a high-speed shear mixer with a speed of up to 10,000 rpm is necessary to obtain a fine dispersion of highly agglomerated CNTs in the polymer matrix.

2.5.4 Comparison of Mixing Techniques

The material characteristics of nanocomposites can be significantly improved by incorporating nanoparticles into epoxy matrices. For maximum effectiveness, nanoparticles must be evenly distributed throughout the epoxy matrix. Several other

types of mixing have been tried to get around the difficulty of dispersing nanoparticles. These include calendering, ultrasonication, and high-shear mixing. Nanoparticle type, loading amount, production size, and desired qualities all play a role in deciding which technique to use. Table 2.1. shows the advantages and disadvantages of three different mixing methods to compare which is better for specific purposes. Ultrasonication is employed in this research as a method of homogenization. Continued research and development in this subject will allow the creation of nanocomposites with unparalleled performance, opening up new paths for different engineering and technological applications.

Table 2.1. Advantages and disadvantages of calendering, ultrasonication and high-shear mixing methods.

	Advantages	Disadvantages
Calendering	• High shear forces generated between the rollers effectively break down agglomerates • Help achieve a narrow particle size distribution of nanoparticles • The operating parameters of a three-roll mill, such as roller speed, gap distance, and feed rate	• Limited to low to medium viscosity materials • The shearing forces generated during the milling process can lead to a rise in temperature • Three-roll mills can be relatively expensive
Ultrasonication	• Effective in dispersing nanoparticles at the nanoscale • Facilitates the incorporation of a wide range of nanoparticle types • Can be used in combination with other mixing methods for improved dispersion	• Potential for degradation of nanoparticles due to prolonged exposure to ultrasonic energy • Not suitable for large-scale production due to the limited volume capacity of ultrasonic baths • Requires optimization of process parameters such as power intensity and duration
High-Shear Mixing	• Enables efficient dispersion of nanoparticles, even at high loading levels • Suitable for both laboratory-scale and industrial-scale production • Allows control over process parameters, including mixing speed and time	• Increased equipment and operational costs compared to conventional mixing methods • Requires careful optimization to prevent degradation of nanoparticles • May lead to localized heating and thermal degradation of the epoxy matrix

2.6 Nanoparticle Incorporated Polymer Nanocomposites

The introduction of nanoparticles into polymers is one of the most exciting developments in the field of material science in recent years. Nanoparticle incorporated polymers are rapidly replacing more typical polymer materials due to their superior mechanical characteristics, usefulness, and performance. Nanoparticles of various materials, including metals, ceramics, organic compounds, and carbon, are inserted into the polymer matrix to enhance its qualities and performance. The type, size, concentration, and distribution of the nanoparticles inside the polymer matrix determine the characteristics and advantages received. Wherever exceptional material qualities are required, such in aircraft, automotive, electronics, packaging, and the biomedical sector, nanoparticle polymers find widespread use.

The capacity to increase fracture toughness is considered a major potential of nanoparticles as a structural element in polymer matrices [19]. The addition of CNTs can significantly enhance epoxy composites' toughness and impact resistance. They function as crack arrestors and energy dissipators, limiting crack propagation and dissipating energy during impact events. This characteristic improves the material's resistance to sudden loads and helps prevent catastrophic failure. Epoxy composites can have their fatigue resistance improved by using CNTs. Crack start and development are inhibited by CNTs, resulting in greater durability under cyclic stress. This is especially crucial in uses that need a long endurance life from their materials after being subjected to repeated stress.

Gojny et al. performed an experimental study for the fracture toughness and tensile strength of CNTs and carbon black incorporated epoxy nanocomposites. They used different types and amounts of nanoparticles, such as CNTs and NH2 functionalized CNTs, as reinforcing material, though they were all originally double-walled CNTs. Fig. 2.11a emphasizes that all nanocomposites had significantly higher fracture toughness than pristine epoxy regardless of the type and amount of reinforcing particles. Since nanotubes have a fiber-like structure and a crack-bridging

mechanism is becoming increasingly dominant, the possible fracture toughness would have been much higher if suitable samples had been available.

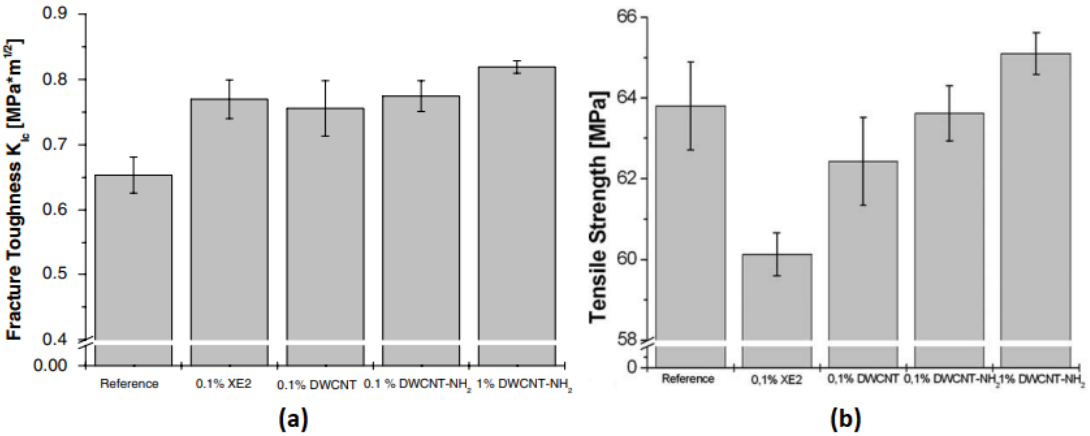

Figure 2.11. (a) Fracture toughness and (b) tensile strength values for pristine epoxy, 0.1% carbon black, 0.1%DWCNT, 0.1%DWCNT-NH2 and 1%DWCNT-NH2 added epoxy [19].

On the other hand, the non-functionalized nanotubes and carbon black had negative effects on tensile strength. The observed behavior could be attributed to their capacity to create agglomerates and a weaker interface with epoxy matrix (compared to the amino-functionalized DWCNTs). At 0.1% nanotube concentration, the tensile strength of samples containing amino-functionalized DWCNTs was similar to that of the pristine epoxy, and at 1%, it was slightly higher. DWCNT-NH2 could be more evenly distributed in the epoxy matrix, leading to fewer and smaller agglomerates than non-functionalized DWCNTs. These findings and the enhanced interface between the amino groups on the nanotube surface and the epoxy resin inhibited the failure initiation at these agglomerates.

Hsieh et al. also conducted a study in terms of the fracture behavior of MWCNT incorporated epoxy nanocomposites. They observed that when the nanotube content of the epoxy polymers was raised up to 0.5% wt, the fracture toughness (Kc) and fracture energy (Gc) increased continuously. The pristine epoxy had a measured Kc of 69 MPa m1/2. Adding 0.5 wt% of MWCNTs improved the value of Kc to 98 MPa m1/2. River lines were observed on the fracture surfaces, which indicates brittle

failures. Also, nanotube pull-out and bridging as toughening processes were detected [29].

Zhou et al. carried out one of the most popular studies about CNTs incorporated epoxy nanocomposites in 2007. The ultrasonic processor was utilized to obtain a homogenous mixture of epoxy resin and multi-walled CNTs. Then, flexural and fracture toughness tests were conducted on pristine and CNT-filled epoxy to determine the impact of the addition of CNTs on the epoxy's mechanical properties (for results Fig. 2.12).

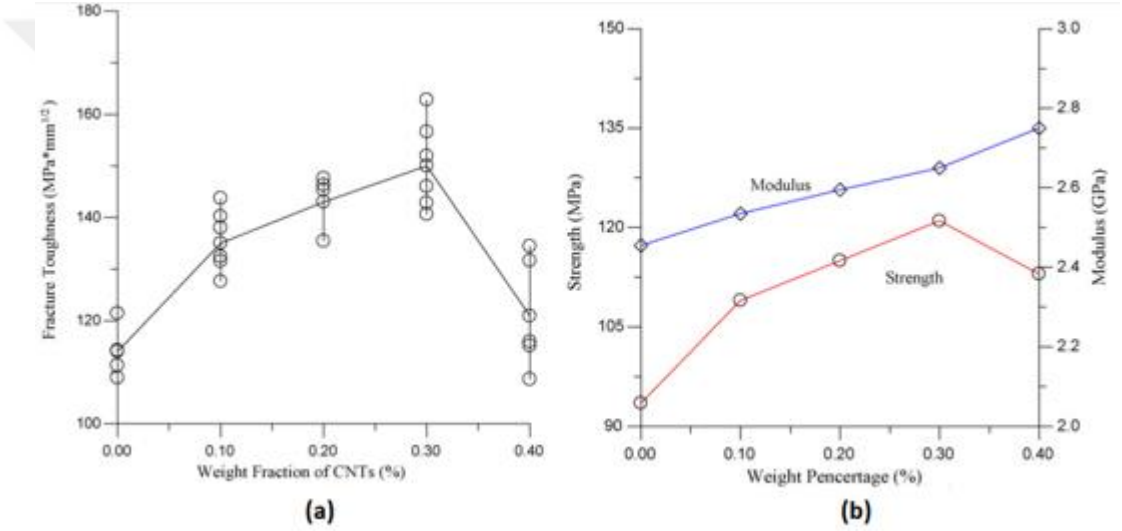

Figure 2.12. (a) Fracture toughness and (b) tensile strength values for pristine epoxy, 0.1% CNTs, 0.2% CNTs, 0.3% CNTs and 0.4% CNTs added epoxy [30].

With increasing fCNTcontent, the epoxy's modulus increased continuously. The introduction of 0.4 wt% CNTs increased the modulus by 11.7%. In contrast, the system with 0.3 wt% addition is the most successful, increasing flexural strength by 28.3% (Fig. 2.12b). At 0.4 wt% addition, the strength starts to decrease, but the improvement in modulus remains. In terms of fracture toughness, the critical stress intensity factor reaches its greatest improvement at 0.3 wt% (Fig. 2.12a). Fracture toughness has been found to decrease with increasing filler loading at higher levels [30].

Another study was conducted by Suresha et al. in 2019. They used nanoclay (N-C) and nano-calcium carbonate (N-CC) as reinforcing particles added to the epoxy matrix. These composites' mechanical properties, such as tensile strength, were investigated [31].

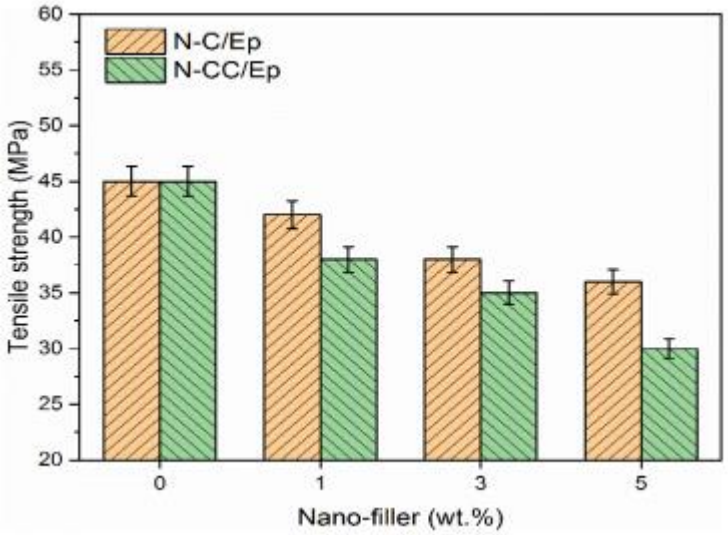

Figure 2.13. Tensile strength of N-C/N-CC epoxy nanocomposites [31].

Fig. 2.13 shows that the tensile strength is lower, no matter what proportion of fillers are added, compared to pure epoxy. 5% N-C filler has resulted in a 22.2% decrease in epoxy's strength compared to epoxy with no filler. N-CC fillers also reduced the strength of the composite by 33.3%.

As a result of these studies, while epoxy composites often benefit from nanoparticle incorporation in terms of enhanced mechanical qualities, these examples show this is not always true. From the literature review, fracture toughness generally increases with the addition of nanoparticles to the polymer matrix. On the other hand, tensile strength decreases typically since the agglomeration of particles creates stress concentration sites. Therefore, the addition of nanoparticles to the epoxy matrix must be done in a proper way and with the right amount to obtain the most valuable results. Nanoparticle dispersion, interfacial bonding, and agglomeration are all variables that might affect the result. It emphasizes the significance of material choice, processing

methods, and optimization in achieving the required mechanical benefits in nanoparticle incorporated epoxy systems.

2.7 Glass Fiber Reinforced Composites with Nanocomposite Matrix

Scientists and engineers have developed innovative methods to improve the qualities of fiber reinforced polymers (FRPs) in their pursuit of stronger, lighter, and more durable materials. Nanoparticle integration into FRPs, creating nanoparticle incorporated fiber reinforced polymers (NP-FRPs), is one such strategy receiving much interest. Fibers and nanoparticles combined provide synergistic benefits, opening up new avenues for innovative material design and use.

Long lauded for their superior strength-to-weight ratio, fiber reinforced polymers are an excellent choice for uses where weight reduction is important without sacrificing structural integrity. High-strength fibers like carbon, glass, or aramid are typically placed in a matrix material like epoxy or polyester to create FRPs. Together, these features allow for uniform stress distribution throughout the material and prevent cracks from propagating, improving the material's mechanical qualities. On the other hand, the small dimension and large surface area of nanoparticles provide them with unique properties. Mechanical strength, thermal stability, and electrical conductivity may all be enhanced when nanoparticles are included in FRPs. For example, the high mechanical strength of carbon nanotubes allows them to bridge the microcracks inside the matrix, increasing the material's toughness and crack resistance. Similarly, the FRP structure may be strengthened, and its performance improved using graphene, renowned for its exceptional mechanical, electrical, and thermal characteristics.

There are a variety of ways to incorporate nanoparticles into FRPs. The most common method involves impregnating fibers with a polymer matrix enhanced with nanoparticles. Nanoparticle decoration of fibers followed by polymer matrix impregnation is yet another method. The interfacial connection between the fiber and

the matrix may be increased by the incorporation of nanoparticles, which also improves the load transfer capacities of the material. FRPs can have their electrical and thermal conductivity altered with the addition of conductive nanoparticles. Lightweight electromagnetic shielding, flexible electronics, and heat dissipation systems are just some of the potential uses made possible by this discovery.

In 2015, Zhang et al. proposed that MWCNTs were significant in enhancing GFRPs' energy-absorbing capacity [32]. They used quasi-static testing to learn about mechanical qualities of GFRPs. In the study, epoxy resins were added with MWCNTs at concentrations of 0.4 wt%, 0.75 wt%, and 1.1 wt%. A high-speed stirrer homogenized the epoxy-CNT mixture, and then S-glass fiber was produced by a wet lay-up process. The findings of the study are shown in Fig. 2.14. According to the results, increasing fCNTconcentration lowers ultimate tensile strength and modulus, with 0.75 wt% showing the maximum tensile strength. The modulus gradually decreases as the percentage of CNTs in the material increases. On the other hand, higher failure strain is demonstrated by CNT-modified GFRPs, as shown in Fig. 2.14b. The 0.4% and 0.75% GFRPs have been steadily increasing, while the 1.1% GFRPs have been decreasing. In terms of fracture work, which is defined as the strain energy of the sample until fracture (Fig. 2.14c), the 0.75%/GFRP displays the greatest value. When comparing the CNT-GFRPs across tensile strength, failure strain, and effort to fracture, the GFRP containing 0.75% fCNTperformed most favorably.

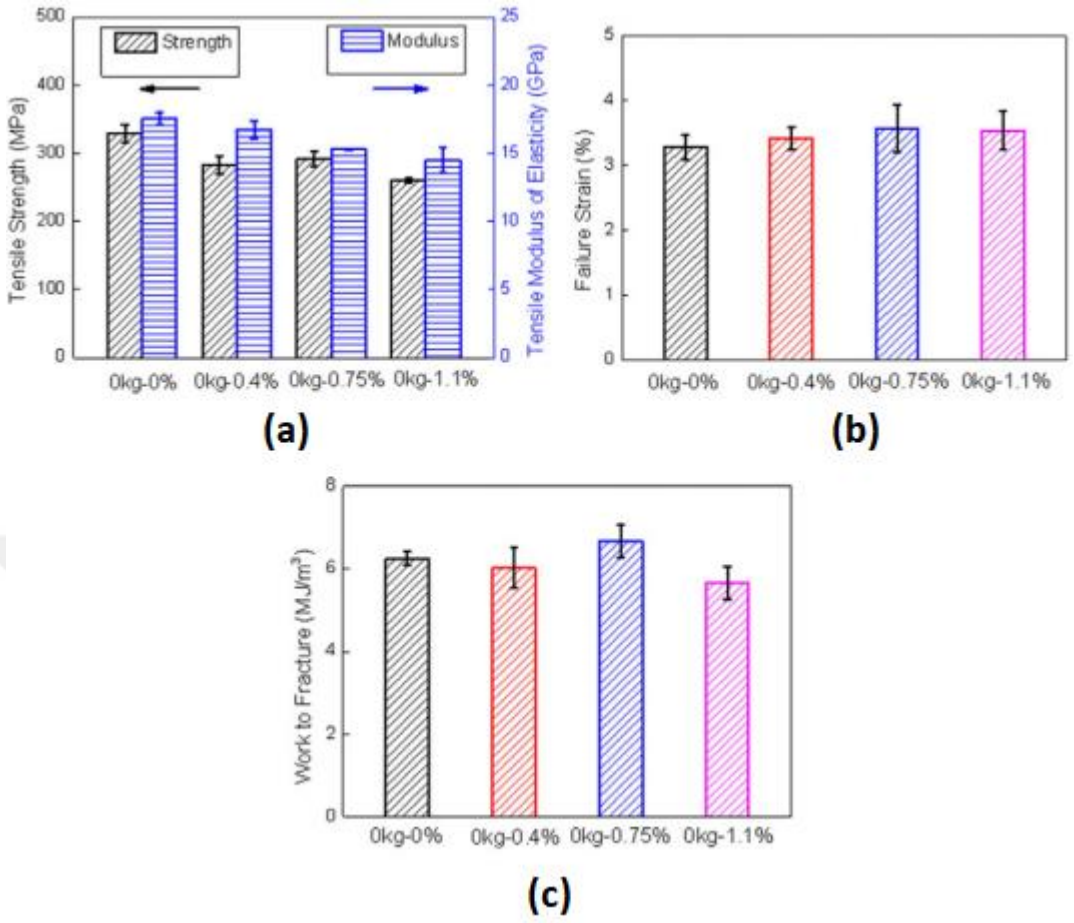

Figure 2.14. (a) Ultimate tensile strength and modulus, (b) failure strain, and (c) work to fracture graphs of GFRPs and GFRPs with 0.4, 0.75, 1.1 wt% MWCNT addition [32].

Mechanical characteristics of fCNTincorporated GFRPs were also studied by Yildiz et al. Two methods of incorporation were investigated. In the first, CNTs (called NRCs in the study) were dispersed in an epoxy matrix. The second method, known as fuzzy architectures, included the direct development of CNTs onto glass fibers. Additionally, composites were fabricated, and reinforcing capacities were determined by employing both NRCs and fuzzy glass fibers, a combination known as fuzzy nanoparticle incorporated composites (F-NRCs). Mode-I fracture toughness and unidirectional composite tensile tests were conducted to learn more about the material's mechanical characteristics. The fracture toughness was improved by 113% with NRCs and by 119% with F-NRCs (Fig. 2.15). On the other hand, the tensile

strength of FNRCs was reduced by 24%, whereas that of NRCs was improved by 16%.

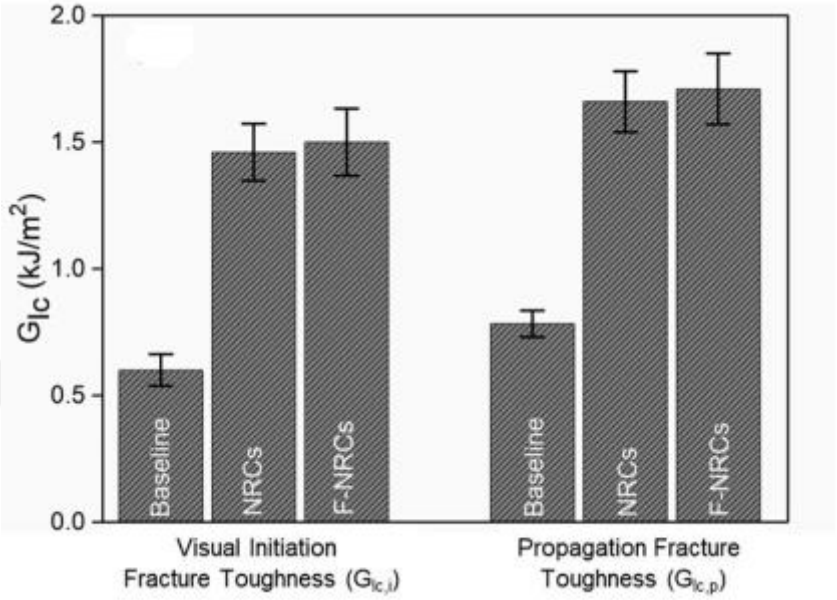

Figure 2.15. Fracture toughness values at initiation and propagation for baseline, NRCs and F-NRCs [33].

CHAPTER 3

METHODOLOGY

3.1 Materials Used

In the study, the Biresin CR80 epoxy resin has been used. Biresin CR80 is an epoxy resin with low viscosity that may be used to make molds and high-performance fiber reinforced composite products with thermal characteristics up to 80 °C. The hardener is CH80-6 with a mixing ratio of 100:30 by weight. The resin was purchased from Odak Kompozit, Ostim Organize Sanayi Bölgesi, 06374 Yenimahalle/Ankara.

Figure 3.1. CR80 - CH80-6 epoxy resin system used in the study.

Because of its low viscosity range, Biresin CR80 is well-suited for infusion and injection procedures. It has a wide range of applications in the marine, wind turbine, and industrial composite applications. Due to its low viscosity and strong wetting characteristic, it allows for quick infusion and good wet-out of fabrics and non-wovens. Table 3.1 details the physical and mechanical characteristics of the resin.

Since these mechanical properties may vary according to the production method and environment, a few of them were measured in this study for consistency.

Table 3.1. Typical properties of CR80 -CH80-6 epoxy system.

Properties	Value
Colour	colorless to yellow
Density	1.17 g/cm³
Tensile Strength	83 MPa
Elastic Modulus	3 GPa
Flexural Strength	126 MPa
Glass Transition Temperature	85 °C

Three different nanoparticles have used in the study as incorporations: COOH-functionalized carbon nanotube (fCNT), nanoclay and cellulose nanofiber (CNF). The fCNT used in this study is a multi-walled carbon nanotube (MWCNT) 8-18 nm in diameter, and its surfaces are functionalized with a carboxyl group (-COOH). On the other hand, no treatment was applied to the surface of the nanoclay and CNF. Nanoparticles were provided by Nanografi, METU Technopolis, 06531 Çankaya/Ankara.

Figure 3.2. fCNT, CNF, and nanoclay used in the study provided by Nanografi.

The diameter and purity values of the nanoparticles are given in Table 3.2. Since nanoclay is not a fiber but a layered structure, it has no diameter or length. Hence its size is provided.

Table 3.2. Characteristic properties of nanoparticles.

Nanoparticle	Purity	Diameter
fCNT	> 96%	8-18 nm
CNF	92%	10- 20 nm
Nanoclay	99.9%	800 in size

In the study, Interglass 92145 has been used as a fabric. Interglass 92145 is a unidirectional glass fiber fabric with a tensile strength of 2000 MPa. Other mechanical properties of Interglass 92145 are given in Table 3.3.

Table 3.3 Typical mechanical properties of Interglass 92145.

Properties	Value
Density	2.6 g/cm³
Tensile Strength	2000 MPa
Elastic Modulus	78 GPa
Shear Modulus	33 GPa
Tensile Strain at Failure	4.8%

Test samples were formed by pouring resin into silicone molds. Verpol RTV-2 mold silicone has been used to create molds. 2 wt% hardener was added to this silicone, and molds were let to cure.

3.2 Sample Preparation

In this study, 3 different amounts of nanoparticles, namely 0.35, 0.75, and 1 wt%, have been added to the epoxy resin to produce nanocomposites. The main purpose

of this study was to find the most suitable nanoparticle amount and production method in terms of the mechanical properties, especially fractue toughness, of the nanocomposites to be used as the matrix of the GFRP composites in the next step. Table 3.4 shows the samples produced for the tests to be performed. The homogenizer's operational parameters, such as power and time, have been determined using only 0.35 wt% fCNT incorporation in the resin representatively. This amount was chosen because the improved mechanical properties presented in literature generally resulted from CNT amounts around this value [30]. Pristine epoxy and all nanoparticles with 0.35 wt%, 0.75 wt%, and 1 wt% are employed in the fracture toughness and tensile strength testing. By using 0.35 wt%, 0.75 wt%, and 1.00 wt%, nanoparticle amounts from lower to higher levels have been covered. Following steps have been used for the production of all samples. Only the amount of the incorporated nanoparticles has been changed.

Table 3.4. All pristine epoxy and epoxy-nanoparticle samples produced in the study with their compositions for the tests they have been used.

	Pristine Epoxy	fCNT (wt%)	CNF (wt%)	Nanoclay (wt%)
Determination of Homogenizer Parameters	-	0.35	-	-
Fracture Toughness Tests	Pristine Epoxy	0.35 0.75 1	0.35 0.75 1	0.35 0.75 1
Tensile Strength Tests	Pristine Epoxy	0.35 0.75 1	0.35 0.75 1	0.35 0.75 1

As the first step of sample preparation, the epoxy resin and nanoparticles have been weighed. The particles were then mixed briefly by hand before being placed in the ultrasonic homogenizer to prevent clumping or flitting.

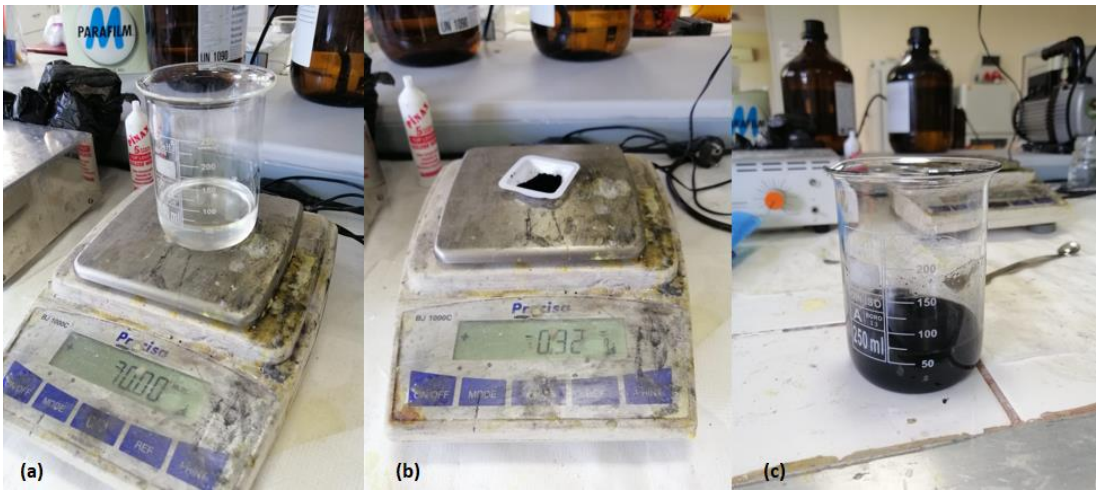

Figure 3.3. Weighed (a) epoxy and (b) fCNT, and (c) hand-mixed mixture of epoxy and fCNT.

NG06LB0202 model ultrasonic homogenizer (Fig. 3.4b) purchased from Nanografi has been used for the dispersion of nanoparticles. The homogenizer, with its horn made of titanium, has a maximum power of 500 watts. The resin was put into the ultrasonicator in an ice bath (Fig. 3.4a) because it overheats the resin during mixing, which damages the particles and the resin. The ice bath prevented overheating. The probe of the ultrasonicator was immersed in the mixture according to the values shown in Table 3.5. In this study, approximately 300 ml of liquid has been used, and therefore the probe was immersed 13 mm.

Table 3.5. Ultrasonicator probe immersion depth with respect to the amount of the mixture.

Capacity	0.5-50 ml	2-100 ml	5-200 ml	10-500 ml	20-1000 ml
Immersion Depth of the Probe Tip	3 mm	6 mm	8 mm	13 mm	16 mm

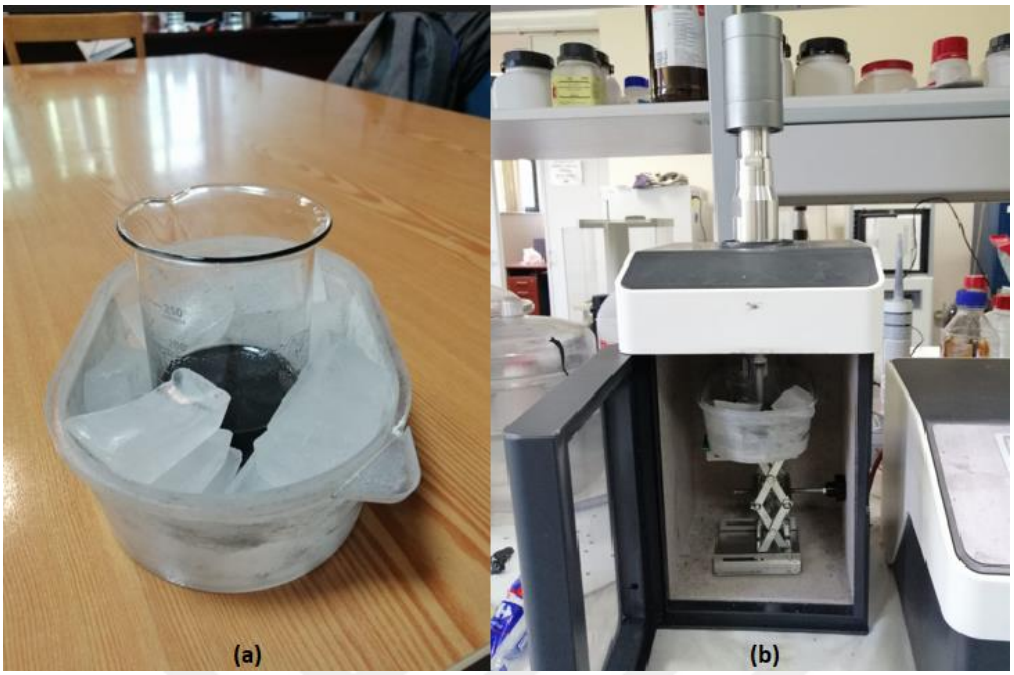

Figure 3.4. (a) The mixture was put into ice bath, and (b) placed in ultrasonic homogenizer.

Fracture toughness and tensile strength samples have been produced by operating the ultrasonicator at 150 watts for 1 hour. The reasons for selecting these parameters as the most appropriate ones have been explained in the result and discussion chapter. After the completion of the mixing process, the nanoparticle incorporated resin leaves the homogenizer at a temperature of about 50 °C. If the hardener were to be added at this temperature, it would rapidly harden, so the temperature was allowed to drop for a while. When the temperature decreased to approximately 30 °C, the hardener was added to the epoxy at a ratio of 100:30. It was hand-mixed for at least three minutes. During mixing processes air bubbles were formed. Therefore, the mixture was placed in a vacuum chamber to eliminate air bubbles and kept in a vacuum of ~10^{-2} mbar for 20 minutes. The Airtech vacuum chamber has been used in this study (Fig. 3.5). The mixture coming out of the vacuum chamber was ready to be poured into the molds prepared with RTV-2 mold silicone.

Figure 3.5. The nanoparticle incorporated epoxy system is kept in the Airtech vacuum chamber to eliminate the air bubbles.

Molds were prepared using RTV-2 mold silicone to be able to produce the specific dimensions of test samples. Models of the samples to be made in accordance with test standards ASTM D638-14 [34] and ASTM D5045-14 [35] were first printed on a 3D printer. Then the models were glued on a flat surface, and a frame, also 3D printed, was glued around them as shown in Fig. 3.6a. Sil-Jet Aerosol silicone mold release agent was sprayed on the models, and the mold silicone mixed with its hardener was poured into the frame. The silicone was allowed to cure for 24 hours before being removed from the frame (Fig. 3.6b).

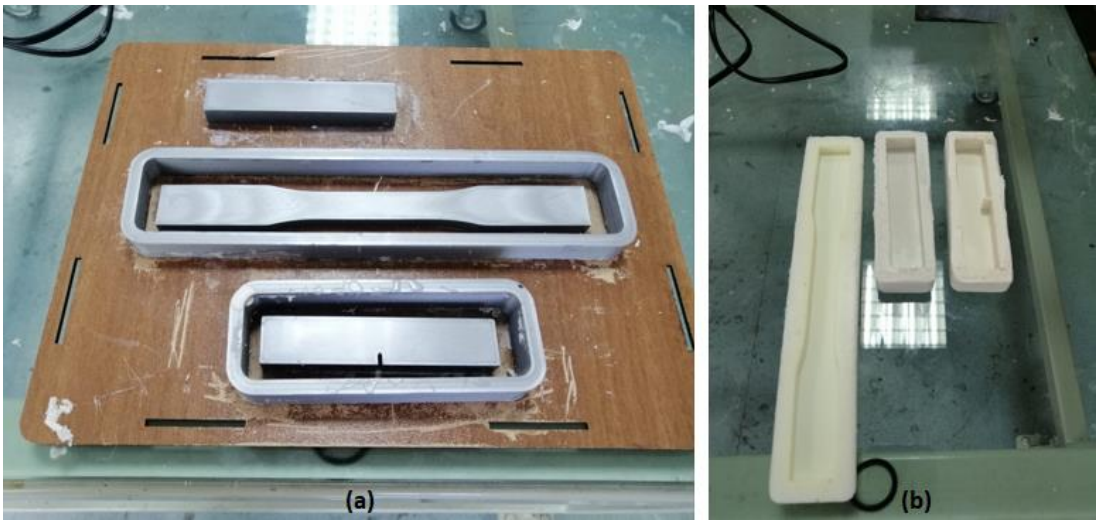

Figure 3.6. (a) 3D printed test sample models and their frames, and (b) resulting silicone molds.

Before the nanoparticle incorporated epoxy resin system has been poured into silicone molds, the Sil-Jet Aerosol silicone mold release agent was sprayed into the molds so that the samples can be easily released from the mold. Nanoparticle-resin mixtures have been poured into the molds after vacuum degassing. The nanoparticle incorporated epoxy resin system was allowed to cure for 24 hours at 25 °C (Fig. 3.7a). The same conditions have been provided for each sample by using a furnace during curing. This is because the laboratory ambient temperature fluctuates during the day which may have changed the curing level of different batches of samples. After 24 hours, the hardened samples have been removed from the molds and placed into the furnace at 80 °C for heat treatment. The heat treatment was applied for 8 hours at 80 °C for post curing. Fig. 3.7 shows the Nuve FN 120 dry heat sterilizer used for all heat treatments.

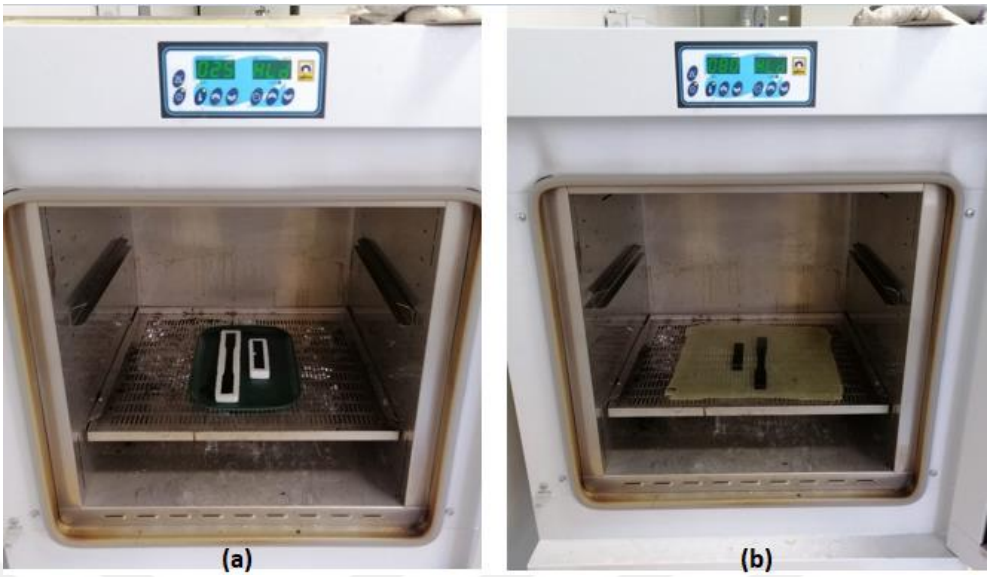

Figure 3.7. (a) Curing of nanoparticle incorporated epoxy resin system at 25 °C, and (b) heat treatment of hardened samples at 80 °C.

As the epoxy resin system cures in the mold, adhesion forces cause it to adhere to the mold. For this reason, the center of the samples remains more dented than the sides (Fig. 3.8a). Therefore, the samples need to be ground following heat treatment. The equipment Metkon 2V Grinder-Polisher has been used for grinding (Fig. 3.8b). For this process, 200-600-1000 grit abrasive grinding papers were used consecutively.

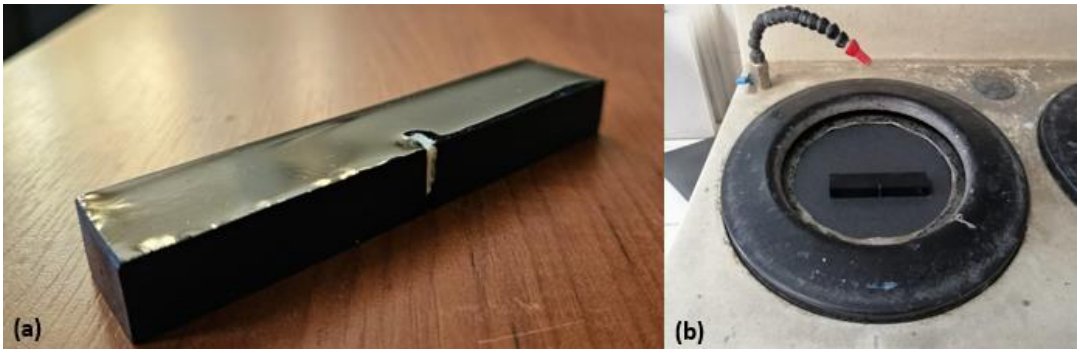

Figure 3.8. (a) Dented structure of samples, and (b) grinding of the samples using Metkon 2V Grinder-Polisher machine.

As the final composite test products, fracture toughness samples produced according to ASTM D5045-14 standard and tensile strength samples produced according to ASTM D638-14 standard have been obtained as shown in Fig. 3.9a and 3.9b, respectively.

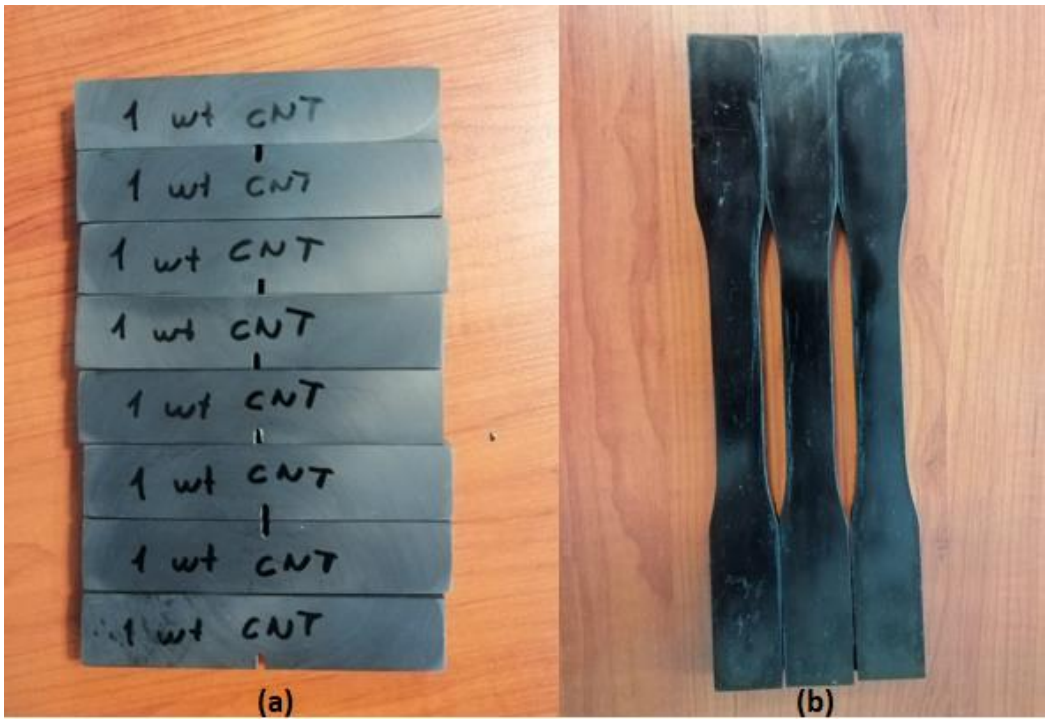

Figure 3.9. (a) Fracture toughness samples produced according to ASTM D5045-14 standard, and (b) tensile strength samples produced according to ASTM D638-14 standard.

3.3 Glass Fiber Reinforced Polymer Composite Production

Interglass 92145 unidirectional fiber glass fabrics have been impregnated with a CR80 - CH80-6 epoxy resin system during GFRP composite production. The standards used for testing composites are given in Table 3.6. Composites were produced to obtain samples complying with these standards. Identical procedures were carried out with pure resin and nanoparticle incorporated resin as the matrix of the GFRP composites to see the effect of nanoparticle addition on the mechanical properties of the composites.

Table 3.6. Composite test standards used in this study and required ply numbers.

Mechanical Property	Test Standard	Ply Number	Ply Orientation
Tensile	ASTM D3039/D3039M-14	12	0°
Fracture Toughness	DIN EN 6033 - DIN EN 6034	16	0°
Ply Drop	-	18 - 12	0°

For composite production, vacuum infusion method has been tried initially. In this method, with the help of vacuum, the resin flows through the unidirectional fabrics parallel to their surfaces stacked on top of each other. A composite sheet was produced successfully using nanoparticle-free pristine resin. However, in the production using nanoparticle incorporated resin, the nanoparticles were filtered between the fibers during the resin flow. Therefore, nanoparticles accumulated on the resin inlet side and the material could not flow uniformly to the vacuum-drawn side (Fig. 3.10). Due to this filtration effect, the vacuum infusion method could not be used in the composite production.

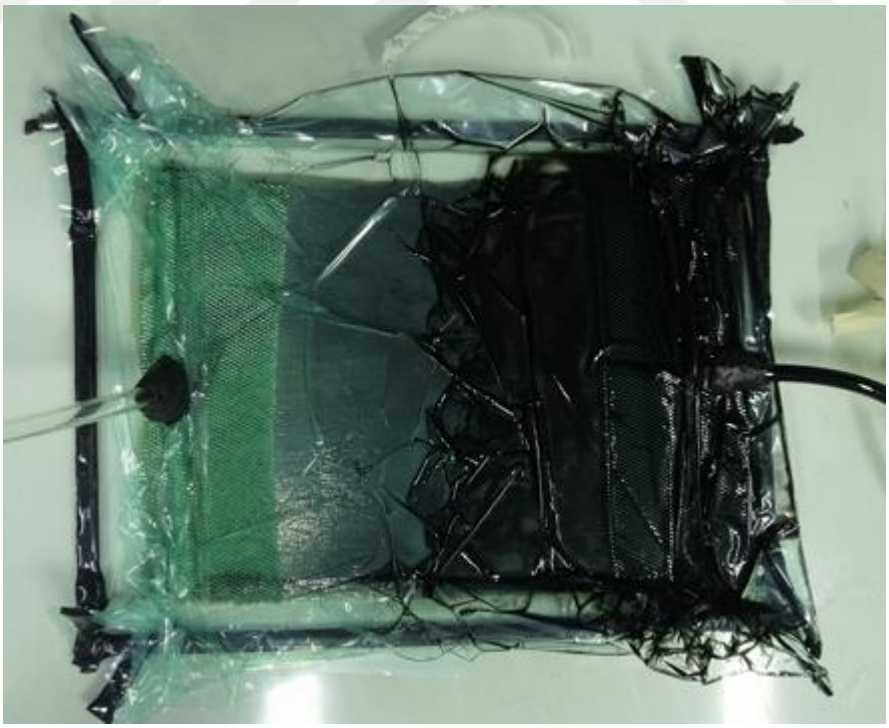

Figure 3.10. Accumulation of CNTs on the resin inlet side during vacuum infusion.

Due to the problems encountered during production with the vacuum infusion method, composite production has been carried out by hand lay-up for both pristine and nanoparticle incorporated resin matrices. First, the mold release agent was applied to the glass working bench surface in two layers to prevent it from sticking to the hand-laid composite surface and allowed to dry for 15 minutes each. Then, while the glass fiber fabric layers were stacked on top of each other, resin was applied to each layer with the help of a brush (Fig. 11a). After the required number of layers were stacked, peel ply and breather were laid on them, respectively. A vacuum bag was placed on the breather with the help of sealing tape and vacuum was applied. The material was left to cure in vacuum for one day (Fig. 11b). After one day, the composite was removed and heat-treated for 8 hours at 80 °C for post curing. Identical procedure was applied in case of composite production with nanoparticle incorporated resin matrix.

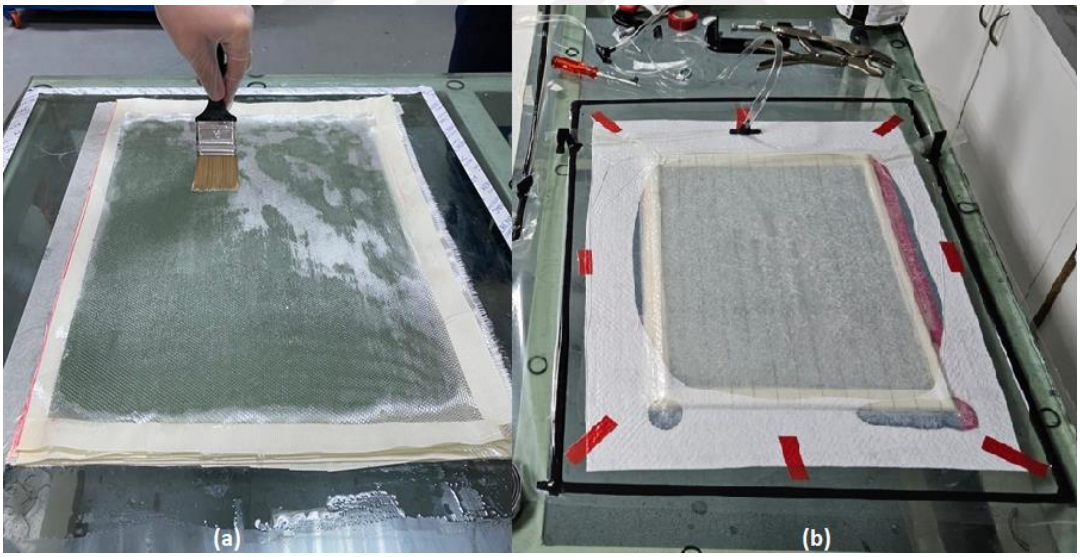

Figure 3.11. (a) Composite production using hand lay-up process and (b) vacuuming.

For tensile testing of the composites, ASTM D3039/D3039M-14 test standard was used. The standard states that the thickness of the specimens should be between 2-2.5 cm. Accordingly, a total of 12 layers of fabrics were laid in 0° orientation to obtain tensile test specimens satisfying the required thickness criterion.

DIN EN 6033 and DIN EN 6033 standards have been used for fracture toughness testing of the composites. Since the specimen thickness should be 3 cm according to the standards, 16 layers of fabrics were laid in a 0° orientation for fracture toughness test specimens called double cantilever beam (DCB). While the fabrics were being laid, after the eighth layer, separator release film was placed on one side of the composite to create the required notch in the middle of the specimen (Fig. 3.12). The remaining eight layers were stacked on top.

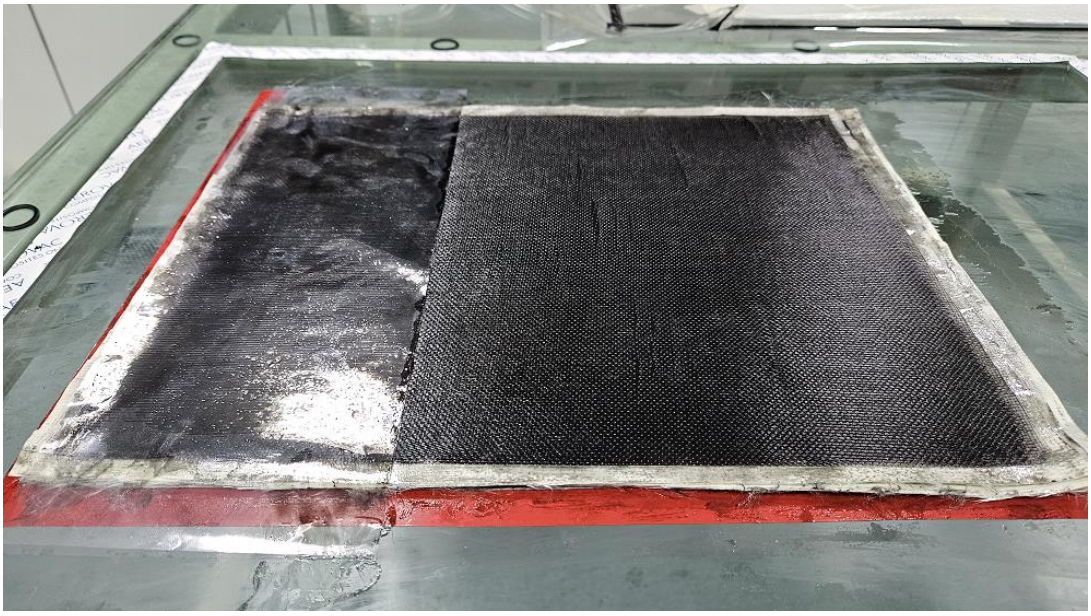

Figure 3.12. Composite production using hand lay-up process for fracture toughness tests.

For samples with ply drop-off zones, no specific test standard exists for FRP composites. Therefore, existing test methods have been adjusted according to composites with ply drop-off zones. To produce these special test samples, six layers of full-size unidirectional fiber fabrics were first laid out. Then, six of the half-sized layers were placed on these layers halfway down the sheet (Fig. 3.13). Finally, six full-sized layers were stacked on top of six half-sized layers. Consequently, in total there were 18 layers of fabrics on one side and 12 layers on the other side of the composite material. With this configuration ply drop has been created by the six half-sized layers in between. When cutting test specimens, the midpoint of the composite,

where the half-sized six layers end, was adjusted such that it was right in the middle of each specimen.

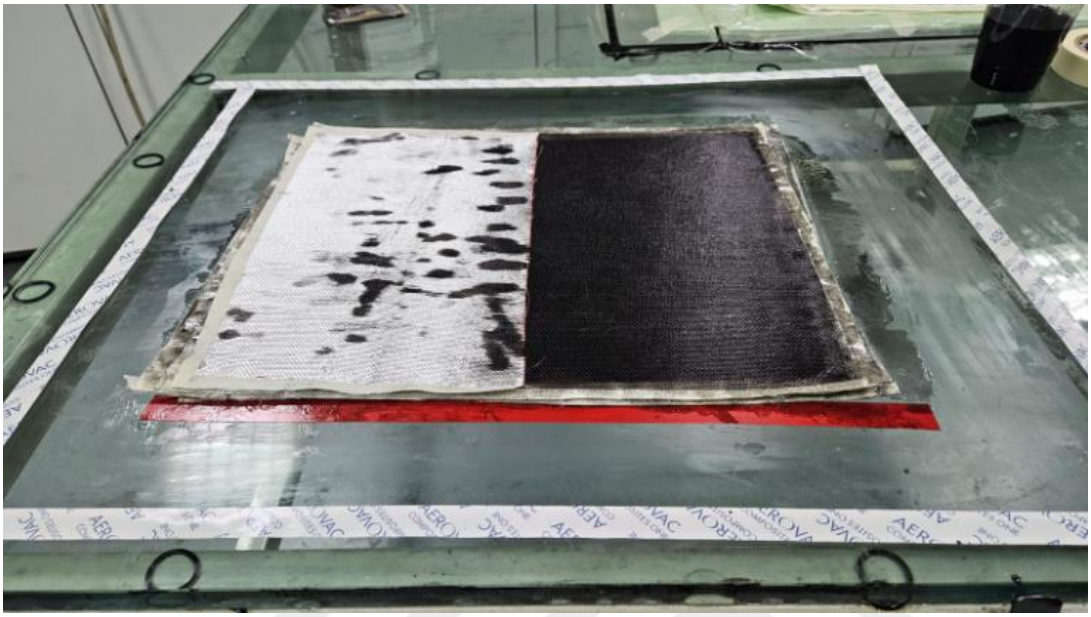

Figure 3.13. Composite production with ply drop-off using hand lay-up process.

After the composite plates were produced, they were sectioned according to the specimen dimensions in the test standards mentioned above. Support was received from Odak Kompozit for these cutting operations.

3.4 Material Characterization

In this study, various experiments have been conducted to determine the effect of nanoparticle incorporation to epoxy resin to obtain nanocomposites. The effect of nanoparticle incorporation on the viscosity of the epoxy resin has been studied. Furthermore, the effect of type and amount of the nanoparticles on the fracture toughness and tensile strength of the nanocomposites as well as those of the glass fiber reinforced composites with nanocomposite matrices has been studied. Finally, composites with ply drop-off regions were mechanically tested to determine the effect of using nanocomposites as the matrix of glass fiber reinforced composites.

Consequently, the modification and development in the mechanical behavior of the composites provided by the nanoparticle usage could be observed.

3.4.1 Viscosity Measurement

Viscosity is described as a measure of a fluid's resistance to flow. In studies where nanoparticle additives are used to improve mechanical properties, the viscosity of epoxy resin increase considerably after the addition of nanoparticles. This increase in viscosity creates significant difficulties in the production of composite materials. The resin flow through the fibers slows down, and fibers remain without being wetted by the nanoparticle-resin mixture. Therefore, the viscosity values of the nanoparticle incorporated resins should be known to avoid manufacturing problems.

In this research, viscosity has been measured using a Brookfield DV-E Viscometer (Fig. 3.14a). The shear rate dependence of fluid viscosity was measured using the viscometer. The viscometer works by rotating a spindle via a calibrated spring while the spindle is immersed in the test fluid. The spring deflection measures the viscous resistance of the fluid against the spindle. The spindle's rotating speed, size, and shape define the viscometer's measuring range. After measuring the viscosity value, the device displays it on the digital screen in the cP unit.

Figure 3.14. (a) Viscometer used in this study and (b) its spindles.

Fig. 3.14b shows the available spindles, and spindle #62 (middle in Fig. 3.14b) has been used in this study. The shapes of these spindles are determined according to the measuring ranges. The viscosity value of the epoxy is suitable for the use of spindle #62. Another variable that must be defined is the spindle's rotational speed. The manufacturer recommends selecting a rotational speed resulting in 50% torque of the maximum level. The percentage of the torque value is displayed on the viscometer's digital display. In this study, three different rotational speeds of 6, 10, and 12 rpm have been employed as spindle rotational speeds. Viscosity tests of all samples have been performed at 25.5 °C in this study to obtain comparable results.

3.4.2 Fracture Toughness Test

Main purpose of this study is to delay the failures caused by delamination in the ply-drop regions of the glass fiber reinforced polymer composites. Resistance to ply delamination is closely related to the fracture toughness value of the resin. For this reason, fracture toughness tests yielded the most important results in this study.

3.4.2.1 Nanoparticle Incorporated Polymer Nanocomposites

To increase the fracture toughness of the polymer resin by nanoparticle incorporation is one of the most important targets of this study. Therefore, the type and amount of nanoparticles to be added to the epoxy resin have been primarily determined by the increase in fracture toughness of the polymer resin.

Fracture toughness tests of the materials have been performed according to ASTM D5045-14, Standard Test Methods for Plane-Strain Fracture Toughness and Strain Energy Release Rate of Plastic Materials. This standard measures the fracture toughness of plastics by measuring the critical-stress-intensity factor, K_{Ic}, and the critical strain energy release rate, G_{Ic} (energy released per unit area of the crack surface) at crack initiation.

The test specimen geometry specified in the standard is shown in Fig. 3.15. This test method is called single-edge-notch bending (SENB). The sample has a length of 100 mm, a width of 20 mm, and a thickness of 10 mm. There is a 0.5 mm deep notch for easy crack opening in the middle of the sample. This geometry of the samples was achieved by pouring liquid resin into silicone molds as described before.

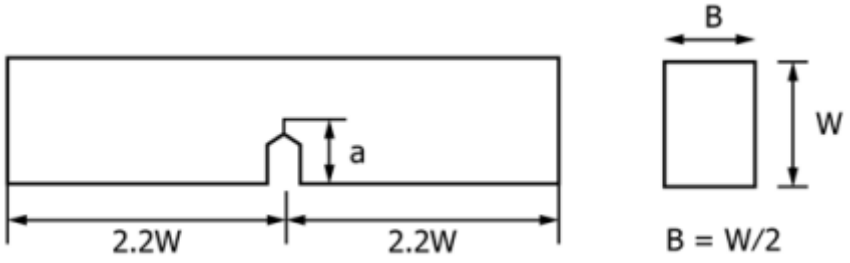

Figure 3.15. SENB test specimen geometry.

In this test, a pre-cracked specimen with a notch is tested. The crack length a must be chosen such that the ratio of a/W is in the range of 0.45 to 0.55. This means that the crack should reach almost half of the depth. The minimum fracture toughness value can only be achieved if the pre-crack is sufficiently sharp. A razor blade has been used to open the pre-crack.

Fracture toughness tests have been performed using the Shimadzu Autograph AGS-J-10 kNJ device that measures constant displacement-rate. Three-point bend test apparatus has been used for measurements (Fig. 3.16). The cross-head speed of $1.67\ x\ 10^{-4}$ m/s (10 mm/min) specified in the standard has been used for the tests. After the fracture of the specimen, the pre-crack was clearly visible and measured for subsequent calculations.

Figure 3.16. Fracture toughness specimen inside testing apparatus.

In order to obtain the fracture toughness values, following calculations were conducted. According to the test standard, the K_Q value must be calculated first to calculate the K_{Ic} value. The K_Q value is calculated with the following equations.

$$K_Q = \left(\frac{P_Q}{BW^{0.5}}\right) f(x) \quad (1)$$

$$f(x) = 6x^{0.5}\left(\frac{1.99 - x(1-x)(2.15 - 3.93x + 2.7x^2)}{(1+2x)(1-x)^{\frac{3}{2}}}\right)$$

$$x = a/W$$

where P_Q is determined from the load vs. displacement graph, B is the thickness and W is the width of the sample. a is the crack length which is measured after fracture. The load vs. displacement graph obtained during the test is drawn to find the P_Q value in the equation (schematic graph given in Fig. 3.17 representatively).

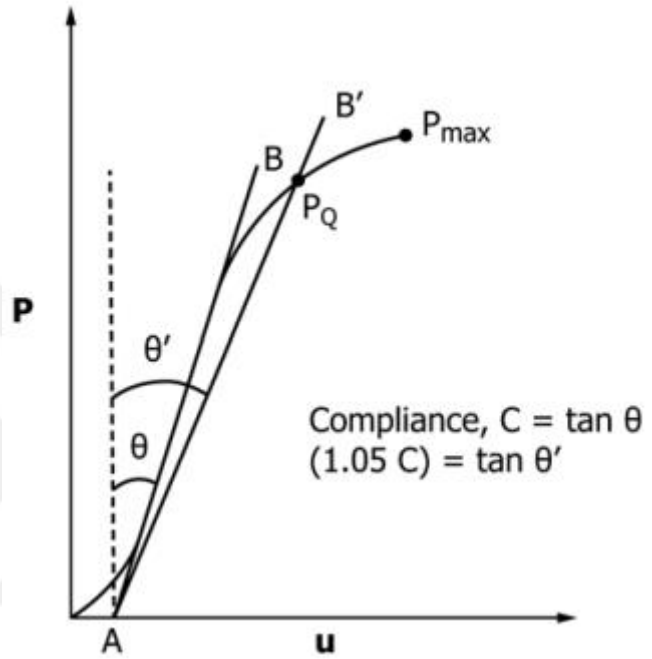

Figure 3.17. Representation of Load vs. Displacement Graph.

In determining the P_Q value from the experimental load vs. displacement graph, first the best straigth line fitting to the initial portion of the curve is drawn (line AB in Fig. 3.17). Another line is drawn by increasing the angle between the best straight line and the y-axis, θ, by 5 degrees (AB' in Fig. 3.17). If the maximum load falls between these two lines, P_Q is considered as maximum load (P_Q = P_{max}). If the maximum load falls outside these two lines, the intersection of the loading curve with the second line is considered to be P_Q (P_Q in Fig. 3.17).

Then, the validity of the K_Q value should be questioned. If the value $2.5(K_Q/\sigma_Y)^2$ (where σ_y is the yield strength of the sample obtained from tensile test) is less than

all of the following, the sample thickness, B, crack length, a, and W-a values, the K_Q is valid and equal to K_{Ic}. If not, the test is invalid.

G_{Ic} is defined as the energy per unit area of the crack surface at fracture initiation. So, the area under the load vs. displacement graph gives the G_{Ic} value. However, displacement correction is required when finding the G_{Ic}. For this, identical test sample should be produced without cracks and notches. Therefore, one notch-free sample has been produced in each batch. They have been tested the same way as in the procedures, and the following equation was used to calculate the corrected displacement.

$$U_C(P) = U_Q(P) - U_i(P) \quad (2)$$

where $U_Q(P)$ is displacement measured with cracked specimen and $U_i(P)$ is displacement measured with uncracked reference specimen. Then, load vs. displacement plot is redrawn with the corrected displacement, and the area under the plot equals the G_{Ic} value.

3.4.2.2 Glass Fiber Reinforced Composites with Nanocomposite Matrix (Mode I)

DIN EN 6033, Determination of Interlaminar Fracture Toughness Energy - Mode I - G_{Ic} [36] standard has been used to measure the mode I fracture toughness of fiber composites. The method for calculating the mode I interlaminar critical strain energy release rate, G_{Ic}, of fiber composites made of unidirectional fabrics is outlined in this standard. The mode describes the process used to apply the load and to make the crack propagate. Peel forces perpendicular to the crack plane cause a mode I crack to extend. For these tests, test specimens called DCB (Double Cantilever Beam) have been produced. The tests have been performed on the Shimadzu Autograph AGS-J-10 kNJ device.

The DCB test specimen geometry specified in the standard is shown in Fig. 3.18. The sample has a length of 250 mm, a width of 25 mm, and a thickness of 3 mm. Release film was placed 25 mm from the starting point of the sample shown as l_1.

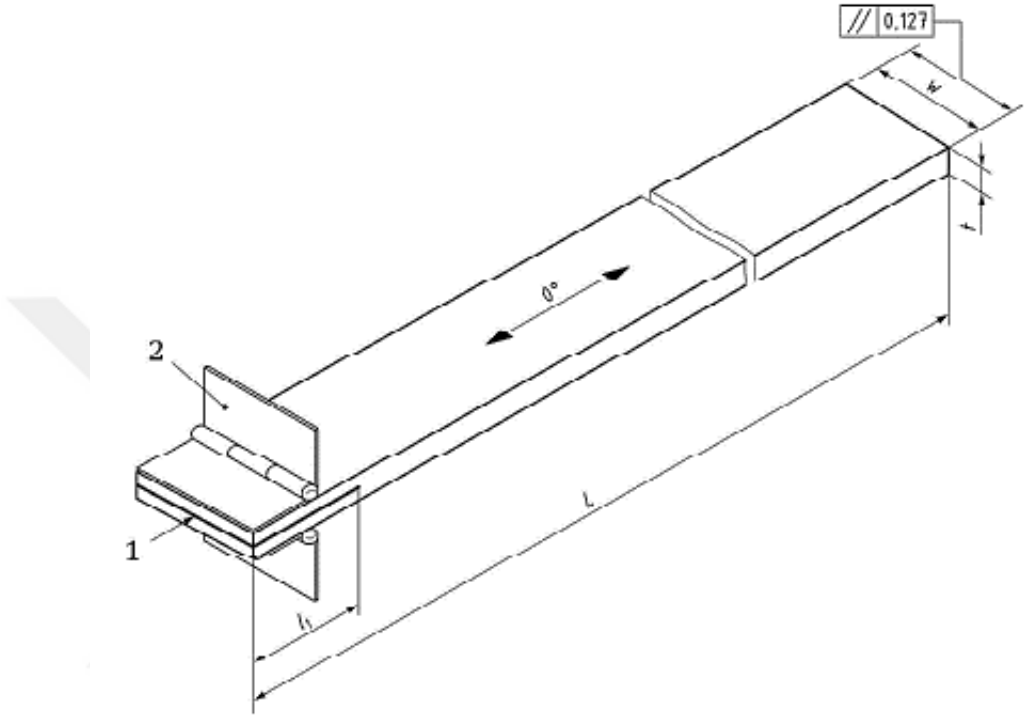

Figure 3.18. Fracture toughness test specimen geometry for fiber reinforced composites.

When performing the test, the sample must first be pre-cracked. For this purpose, mode I peel forces were applied to the sample so that the pre-crack length is 10-15 mm. During the tests the device records load-displacement information. The pre-cracked sample was exposed to mode I peel forces again until a crack of at least 100 mm was formed (Fig. 3.19). The device's cross-head speed was set to 10 mm/min.

Figure 3.19. Test fixture to measure mode I interlaminar fracture toughness energy according to DIN EN 6033.

Following the tests Load vs. Displacement graphs were drawn similar to the one shown in Fig. 3.20. In the figure, D_1 is the cross-head displacement at initial crack length, D_2 is the cross-head displacement at final crack length and A is the area underneath the graph used to find the fracture energy.

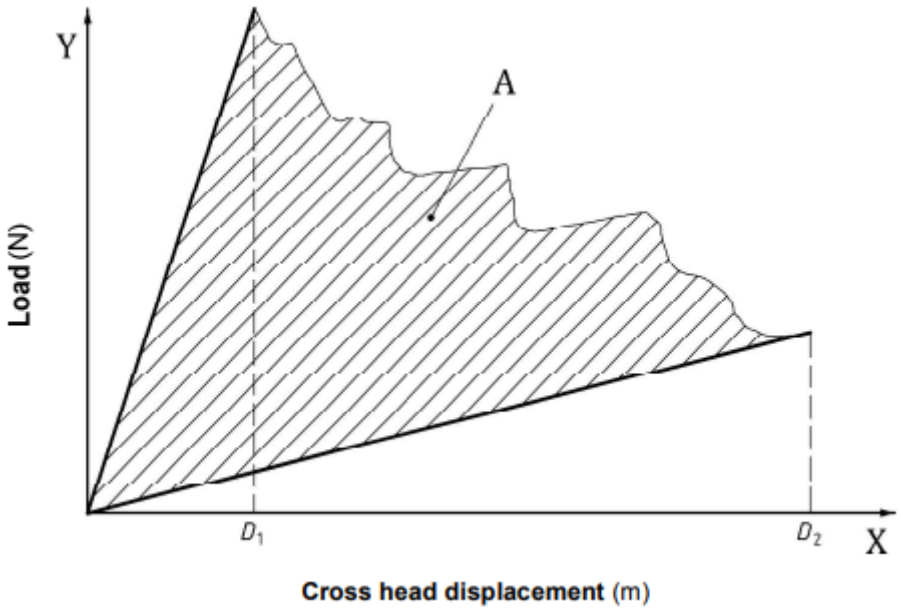

Figure 3.20. Scematic representation of Load vs. Displacement Graph for DCB test.

Critical strain energy release rate G_{Ic} is calculated according to the equation below.

$$G_{Ic} = \frac{A}{a\,w}\ 10^6 \tag{3}$$

where A is area underneath the Load vs. Displacement graph, a is the propagated crack length (difference between final and initial crack length) and w is the width of the specimen.

3.4.2.3 Glass Fiber Reinforced Composites with Nanocomposite Matrix (Mode II)

DIN EN 6034 - Determination of Interlaminar Fracture Toughness Energy - Mode II – G_{IIc} [37] standard has been used to determine the mode II fracture toughness of fiber reinforced composites. The method for calculating the mode II interlaminar fracture toughness energy G_{IIc} of fiber reinforced composites composed of unidirectional fabrics is outlined in this standard.

This test standard is linked to the DIN EN 6033 standard, which is mentioned above. According to this standard G_{IIc} test should only be conducted on specimens with the initial crack introduced through a defined mode I procedure. Therefore, these test specimens were cut from the remaining part of a previously tested G_{Ic} specimen subjected to loading and cracking as outlined in DIN EN 6033. The cut specimen must be at least 112 mm long at the crack side.

The tests have been performed on the Shimadzu Autograph AGS-J-10 kNJ device. Mode II crack propagation has occured due to shear forces at the crack tip, typically introduced during flexural testing. This test method, in which three-point bending forces are applied to the sample with a crack on one side, is also called the End Notched Flexure (ENF) test. In this testing method, a pre-cracked specimen was placed in a three-point bending fixture (Fig. 3.21), and loading (1 mm/min) was applied until the onset of crack propagation. Throughout the test, the applied load to the specimen and the cross-head displacement of the testing machine were continuously recorded. After the load drop, the test was stopped. The total fracture toughness energy was then calculated using the initial crack length and the load-displacement diagram.

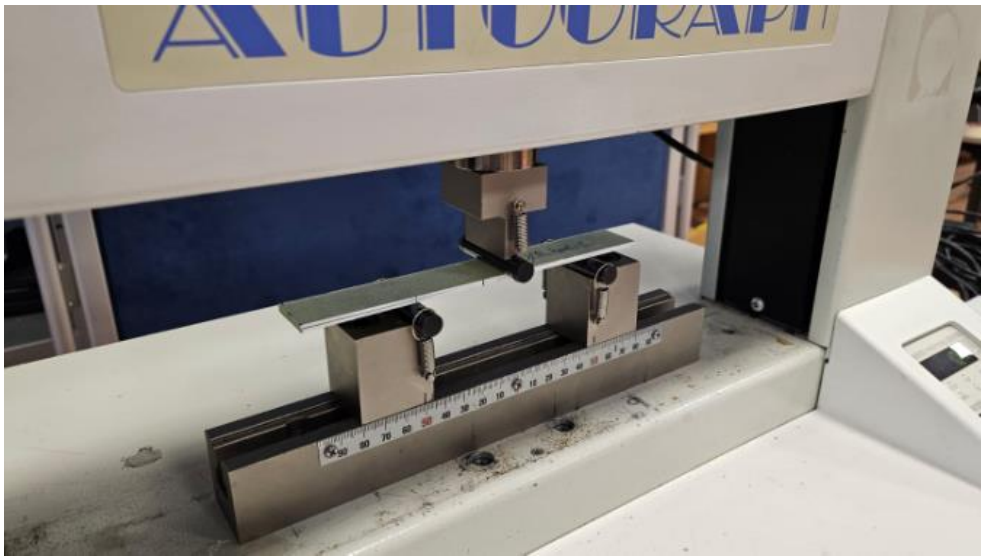

Figure 3.21. Three-point bend fixture to measure mode II interlaminar fracture toughness energy according to DIN EN 6034.

Fracture toughness energy G_{IIC} is calculated according to the equation below.

$$G_{IIC} = \frac{9\,P\,a^2\,d\,1000}{2\,w\,(\frac{1}{4}L^3 + 3\,a^3)} \quad (4)$$

where P is the critial load to start the crack (where the load drop is observed), a is the initial crack length (35 mm), d is the cross-head displacement at crack delamination, w is the width of the specimen and L is the span length (100 mm).

3.4.3 Tensile Test

The tensile test is another mechanical test used in the study. Tensile properties have been measured for both nanoparticle incorporated polymer nanocomposites and glass fiber reinforced composites with either pristine epoxy matrix or with nanoparticle incorporated polymer (nanocomposite) matrix.

3.4.3.1 Nanoparticle Incorporated Polymer Nanocomposites

Literature studies generally show that by the incorporation of nanoparticles to the epoxy resin the tensile properties either reduce or, at best, remain constant. Therefore, tensile properties should be taken into account when choosing nanoparticles to be used. In this study, ASTM D638-14, Standard Test Method for Tensile Properties of Plastics, test standard has been used to find tensile properties of nanoparticle incorporated polymer nanocomposites.

The dumbbell-shaped geometry of the test specimen is shown in Fig. 3.22. The sample has 210 mm length (L0), 23 mm width (W0), 57 mm inner length (L), 16 mm inner width (W), 7 mm thickness (T) and 76-degree radius R.

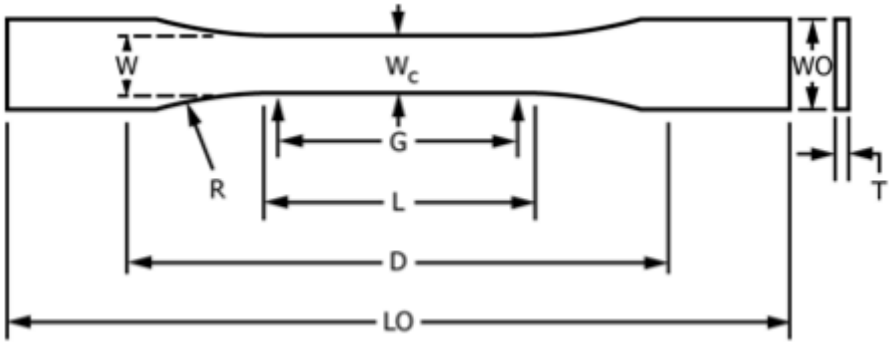

Figure 3.22. Tensile test specimen geometry according to ASTM D638-14.

Tensile tests have been performed on the MTS 809 Axial/Torsional Test device with a load cell capacity of 100 kN. The device records the load, and the displacement is recorded with the help of the camera. Tension is performed at a speed of 5 mm/min until fracture occurs, as specified in the standard (Fig. 3.23).

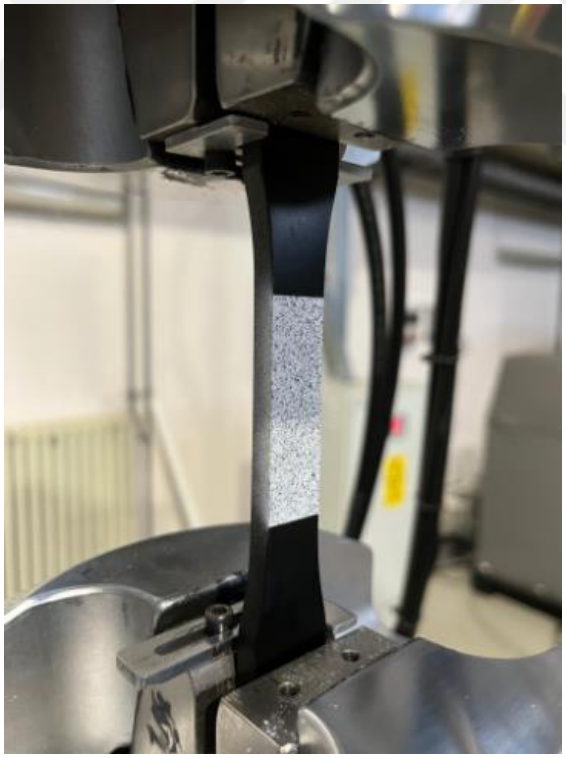

Figure 3.23. Tensile test specimen inside testing apparatus.

Tensile strength is calculated by dividing the maximum load to the cross-sectional area (Eqn. 5). The stress vs. strain graph is used to calculate the elastic modulus, which is the slope of the curve in this graph.

$$\sigma_T = P \,/\, W_C\, T \tag{5}$$

where P is the maximum load, W_c is the inner width and T is the thickness.

3.4.3.2 Glass Fiber Reinforced Composites with Nanocomposite Matrix

ASTM D3039/D3039M-4, Standard Test Method for Tensile Properties of Polymer Matrix Composite Materials [38] has been used to measure the in-plane tensile characteristics of polymer matrix composite materials reinforced with high-modulus fibers. These tests have been performed on the MTS 809 Axial/Torsional Test device with a load cell capacity of 100 kN. The device recorded the load, and the displacement was recorded with the help of the camera. Tension was performed at a speed of 2 mm/min until fracture occurs, as specified in the standard. The test specimen geometry specified in the standard is shown in Fig. 3.24. The sample has a length of 250 mm, a width of 25 mm, and a thickness of 2.5 mm.

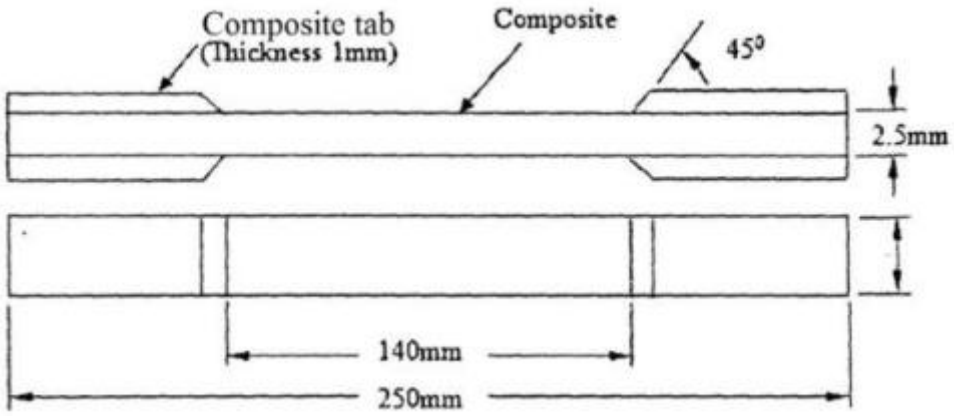

Figure 3.24. Tensile test specimen geometry according to ASTM D3039/D3039M-14.

Tensile strength is calculated by dividing the maximum load to the cross-sectional area (Eqn. 6). The stress vs. strain graph is drawn to calculate elastic modulus, which is the slope of the curve in this graph.

$$\sigma_T = P \,/\, A \tag{6}$$

where P is the maximum load and A is the cross-sectional area.

3.4.4 Ply Drop-off Test

The final point this thesis aims to reach is to observe the effect of nanoparticle incorporation on the matrix of GFRP composites with ply drop-off zone. However, no specific test standard exists for FRP composites with ply drop-off zone. Therefore, existing test methods have been adjusted according to the presence of ply drop-off in fiber reinforced composites. This modified test method constitutes an application of a typical tensile test on the ply drop-off sample similar to ASTM D3039/D3039M-14. In the ply drop-off sample, which resembles the geometry defined in this test standard, a drop-off was created by placing six extra half layers of fabrics sandwiched between two groups of six full-sized layers (Fig. 3.25). The tensile tests were performed with a 0.5 mm/min displacement rate.

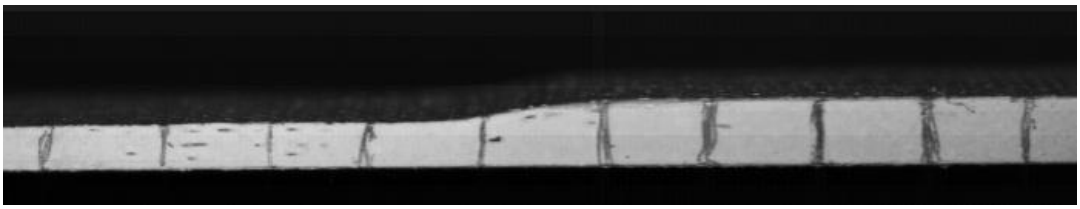

Figure 3.25. Side view of the specimen with ply drop-off region.

While the modified ply drop-off test has been conducted, a ticking sound was heard from the specimens when the applied load reached to a specific value. When the specimen was observed after the sound was heard, in GFRP specimens without nanoparticle additives, delamination initiation was visible with color change (Fig. 3.26). Therefore, a connection between ticking sound and delamination initiation

was observed. Accordingly, audio recording was started with the start of the modified ply drop-off test. The time at which the ticking sound was heard was noted, and the onset of delamination was determined accordingly. Also, when the stress vs. strain graph was drawn, a load drop was observed as soon as delamination started. With this two-way verification, the moment of delamination could heve been detected.

Figure 3.26. Delamination identification during the test.

After the test, stress vs strain graphs were drawn for GFRP and GFRP with nanocomposite matrix having ply drop-off region samples. The tensile strength (σ_U), delamination strength (σ_{Del}), and failure strain values were obtained from this graph. Moreover, the work of fracture (W_f) values were calculated as the area under the graphs. The results were discussed according to the moment of delamination initiation, post-delamination load-bearing capacity and work of fracture.

3.5 Summary of the Methodology

The composite materials to be produced and the characterization methods to be applied within the scope of the study are summarized in the flowchart given in Fig. 3.27. The road map of this study can be followed from this diagram.

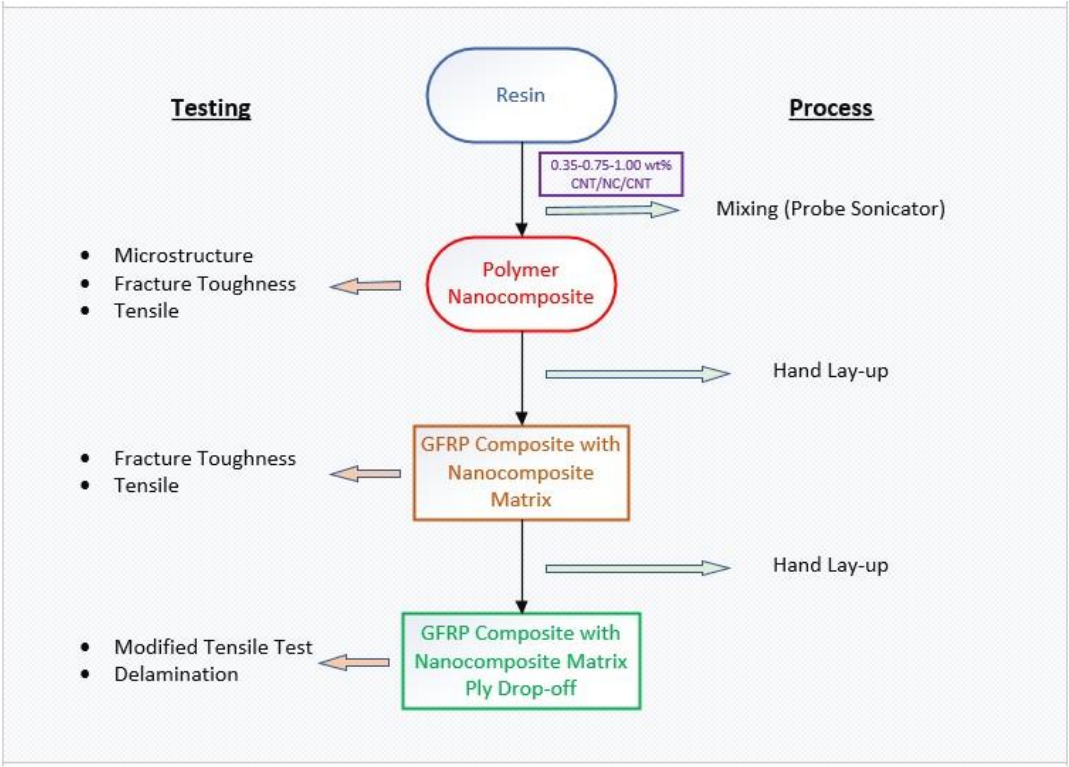

Figure 3.27. Flowchart showing the production and characterization methods used within the scope of this study.

CHAPTER 4

RESULTS AND DISCUSSIONS

4.1 Properties of Pristine Polymer

In this study, Biresin CR80-CH80-6 epoxy resin system has been used to increase its mechanical properties. First, the mechanical properties of the pristine epoxy resin were measured as the initial level to see the effect of nanoparticle additives.

The mechanical properties of pristine resin were measured according to the test standards given in Chapter 3. The energy required for fracture, G, the resistance of the material to fracture, K, tensile strength, σ_U, elastic modulus, E, and viscosity, η, values of the pristine resin all measured in this study are tabulated in Table 4.1. In the table, CV% represents the coefficient of variation. The coefficient of variation is defined as the ratio of the standard deviation to the mean and is often expressed as a percentage. Since standard deviation values are meaningful when compared to the average value, they are given as CV% in this thesis.

Table 4.1. Mechanical properties of the pristine epoxy resin used in this study.

Pristine	K_{Ic} (MPam$^{1/2}$)	G_{Ic} (J/m^2)	σ_u (MPa)	E (GPa)	η (cp)
Avg	0.716	128.60	77.77	3.04	1149
CV%	8	21	2	2	0

The measured tensile strength and elastic modulus values are close to those provided in the product catalog (Table 3.1). Tensile strength was measured as 77.77 MPa, which is given as 83 MPa in the catalog. In comparison, the elastic modulus is given as 3 GPa in the catalog and was measured as 3.04 GPa. Since product catalogs generally provide the best possible values, slightly deviating values are expected.

4.2 Determination of Ultrasonicator Operating Parameters for Mixing

In this work, an ultrasonic homogenizer has been used to disperse the nanoparticles in the epoxy resin. As the homogenizer operating parameters, power and time used for mixing should be determined. The aim is to find the most appropriate operating parameter to ensure the most effective dispersion and improvement in the mechanical properties of the resulting nanocomposites. Literature research showed that the device is usually operated with a power between 50 and 250 W. Run time ranges from 45 minutes to 2 hours [39]. Therefore, tests were carried out at 100, 150, and 200 W for 30, 60, 90, and 120 minutes to find the optimal operating parameter. 0.35 wt% fCNT added epoxy was used in these prelimary tests. The reason for choosing this amount was that 0.3-0.5 wt% fCNT incorporation results in the most effective values in the related literature [30].

First, viscosity tests were performed to determine the optimal operating parameters leading to the best dispersion of nanoparticles. Viscosity values of pristine resin and 0.35 wt% fCNTadded and only hand-mixed resin were measured. These values are given in Table 4.2. In viscosity measurements, tests were performed with 3 different spindle speeds and the coefficient of variation (%CV) was as low as ~3-5‰. For this reason, %CV values were not provided in the tables where viscosity measurement results are given.

Table 4.2. Viscosity values of pristine and 0.35 wt% fCNT containing only hand-mixed resin.

	Pristine	Hand-mixed
η (cp)	1149	1163

Then, 0.35 wt% fCNTadded resins were mixed using the ultrasonicator at 100, 150, and 200 W power for 30, 60, 90 and 120 minutes. The viscosity values obtained as a result of mixing are given in Table 4.3 and plotted in Fig. 4.1.

Table 4.3. Viscosity values of 0.35 wt% fCNTadded resins mixed with different parameters.

Power (Watt)	100 W				150 W				200 W			
Time (min)	30	60	90	120	30	60	90	120	30	60	90	120
η (cp)	1227	1295	1313	1448	1297	1290	1332	1493	1218	1358	1350	2054

According to the test results, viscosity significantly increased when the 0.35 wt% fCNT incorporated samples were mixed at 200 W for 120 minutes (Fig. 4.1). Normally, higher viscosity values can be interpreted as a better mixture. It is known that nanoparticle addition increases the viscosity of the resins. With better mixing, regions of pristine resin, i.e., sites of lower viscosity, will be reduced. Therefore, the viscometer takes measurements from high-viscosity regions with nanoparticles. Accordingly, it can be said that the best mixing takes place at 200 W for 120 minutes, as viscosity is the highest. However, it should be considered that dispersion methods that involve high-energy input can lead to the fracture of CNTs.

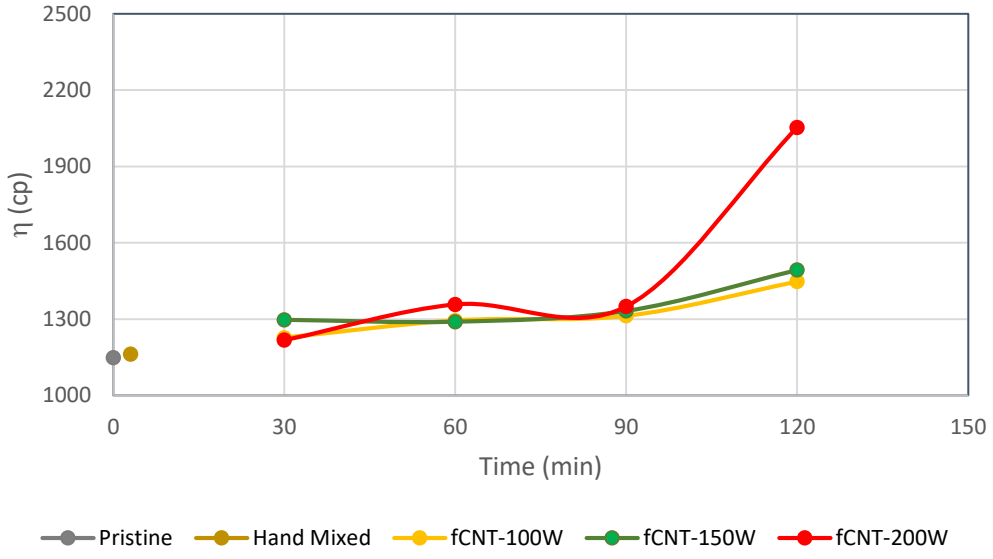

Figure 4.1. Viscosity vs. time graph of 0.35 wt% fCNT incorporated resins which were mixed with different powers.

The fracture of CNTs is a relevant phenomenon especially in ultrasonication, where literature studies have validated the occurrence of fCNT fracture during the sonication process. Montazeri et al. found that in the Gaussian distribution of CNTs (Fig. 4.2), the ratio of tube length over 0.8 μm was high when exposed to ultrasonic treatment for 1 hour. In comparison, tube length over 0.8 μm was not observed much when exposed to ultrasonic treatment for 10 hours, and tube length generally decreased to 0.4 [40].

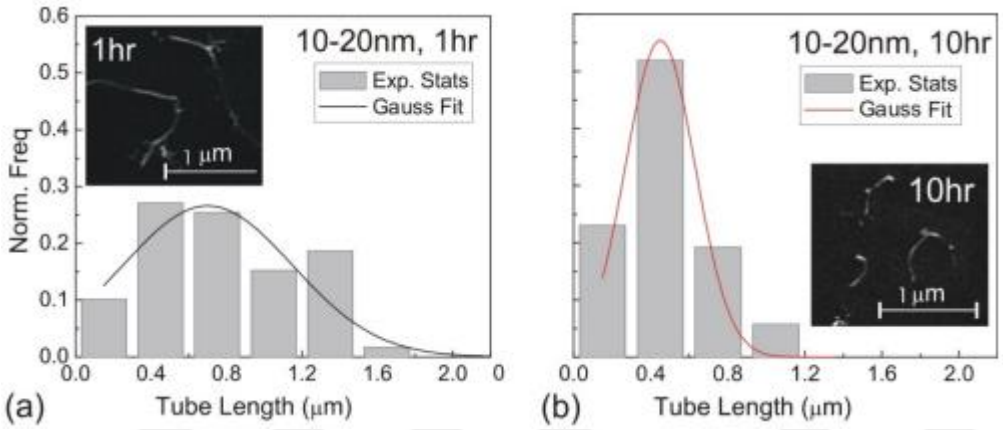

Figure 4.2. Histogram of length distribution of CNTs after the (a) 1 h, and (b) 10 h horn sonication treatment [39].

For the reasons mentioned above, the microstructure of the samples should be examined before selecting the operating parameter of the ultrasonicator as 200W-120min solely according to the maximum viscosity achieved. A different nanoparticle has also been tested to see if the observed viscosity increase was due to the fracture of fCNTs. This time, 0.35 wt% CNF (cellulose nanofibrils) incorporated epoxy resin was mixed at 200W for 30, 60, 90, and 120 minutes, and the viscosity values were measured. The results are given in Table 4.4.

As seen in Table 4.4, no significant increase was observed for the CNF incorporated resin in the mixing parameter of 200W-120min. These results confirm the fracture of CNTs with ultrasonic mixing at 200 W for 120 minutes.

Table 4.4. Viscosity values of 0.35 wt% CNF added resins dispersed at 200W.

Power (Watt)	200 W			
Time (min)	30	60	90	120
η (cp)	1174	1199	1267	1268

In Fig. 4.3, SEM images of 0.35 wt% fCNT-epoxy nanocomposites ultrasonicated at 150W-60min and 200W-120min are given at the same magnification side by side for comparison. The lengths of the fCNTs mixed at 150W-60min are clearly longer than those mixed at 200W-120min.

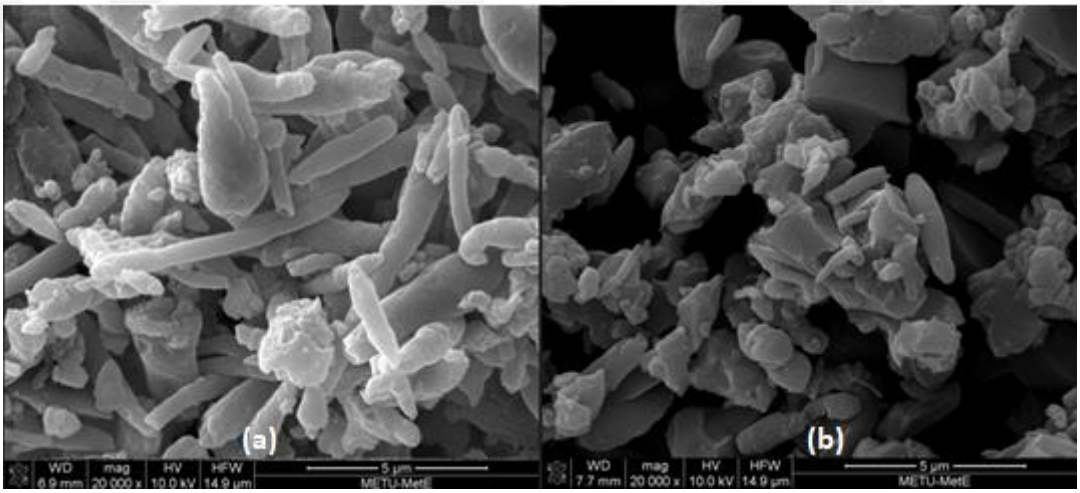

Figure 4.3. SEM images of 0.35wt% CNT-epoxy nanocomposites ultrasonicated at (a) 150W-60min and (b) 200W-120min at 20000x magnification.

The lengths of these fCNTs were measured with the help of the software included in the SEM system as shown in Fig. 4.4 and Fig. 4.5. The lengths of fCNTs were, on average, 4-6 μm for 150W-60min mixed, and 1-2 μm for 200W-120min mixed nanocomposites. According to these values, the fracture of fCNTs upon prolonged ultrasonication at high power has been clearly evidenced. However, mechanical tests must be performed to determine whether decrease in the length of the fCNTs due to fracture negatively affects the mechanical properties.

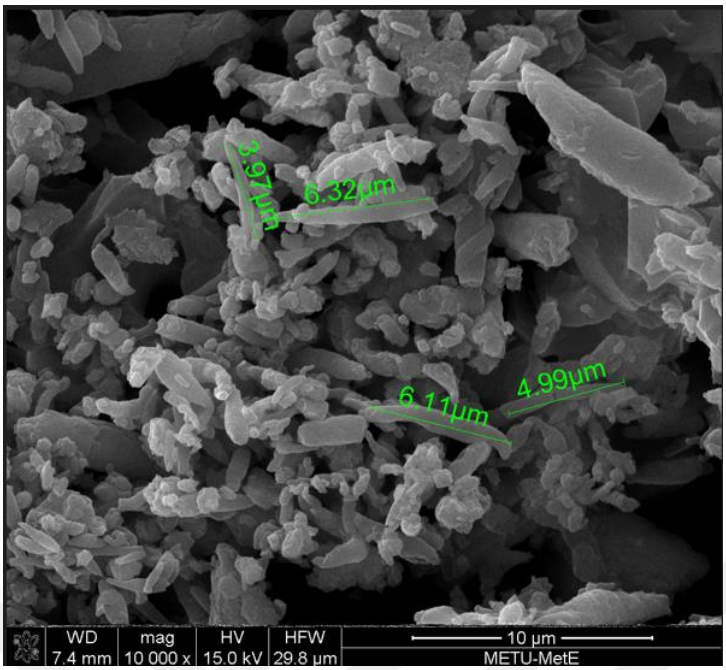

Figure 4.4. SEM image of 0.35wt% fCNT-epoxy nanocomposites ultrasonicated at 150W-60min at 10000x magnification.

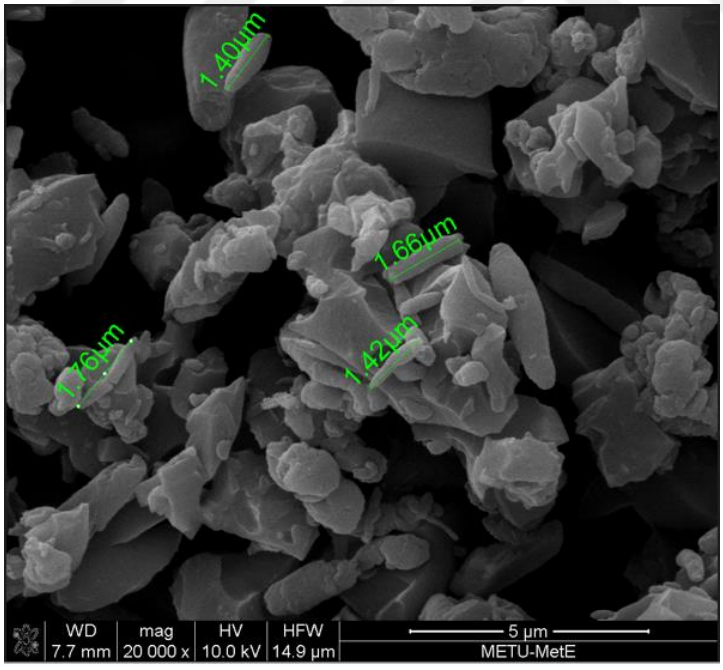

Figure 4.5. SEM image of 0.35wt% fCNT-epoxy nanocomposites ultrasonicated at 200W-120min at 20000x magnification.

As a result, viscosity tests did not provide sufficient data to select the operating parameters of the ultrasonicator. In order to make this choice, fracture toughness and tensile tests should be performed. However, the viscosity test results were used to eliminate some of the mixing parameter combinations to reduce extra workload before conducting mechanical tests. For instance, 30 minutes of mixing always resulted in the lowest viscosity values. Therefore, it can be said that the nanoparticles could not mix sufficiently in 30 minutes, so samples prepared with 30 minutes mixing were omitted for mechanical testing. On the other hand, the viscosity values generally increased in samples mixed for 120 minutes, so samples should be produced with 120 minutes mixing. As there was no remarkable difference in the viscosity values of the mixtures when mixed for 60 minutes and 90 minutes at all powers, samples prepared with the intermediate mixing time of 90 minutes were also omitted for further mechanical testing.

For the reasons stated, fracture toughness and tensile tests have been performed on nanocomposite samples prepared by mixing 0.35 wt% fCNT and epoxy resin at 100, 150, and 200 W for 60 and 120 minutes. Since the delamination resistance of a fiber reinforced composites is related to the resin's fracture toughness [7], the fracture toughness results are of high priority in selecting nanocomposites to be the matrix material of the intended glass fiber reinforced composites and especially with ply drop-off regions. However, it is also critical that the tensile properties of the nanocomposites do not downgrade remarkably, while increasing their fracture toughness.

Fracture toughness test results, performed according to ASTM D5045 – 14, are shown in Table 4.5 and in Fig. 4.6. Properties of pristine resin given in Table 4.1 can be considered for comparison. The critical strain energy release rate, G_{Ic} (energy released per unit area of the crack surface) and the critical-stress-intensity factor at crack initiation, K_{Ic}, values obtained from the tests are presented in Fig. 4.6 in bar chart form for better comparison. Typically, in fracture toughness calculations the K_{Ic} value can be correlated with the G_{Ic} value using the following relationship: $G_{Ic} = K_{Ic}^2 / E$, where E is the Young's Modulus of the material. However, in the test

standard used in this study, K_{Ic} and G_{Ic} calculation methods are specified. For this reason, the calculation method explained in Chapter 3 has been used to calculate the K_{Ic} and G_{Ic} values instead of the above-mentioned relationship.

Table 4.5. Fracture toughness test results of 0.35 wt% fCNTadded resin mixed with different parameter.

0.35 wt% CNT		100W		150W		200W	
		G_{Ic} (J/m^2)	K_{Ic} (MPam$^{1/2}$)	G_{Ic} (J/m^2)	K_{Ic} (MPam$^{1/2}$)	G_{Ic} (J/m^2)	K_{Ic} (MPam$^{1/2}$)
60 min	**Avg**	143.16	0.832	181.12	0.911	143.53	0.774
	CV%	26	12	19	9	5	6
120 min	**Avg**	199.93	0.909	233.94	1.000	198.04	0.838
	CV%	34	23	33	24	9	3

K_{Ic} represents the resistance of the material to fracture. According to the results of this parameter, the highest increase in fracture toughness value compared to that of the pristine resin was ~40% at 150W-120min mixing. Similarly, the increase was ~28% for parameters 100W-120min and 150W-60min. According to these test results, the standard deviations for 120 minutes of mixing at 100 and 150 W are considerably high to be trusted when making selection.

G_{Ic} represents the energy required for fracture. Considering obtained results in terms of G_{Ic} values, with 120 minutes of mixing at 150 W power, fracture energy showed the highest increasen by ~82% compared to pristine resin. In the fracture energy values, there was a ~55% increase for the 100W-120min parameter, while there was a ~53% increase in the 200W-120min mixing. However, according to Table 4.5, it should be considered that the standard deviation in the G_{Ic} is relatively high for 120 minutes of mixing at 100 and 150 W, as in the case of K_{Ic} results. It would be unreliable to select these parameters with such high standard deviations.

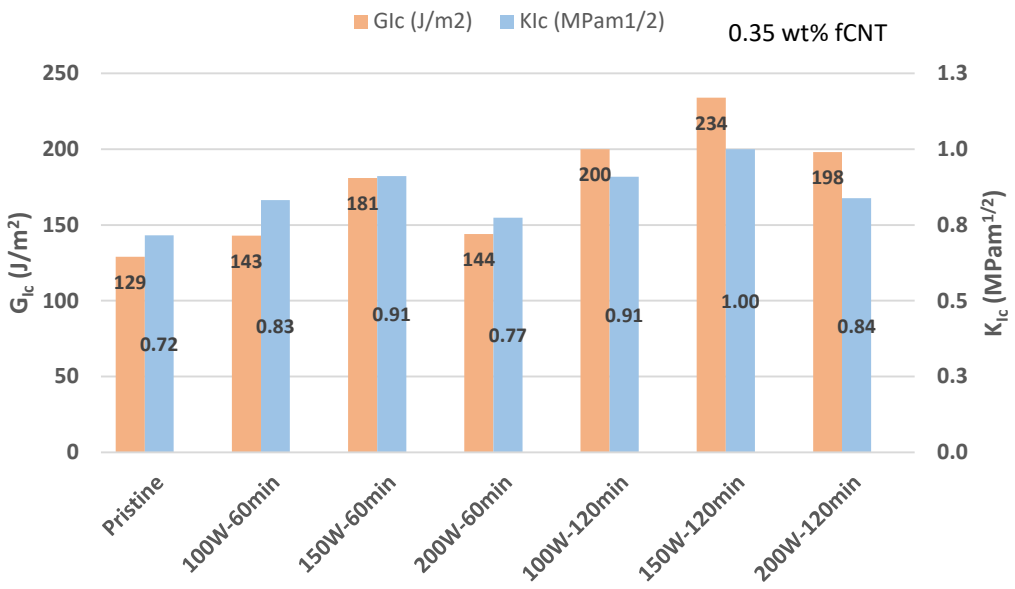

Figure 4.6. Fracture energy G_{Ic} and fracture toughness K_{Ic} values of pristine and nanoparticle incorporated epoxy resins mixed with different parameters.

Even though all of the fCNT containing nanocomposites have been produced with different parameters, increase in the fracture energy and toughness of the pristine resin was observed after nanoparticle addition for all mixing conditions. SEM images were taken to understand the reasons of this increase in fracture energy and toughness values with nanoparticle addition. Fig. 4.7a and Fig. 4.7b show the fracture surfaces of pristine and 0.35 wt% fCNT incorporated samples at 250x magnification after the fracture toughness test, respectively. Pristine epoxy showed typical brittle fracture behavior with smooth fracture surface resulting in lower fracture toughness values due to weak crack initiation and propagation resistance. In Fig. 4.7c and Fig. 4.7d, fCNT agglomerates are visible at higher magnification protruding out of the surface. Even though fCNTs are in agglomerated form, they have a retarding effect on crack propagation. Zhou et al. indicated that crack propagation changes direction during the failure process as it crosses CNTs. The bridging effect, which prevents crack opening, was shown to enhance the strength of the CNT/epoxy matrix [30]. fCNTs, seen in SEM images, increase fracture energy and toughness values with their impact on slowing down the crack propagation.

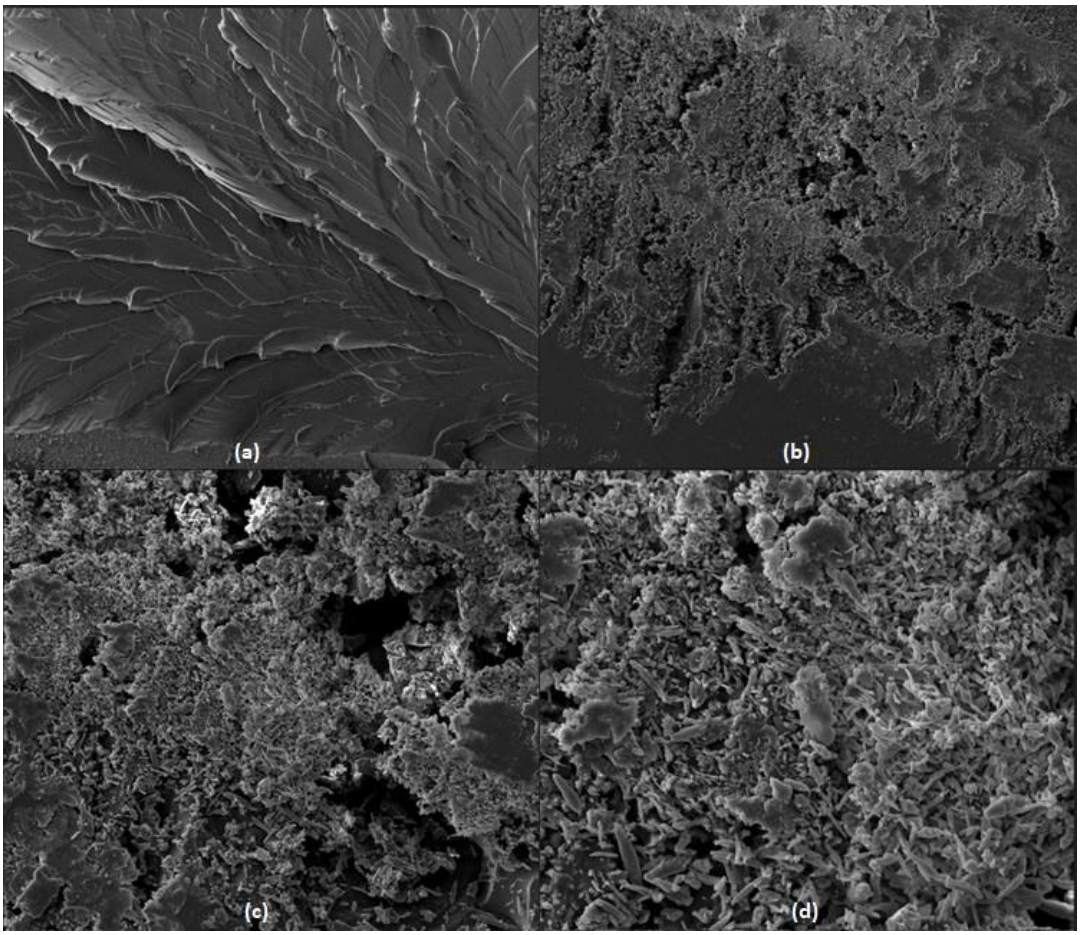

Figure 4.7. SEM images of fracture surfaces of (a) pristine epoxy, and 0.35 wt% fCNT-epoxy nanocomposite ultrasonicated at 150W-60min (b) at 250x, (c) 1000x and (d) 2500x magnification after fracture toughness tests.

If the ultrasonicator working parameters were to be selected only according to the fracture toughness test results, there would be three important candidates in terms of the G_{Ic} and K_{Ic} values of the nanocomposites; 150W-60min, 100W-120min and 150W-120min. Among these, 100W-120min and 150W-120min are unreliable as they provide values with high standard deviations. Therefore, although 150W-60min is considered as the most reliable parameter set, tensile tests have also been performed on all samples produced with all of the considered parameter sets.

Ultimate tensile strength, σ_u, and elastic modulus, E, values obtained in tensile tests, performed according to ASTM D638-14, are given in Table 4.6. Pristine resin results

given in Table 4.1 can be considered for comparison. The results of Table 4.6. are also plotted in bar chart form in Fig. 4.8for better comparison.

Table 4.6. Tensile test results of 0.35 wt% fCNTadded resin mixed with different parameter sets.

0.35 wt% fCNT		100W		150W		200W	
		σ_u (MPa)	E (GPa)	σ_u (MPa)	E (GPa)	σ_u (MPa)	E (GPa)
60 min	**Avg**	64.85	3.19	78.06	3.08	67.40	3.07
	CV%	7	2	1	2	10	3
120 min	**Avg**	72.71	3.07	74.92	3.01	64.00	3.09
	CV%	11	2	2	1	9	1

According to the tensile strength values of the nanocomposites, the only increase with respect to pristine epoxy was obtained from the sample mixed at 150W-60min; while decrease in tensile strength was observed for the remaining parameters. The decrease was ~7% for 100W-120min and ~4% for 150W-120min conditions.

Elastic modulus values of the nanocomposites were very close for each parameter, and the variation was within ~5%. Therefore, the elastic modulus results could not be used to select the operating parameter of the ultrasonicator as a decisive mechanical property.

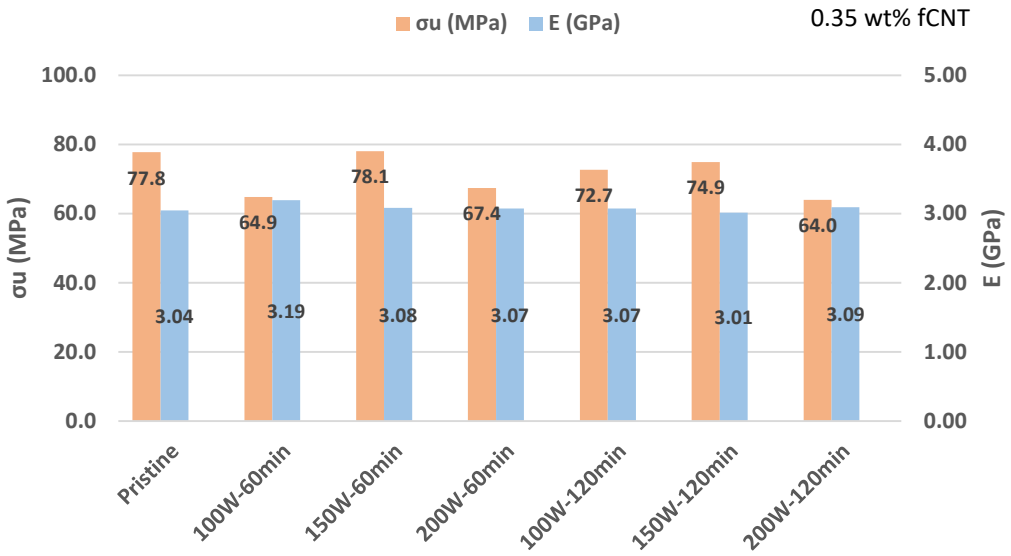

Figure 4.8. Ultimate tensile strength and elastic modulus values of pristine and nanoparticle incorporated epoxy nanocomposites mixed with different parameters.

Despite the studies showing increase in tensile strength with the addition of CNTs to epoxy, there are also many studies in which nanoparticle incorporation decreased tensile strength or did not affect it considerably. For instance, Gojny et al. showed that the tensile strength of samples containing CNTs remained on the same level as the pristine epoxy at 0.1 wt% and slightly increased with 1 wt% nanotube content [19]. In addition, Tang et al. found out that with the addition of MWCNT to epoxy resin, the tensile strength decreased slightly, by ~4% [41]. In these studies, it was determined that especially agglomeration of the CNTs reduced the tensile strength. Based on this, the formation of agglomerates, as evidenced in Fig. 4.7.b-d, seems to have prevented the increase of tensile strength in this study.

In the light of these results, it was seen that after nanoparticle incorporation, fracture toughness of the fCNT incorporated epoxy nanocomposites tended to increase as opposed to tensile strength. Similar results have been described in the literature. This behavior was observed because nanoparticles change the crack direction by acting as an obstacle during crack propagation, which increases fracture energy and toughness. However, since nanoparticles formed agglomerates, they baheved as

stress concentration sites against tensile force, and hence tended to reduce tensile strength.

Consequently, in terms of mixing parameter selection based on the examinations on the mechanical behavior of fCNT incorporated epoxy nanocomposites, 100W-120min and 150W-120min could not be selected, as they did not provide reliable data due to the high standard deviations while also leading to significantly reduced tensile strength. Therefore, 150W-60min parameter set was chosen as the operating parameter of the ultrasonicator, since it did not cause a remarkable decrease in tensile strength while increasing the fracture toughness significantly. The 150W-60min parameter set was optimal where a sufficiently effective mixture could have been obtained and fCNT fracture did not deteriorate the mechanical properties.

4.3 Properties of Nanoparticle Incorporated Polymer Nanocomposites

In the previous section it was shown that the optimum ultrasonicator parameter set in mixing fCNTs with epoxy resin is 150 W and 60 minutes in terms of mixing power and time, respectively. This section discusses the effect of type and amount of nanoparticles incorporated in epoxy resin on the mechanical properties of the resulting nanocomposites produced with the predetermined mixing parameter set. For this purpose, fCNT, nanoclay, and CNF (cellulose nanofibrils) type of nanoparticles in varying amounts of 0.35, 0.75 and 1.00 wt% have been mixed with epoxy resin, and their mechanical properties were examined. By using nanoparticle amounts from 0.35 to 1.00 wt%, a relatively wide nanoparticle amount range was studied.

To find the combination of 150W-60min, which was determined as the mixing parameter of the ultrasonicator, 0.35 wt% fCNT added resin was used. In addition to this amount, 0.75 and 1.00 wt% incorporations were tried to select the most effective nanocomposite composition. Despite this amount increase in nanoparticle content, the mixing parameter could not be used at a higher intensity value, because CNT

breakage was observed in the scenario where the power was 200W and the time was 120 min. Therefore, the 150W-60min parameter set was continued to be used for different nanoparticle compositions.

Fracture toughness and tensile tests have been performed to examine the mechanical properties of the nanoparticle incorporated polymer nanocomposites. As described previously, the priority was to increase fracture toughness, as these nanocomposites were intended to be used as matrix material in fiber reinforced composites, where delamination resistance is mainly dependent on the fracture toughness of the matrix [7]. However, it was also essential that the tensile properties do not deteriorate remarkably by the formation of these nanocomposites.

4.3.1 Fracture Toughness

Fracture toughness tests have been performed, according to ASTM D5045 – 14, for 0.35, 0.75, and 1.00 wt% fCNT, nanoclay, and CNF incorporated epoxy resin. The nanoparticles have been mixed with the epoxy using an ultrasonicator at 150 W for 60 minutes. The results are given in Table 4.7. The values in Table 4.1 can be viewed for comparison with pristine resin.

Table 4.7. Fracture energy and toughness results of 0.35, 0.75, and 1.00 wt% fCNT, nanoclay, and CNF incorporated epoxy nanocomposites.

		0.35 wt%		0.75 wt%		1.0 wt%	
		G_{Ic} (J/m^2)	K_{Ic} ($MPam^{1/2}$)	G_{Ic} (J/m^2)	K_{Ic} ($MPam^{1/2}$)	G_{Ic} (J/m^2)	K_{Ic} ($MPam^{1/2}$)
fCNT	**Avg**	181.12	0.911	158.40	0.733	111.03	0.764
	CV%	21	11	13	14	22	8
Nanoclay	**Avg**	156.19	0.870	193.55	0.879	183.40	0.960
	CV%	18	9	12	7	19	6
CNF	**Avg**	120.41	0.726	130.04	0.699	86.93	0.726
	CV%	18	19	12	15	13	6

Fig. 4.9 has been plotted to compare the fracture toughness, K_{Ic}, and the fracture energy, G_{Ic}, values of the produced nanocomposites. According to the nanocomposites' resistance to fracture, K_{Ic}, results, the most significant increase was obtained in all nanoclay compositions along with 0.35 wt% fCNT incorporation. The highest increase in fracture toughness with respect to pristine epoxy was observed in 1.00 wt% nanoclay incorporation reaching to ~34%. In case of 0.35 wt% fCNT incorporation the increase in fracture toughness was also significant (~28%).

According to the G_{Ic} results, nanoclay significantly increased fracture energy. The highest increase in G_{Ic} at a value of ~50% was obtained with 0.75 wt% nanoclay incorporated expoxy nanocomposite. 0.35 wt% and 1.00 wt% nanoclay incorporation increased fracture energy by ~21% and ~42% compared to that of the pristine epxoy, respectively. fCNT incorporation also resulted in a significant increase in fracture energy, which is ~40% with 0.35 wt% fCNT incorporation. CNF incorporation did not have a positive effect on fracture toughness and energy. In fact, 1.00 wt% CNF contribution reduced fracture toughness by ~33%.

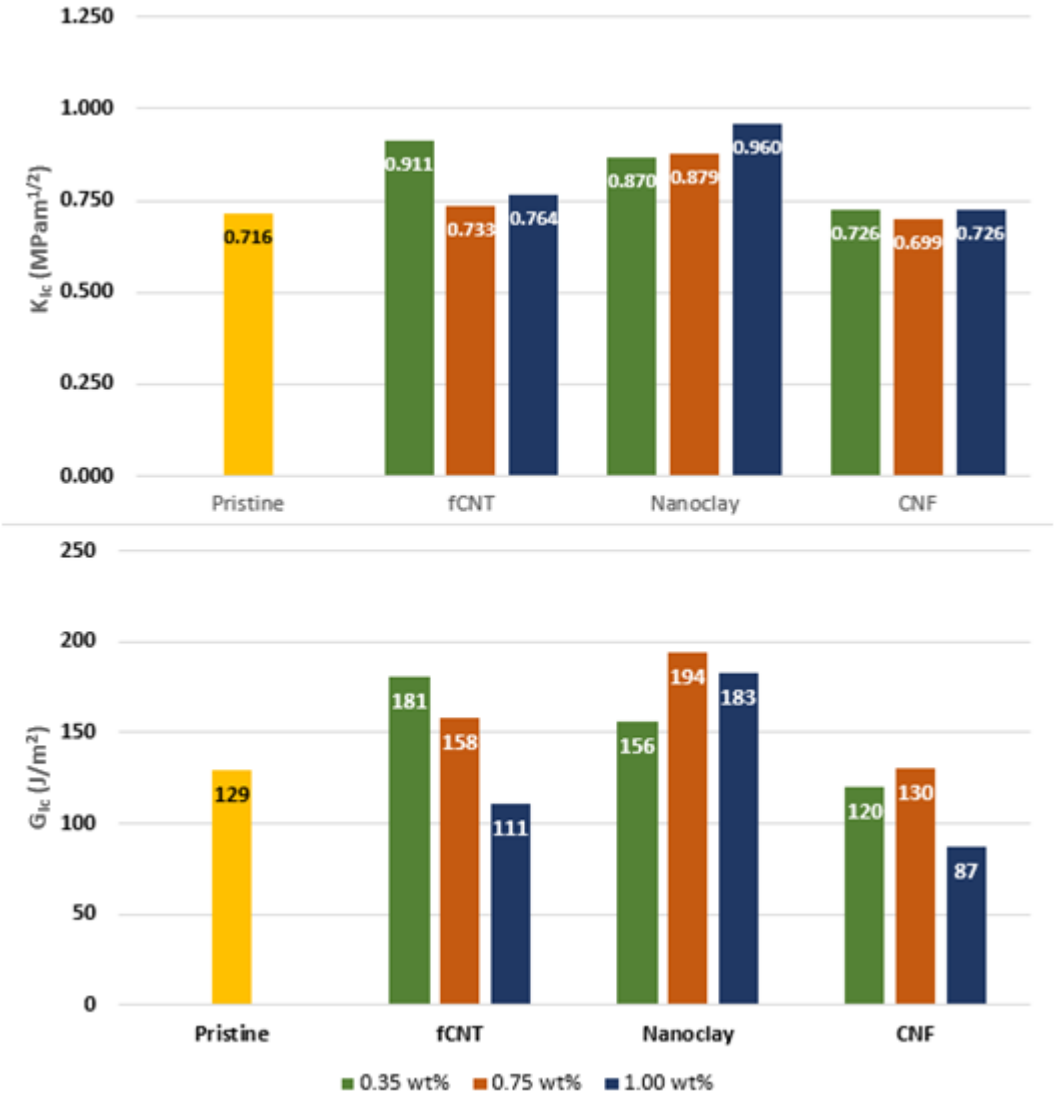

Figure 4.9. Fracture toughness, K_{Ic}, and fracture energy, G_{Ic}, values of pristine epoxy and nanocomposites incorporated with different types and amounts of nanoparticles.

Based on the fracture toughness test results, 0.35 wt% fCNT and nanoclay incorporation in all compositions were determined to lead to the most effective nanoparticle containing epoxy nanocomposites. However, in addition to fracture toughness, effect of nanoparticle incorporation on the tensile strength of the nanocomposites should also be considered in selecting the optimal nanoparticle type and amount combination.

4.3.2 Tensile Strength

Although the main aim of this study was to increase the fracture toughness of the nanocomposites, it was never desired to decrease tensile propertiesby nanoparticle incorporation. Tensile tests have been performed, according to ASTM D638-14, only for compositions that showed effective fracture toughness development to reduce the workload. For this purpose, 0.35, 0.75, and 1.00 wt% nanoclay and 0.35 wt% fCNT incorporated epoxy nanocomposites have been tested. The nanoparticles and epoxy resin were mixed with an ultrasonicator at 150 W for 60 minutes. Ultimate tensile strength values are given in Table 4.8 and also summarized in Fig. 4.10. Table 4.1 can be reviewed for comparison with pristine resin.

Table 4.8. Tensile test results of 0.35, 0.75, and 1.00 wt% nanoclay and 0.35 wt% fCNT incorporated epoxy nanocomposites.

		σ_u (MPa)		
		0.35 wt%	**0.75 wt%**	**1.0 wt%**
fCNT	**Avg**	78.06	-	-
	CV%	1	-	-
Nanoclay	**Avg**	65.05	57.62	55.01
	CV%	2	4	5

According to the tensile test results, the addition of nanoclay affected the tensile properties quite negatively due to high agglomeration. 1.00 wt% nanoclay incorporation, showing the highest increase in fracture toughness, K_{Ic}, reduced tensile strength by ~30%. Similarly, 0.35 wt% and 0.75 wt% nanoclay incorporation

reduced tensile strength by ~17% and ~26%, respectively. Continuous reduction in tensile strength with increasing nanoclay amount shows that agglomeration effect becomes more pronounced at higher nanoparticle loadings.

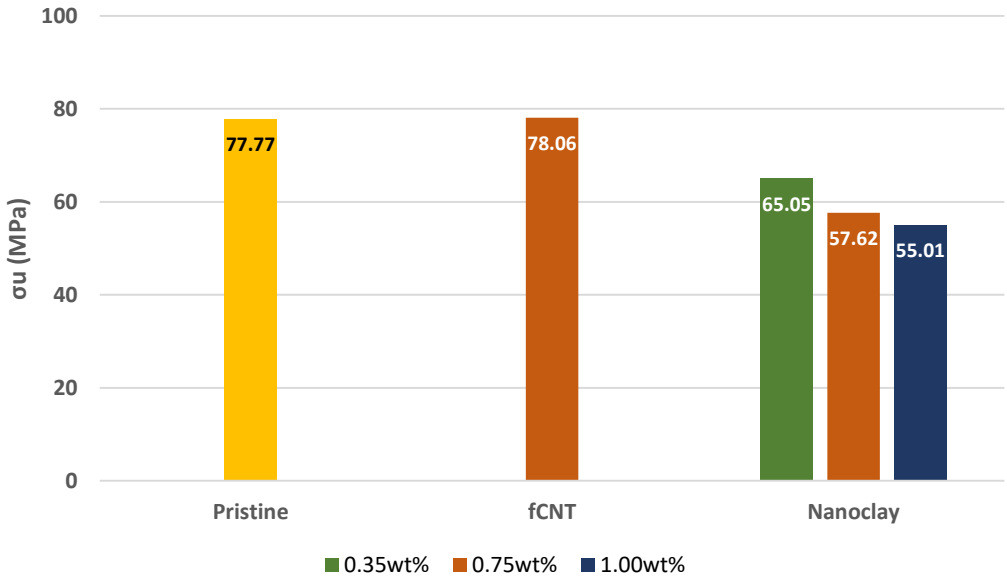

Figure 4.10. Tensile strength values of pristine epoxy along with epoxy resins incorporated with different types and amounts of nanoparticles.

The results are similar to the studies in the literature in which nanoclay has been used as a reinforcing nanoparticle. Suresha et al. found out that irrespective of the percentage of the nanoclay fillers loaded, tensile strength was lower than pristine epoxy. Adding 1 wt% nanoclay to the epoxy resin reduced the tensile strength by ~7%. In that study the decrease was attributed to the agglomerated structure of nanoclay particles serving as stress concentration sites, when applied stress induces interfacial failure between the particles and the matrix. The agglomeration created defects that led to stress concentration within the matrix, consequently causing a reduction in both tensile and flexural strengths [31].

As opposed to the effect of nanoclay incorporation, tensile strength remained similar with that of the pristine resin as a result of 0.35 wt% fCNT incorporation in the current study. This composition also increased fracture toughness (K_{IC}) by ~28%.

Therefore, 0.35 wt% fCNT has been selected as the most effective nanoparticle composition. Consequently, this composition has been used as the nanocomposite matrix of the glass fiber reinforced composites targeted in this study.

Table 4.9 summarizes the increase in fracture toughness and tensile strength, with respect to those of the pristine epoxy, achieved in this study and reported in the literature. ~28% increase in fracture toughness in this study is almost equal to the values obtained in the pioneering studies of this field by Zhou and Gojny. Additionally, Cha and Hsieh achieved ~40% increase in fracture toughness, which was positively affected by efficient dispersion and strong resin-particle interactions. With nanoparticle addition, the increase in tensile strength is not at levels similar to the increase in fracture toughness. While Zhou achieved the highest increase in tensile strength by ~12%, it generally remained similar with that of the pristine epoxy. ~1% increase in tensile strength obtained in the current study aligns with the literature data.

Table 4.9. Comparison of the increase in fracture toughness and tensile strength of CNT incorporated polymer nanocomposites achieved in the current study and in the literature.

Study	CNT content	Fracture Toughness (K_{IC}) Increase	Tensile Strength Increase
Zhou et al. [30]	0.30 wt%	~28%	~12%
Gojny et al. [19]	1.00 wt%	~26%	~2%
Hsieh et al. [29]	0.50 wt%	~42%	NA
Cha et al. [42]	0.50 wt%	~40%	~5%
Current study	0.35 wt%	~28%	~1%

4.4 Properties of Glass Fiber Reinforced Polymer (GFRP) Composites

In this study, Biresin CR80-CH80-6 epoxy system and Interglass 92145 glass fiber have been used to manufacture GFRP composites. To determine the effect of nanoparticle incorporated epoxy nanocomposites as the matrix of these GFRP

composites, firstly, the mechanical properties of GFRP composites with nanoparticle-free pristine epoxy matrix were measured as reference.

The mechanical properties of the reference GFRP composite have been measured according to the test standards given in Chapter 3. The mode I, G_{IC}, and mode II, G_{IIC}, interlaminar fracture toughnesses as well as tensile strength, σ_U, values of the reference GFRP composite are tabulated in Table 4.10.

Table 4.10. Mechanical properties of GFRP composite.

GFRP	G_{Ic} (J/m²)	G_{IIc} (J/m²)	σ_u (MPa)
Avg	666	984	764
CV%	12	4	14

4.5 Properties of Glass Fiber Reinforced Composites with Nanocomposite Matrix

Fracture toughness and tensile tests have been performed on the GFRP composite with nanocomposite matrix incorporated by 0.35 wt% fCNT to its resin. The mode I, G_{IC}, and mode II, G_{IIC}, interlaminar fracture toughnesses as well as tensile strength, σ_U, values of GFRP composite with nanocomposite matrix were measured.

4.5.1 Fracture Toughness

It has been a focus to increase fracture toughness, since sufficient fracture energy absorption capability is a crucial design requirement for fiber reinforced polymer composites. The ability of a fiber reinforced composite to withstand different forms of crack propagation determines its structural performance. In this study fracture toughness values have been investigated under two different loading types, namely mode I and mode II. In mode I type, the sample was pulled apart by tensile force, according to DIN EN 6033 (Fig. 3.19). On the other hand, shear forces were applied

using a 3-point bending fixture in mode II type loading according to DIN EN 6034 (Fig. 3.21).

For mode I fracture toughness tests, a load that created a 100 mm crack was first applied to the DCB specimen. Then, by unloading, the applied load was released. Load vs. displacement curves were drawn, and the area between the two curves, loading and unloading, was used for fracture toughness calculations. In Fig. 4.11, these graphs are given for representative specimens of GFRP and GFRP with nanocomposite matrix to show how the curves emerge. The upper curve represents loading, and the lower curve indicates unloading. The area between the two curves of the GFRP with nanocomposite matrix is noticeably larger than that of the GRFP.

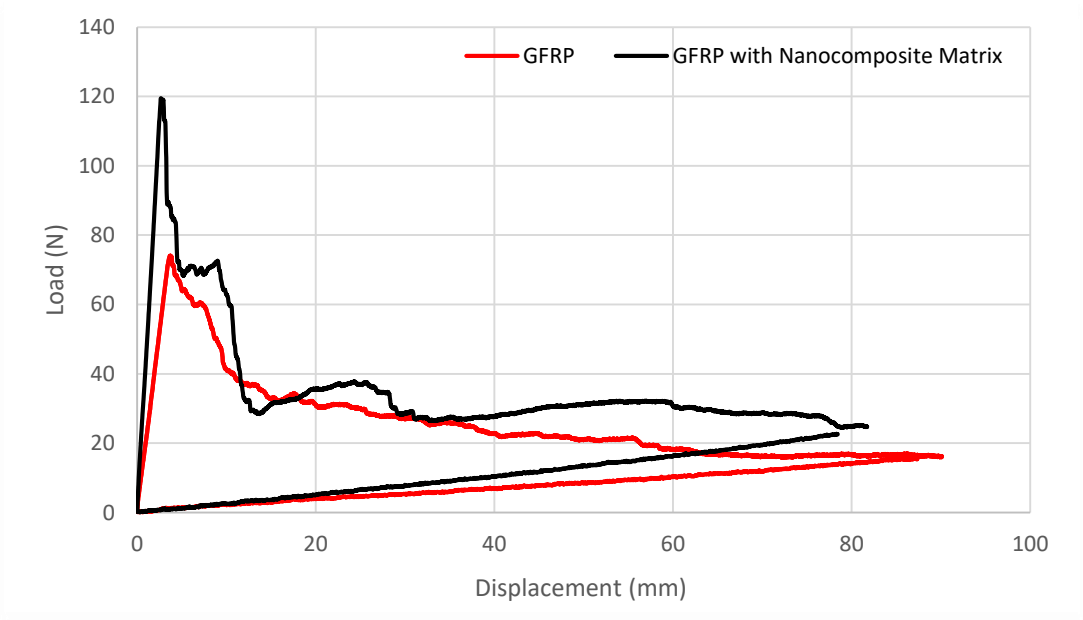

Figure 4.11. Load vs. displacement graph plotted after mode I fracture toughness test for representative specimens of GFRP and GFRP with nanocomposite matrix.

After the tests have been performed for each sample, the average mode I fracture toughness values were calculated which are shown in Table 4.11. As it is reported in the literature, mode I delamination resistance is a matrix-dominated feature of GFRP composites. Accordingly, an overall advanced mode I fracture behavior of GFRP is expected to be obtained by the improvement in the fracture toughness of its matrix

[43]. Therefore, increasing the fracture toughness of the epoxy resin by nanoparticle incorporation and formation of a nanocomposite was one of the aims of this study. It has been discussed in previous sections that the fracture toughness of the resin was increased by ~28% with the addition of 0.35 wt% fCNT. For this reason, the increase in mode I fracture toughness of the GFRP with nanocomposite matrix was an expected result.

Table 4.11. Mode I fracture toughness test results of GFRP and GFRP with nanocomposite matrix.

Mode		GFRP	GFRP with Nanocomposite Matrix
G_{Ic} (J/m^2)	Avg	666	721
	CV%	12	13

When the mode I fracture toughness, G_{IC}, values are compared, it is seen that fCNT incorporation to the matrix provided an ~8% increase compared to the GFRP composite with pristine matrix. This increasing fracture toughness behavior can be attributed to the large aspect ratio of fCNTs, which enabled them to act as nano-bridges between the surfaces of the crack as the DCB specimen pulled apart with tensile force. It took more energy to break or pull them out from the matrix to initiate the crack propagation resulting in an increase in fracture toughness. SEM images given in Fig. 4.12 were taken from a study in the literature. While Fig. 4.12a shows the GFRP composite produced with pristine epoxy matrix, Fig. 4.12b shows the GFRP nanocomposite manufactured with 1.00 wt% CNT added matrix. CNT pull-out and frcature, which contributed to higher G_{IC}, values, were observed in the sample with CNT added matrix. In that study, ~50% increase in mode I fracture toughness was observed by adding 0.5 wt% CNT to the matrix [43]. ~8% increase in mode I fracture toughness obtained in this study is lower than those of the studies in the literature. However, the positive effect of fCNT incorporation on mode I fracture toughness was observed regardless of the level of the increase. The level of

the increase can be enhanced with improved GFRP composite production techniques and better nanoparticle dispersion.

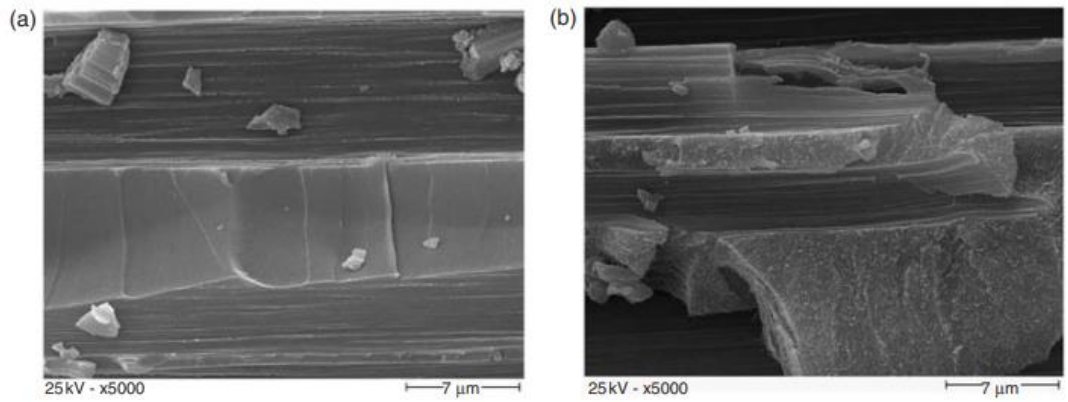

Figure 4.12. SEM images of (a) GFRP composite produced with pristine epoxy and (b) GFRP nanocomposite manufactured with 1.00 wt% CNT added epoxy from a literature study [43].

Following the mode I fracture toughness test results, mode II fracture toughness test results were investigated. End notched flexure (ENF) method was used for mode II fracture toughness tests. Three-point bending forces were applied to the pre-cracked specimen until load drop began. When the load drop began, the test was stopped, and a load versus displacement graph was drawn. Fig. 4.13 shows corresponding curves drawn for representative samples of GFRP and GFRP with nanocomposite matrix to give examples of how curves emerge after ENF tests. In calculating the G_{IIC} values ultimate load and displacement corresponding to the ultimate load have been used.

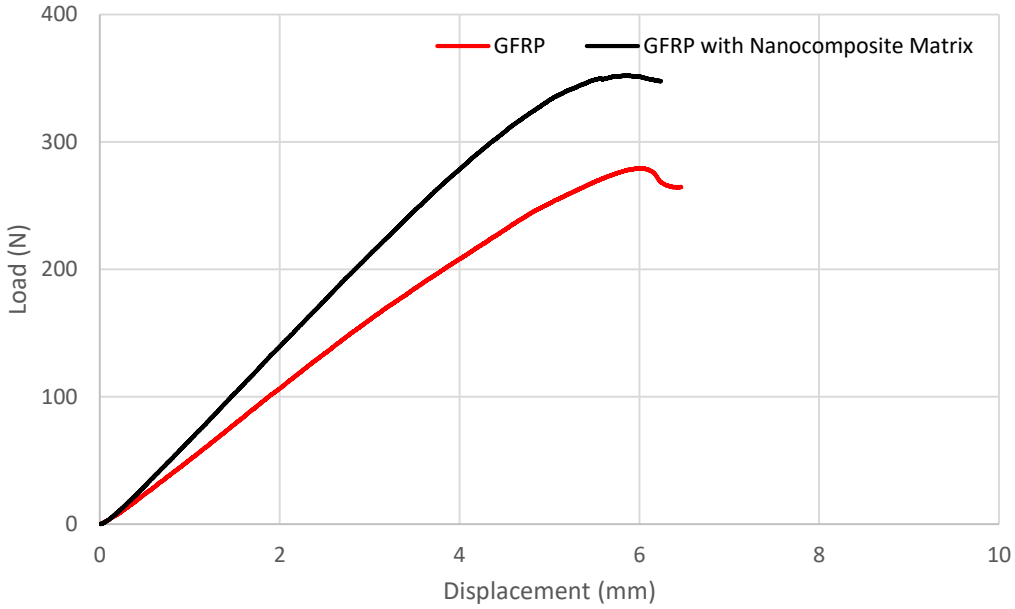

Figure 4.13. Load vs displacement graph plotted after mode II fracture toughness tests for representative specimens of GFRP and GFRP with nanocomposite matrix.

After the tests have been performed for each sample, the average mode II fracture toughness, G_{IIC}, values were calculated as shown in Table 4.12.

Table 4.12. Mode II fracture toughness, G_{IIC}, of GFRP and GFRP with nanocomposite matrix.

Mode		GFRP	GFRP with Nanocomposite Matrix
G_{IIc} (J/m^2)	Avg	984	1328
	CV%	4	15

With the incorporation of 0.35 wt% fCNT to the epoxy resin, ~35% increase was observed in the mode II fracture toughness of the GFRP. The presence of fCNTs in the epoxy resin led to the operation of energy-absorbing mechanisms as also presented in the literature. Ma et al. calculated a ~20% increase in the energy absorption of the composite with the addition of 0.5 wt% MWCNT. MWCNT breakage and matrix cracking caused a large amount of energy absorption when the

displacement increased [44]. Similarly, higher fracture toughness values resulted from the additional energy required for the fCNTs to break and pull out from the epoxy [45]. Mode II fracture toughness results presented in this study are similar to those given in the literature. Karapappas et al. observed a ~40% increase in mode II fracture toughness with the addition of 0.5 wt% CNT [43]. ~35% increase obtained in this study was in line with the literature data.

As a result, understanding the fracture behavior of nanocomposites depends critically on the degree of interfacial adhesion between nanoparticles and polymers, which is a key factor in the synthesis of fCNT incorporated nanocomposites and their physical characteristics. Therefore, the nanoparticle-resin interface can be examined in more detail to improve the fracture behavior of nanoparticle incorporated polymers and, thus, that of GFRPs with nanocomposite matrix.

4.5.2 Tensile Strength

Tensile tests of GFRP with pristine epoxy matrix and GFRP with nanocomposite matrix have been carried out according to ASTM D3039/D3039M-14 standard. After the tests, stress vs. strain graphs of representative samples from GFRP and GFRP with nanocomposite matrix have been drawn to show how the curves were formed. At first glance, it is observed that the tensile strength decreased with fCNT incorporation as seen in Fig. 4.14. After the tests have been performed for each sample, the average tensile strength values were obtained as given in Table 4.13.

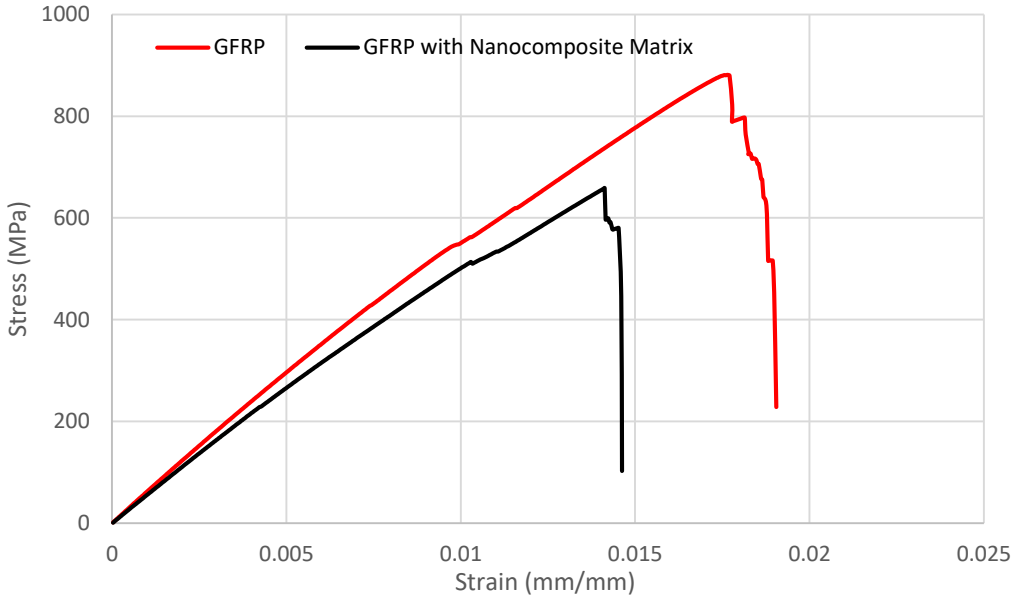

Figure 4.14. Stress vs. strain graphs for representative specimens of GFRP and GFRP with nanocomposite matrix obtained by the tensile tests.

Table 4.13. Tensile test results of GFRP and GFRP with nanocomposite matrix.

Tensile		GFRP	GFRP with Nanocomposite Matrix
σ_u (MPa)	Avg	764	651
	CV%	14	3

According to Table 4.13, it is observed that tensile strength decreases by ~15% with 0.35 wt% fCNT incorporation. Although the decrease in tensile strength is slightly higher than expected, this decrease was similarly observed in the literature studies. Zhang et al. performed tensile testing on GFRP composites incorporated with CNTs in different compositions. For each composition (0.4, 0.75, 1.1 wt%), tensile strength decreased with CNT incorporation. With the addition of 0.4 wt% CNT, tensile strength fell by ~10% [32]. The decrease was attributed to the development of CNT agglomerates considered as composite defects. Furthermore, as the CNT content rises, viscosity of the epoxy increases as well, which causes the epoxy to behave poorly when wetting during composite processing by hand lay-up. In addition, higher amount of trapped air voids in the composite resulted from increased viscosity. Both

of these drawbacks led to a decrease in the modulus and tensile strength of the GFRP. However, these production issues were unrelated to fracture toughness outcomes. The interfacial bonding was improved by the addition of CNTs, which contributed to the toughness enhancement of the GFRP. This was attributed to the optimal interlaminar shear strength contributed by various strengthening mechanisms resulting from CNT, including pull-outs, debonding, and crack bridging.

4.6 Properties of Glass Fiber Reinforced Composites with Nanocomposite Matrix Having Ply Drop-off Regions

A modified test method was used, since no standard test method exists for ply drop-off regions. While the modified tensile test has been applied to the specimens having drop-off regions, an audio recording was made to hear the ticking sound at the beginning of delamination. Even if there is no sound, the beginning of delamination can be seen from the small load drop on the stress vs strain curve. Load drops, pointing out the beginning of delamination, are shown in Fig. 4.15 with arrows.

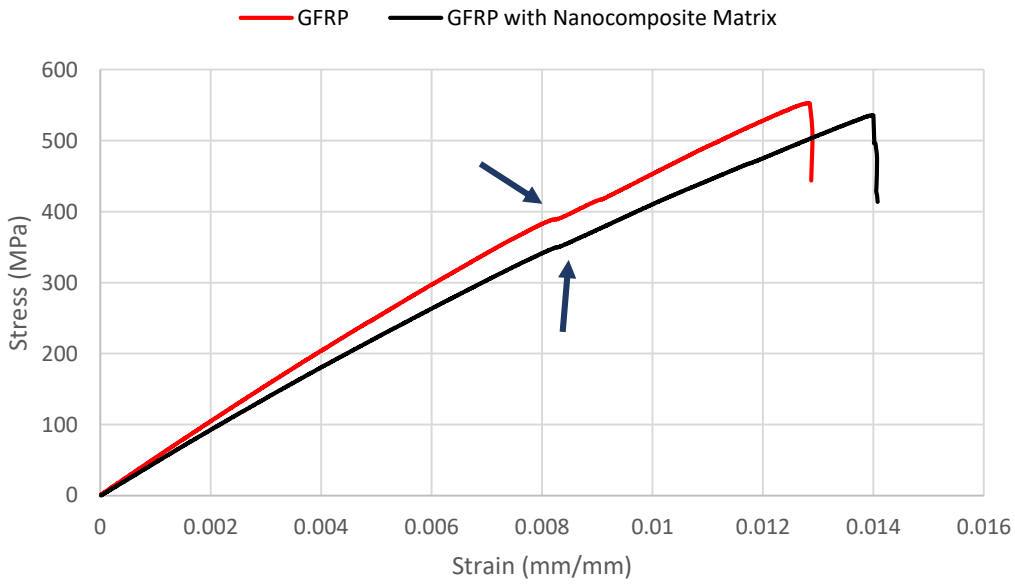

Figure 4.15. Stress vs. strain graphs of GFRP and GFRP with nanocomposite matrix having ply drop-off regions.

Table 4.14 shows the tensile strength (σ_U), delamination strength (σ_{Del}), work of fracture (W_f) and failure strain values obtained from drop-off tests of GFRP and GFRP with nanocomposite matrix having ply drop-off regions. The decrease in tensile strength is seen to be ~3% in the composites produced with fCNT incorporated nanocomposite matrix compared to GFRP with pristine epoxy matrix. In previous chapters, ~15% decrease in tensile strength was observed in GFRP produced with fCNT incorporated matrix as a result of the standard tensile test without ply drop-off. The improvement in this value (the decrease in tensile strength changing from ~15% to ~3%) shows that the contribution of fCNT incorporation on the mechanical behavior of GFRP composites is more pronounced with the existence of compelling regions like ply drop-off. Since delamination is a more critical problem in structures with ply drop-off, stress concentration sites resulting from fCNT agglomeration do not play a significant role. Therefore, fCNT agglomerates caused a slight decrease (~3%) in tensile strength. In terms of the delamination strength, GFRP with nanocomposite matrix showed ~10% decrease compared to GFRP with pristine epoxy matrix. Delamination strength and tensile strength are the features where tensile properties come to the fore, and the negative effect of fCNT incorporation on these features were also shown in previous chapters. However, although fCNT incorporation reduces the delamination strength, it increases the amount of post-delamination strain (Fig. 4.15). Since preventing delamination in structures with ply drop-off is very challenging, the longer the structure can continue load bearing after delamination, the more beneficial it will be.

Finally, the fracture behavior of structures with ply drop-off, which is the main point of this study, has been examined. GFRP with nanocomposite matrix showed ~6% increase in work of fracture (W_f) values compared to GFRP with pristine epoxy matrix. The W_f is defined as the strain energy absorbed by the sample until fracture and is calculated as the area under the stress vs. strain graph. As W_f increases, the work capacity of the material increases. In structures such as wind turbines, catastrophic failures can be prevented by increasing absorbed strain energy. Zhang

et al. also increased W_f values of GFRP with 0.75 wt% fCNT added matrix by ~6% compared to GFRP with pristine matrix. However, in that study with 0.4 wt% fCNT incorporation W_f decreased by ~4% [32]. Even though no ply drop-off effect has been considered in the study of Zhang et al., a similar amount of fCNT incorporation applied in the current study, 0.35 wt%, resulted in ~6% improvement in W_f when drop-off is considered. Here it should be emphasized that not many studies have been found in the literature which examine the characteristics of ply drop-off zones as in this study.

Table 4.14. Tensile test results of GFRP and GFRP with nanocomposite matrix having ply drop-off regions.

	GFRP	GFRP with Nanocomposite Matrix	Variation
σ_U (MPa)	553.06	535.85	~ -3%
σ_{Del} (MPa)	389.01	349.58	~ -10%
Work of Fracture (MJ/m^3)	4.062	4.297	~6%
Failure Strain	0.0129	0.0140	~9%

As a result, ~6% increase in W_f compared to GFRP with pristine epoxy matrix is a significant increase. Ply drop-off structures produced with CNT incorporated resin can be considered for industrial applications because of its contributions to fracture behavior, when the negative effects on tensile properties can be mitigated. The negative effects of nanoparticle incorporation on tensile properties should be minimized before considering its contribution to the fracture behavior. However, ~3% and ~10% decreases in ultimate tensile strength and delamination strength, respectively, observed in the current study may be acceptable considering the advantages of the fCNT incoporation in fracture behavior in terms of enhanced energy absorption and post-delamination load bearing capability.

CHAPTER 5

CONCLUSIONS

In the scope of this study, the effect of nanoparticle additives on the structural integrity of the ply-drop regions of glass fiber epoxy composite structures has been studied. Three different nanoparticles, functionalized carbon nanotube, nanoclay, and cellulose nanofiber, have been tested to improve the mechanical properties. Nanoparticles have been used in quantities of 0.35, 0.75, and 1.00 wt%. The nanoparticles were dispersed in the epoxy resin to obtain nanocomposites using the ultrasonication method using sound waves.

Viscosity of the mixtures as well as the fracture toughness and tensile strength of the resulting nanocomposites have been measured to optimize the working parameters of the ultrasonicator. 0.35wt% fCNT dispersed in epoxy was used in these tests. Initially, viscosity measurements have been performed. Mixing time and power were used as the process parameters to be optimized, where the ultrasonicator was operated at 100, 150, and 200 W power for 30, 60, 90, and 120 minutes.

- As a result of these tests, the viscosity of the mixture increased significantly at the 200 W-120 min condition, and the viscosity remained approximately constant in the remaining combinations. Since the change in viscosity was very minimal at 30 and 90 min compared to 60 and 120 min, the mixtures processed at 30 and 90 min were not used to prepare composites for further mechanical testing.
- Fracture toughness and tensile tests were performed on composites produces from mixtures processed at 100, 150, and 200 W power for 60 and 120 min. Fracture toughness values of the composites were higher than that of the pristine sample for each parameter. The highest increase was observed in the

case of 150 W-120 min combination with ~82%. The 150 W-60 min combination have increased the fracture toughness by ~40%.

- Tensile strength of the processed nanocomposites, on the other hand, always decreased with respect to that of the pristine resin, except for the 150 W-60 min combination, in contrast to fracture toughness. While a decrease of ~4% in tensile strength was observed for the composite obtained from the mixture processed at 150 W-120 min combination, the tensile strength remained almost constant in the case of 150 W-60 min combination.
- 150 W-60 min combinagtion was selected as the optimum mixing parameter set of the ultrasonicator due to the high standard deviation and decrease in tensile strength observed with 150 W-120 min combination.

Fracture toughness and tensile tests have been performed to select the best nanoparticle type and quantity using the initially selected optimum mixing parameter combination. In these tests, fCNT, nanoclay, and cellulose nanofiber dispersed in epoxy polymer have been tested in amounts of 0.35, 0.75, and 1.00 wt%. The dispersion process has been carried out by running ultrasonication at 150 W power for 60 min.

- As a result of the fracture toughness tests of the nanoparticle incorporated resin, the most remarkable increase was seen in the nanocomposites containing nanoclay. The sample containing 0.75 wt% nanoclay showed ~50% increase in fracture toughness, while the sample containing 1.00 wt% nanoclay showed ~42% increase.
- As a result of the fracture toughness tests of the fCNT incorporated resin, fracture toughness was observed to decrease as the amount of nanoparticles increases. 0.35 wt% fCNT incorporation increases fracture toughness by ~40%. On the other hand, incorporation of 0.75 wt% and 1.00 wt% fCNT caused an in increase in fracture toughness by ~22% and ~14%, respectively, compared to that of pristine resin.

- No increase was observed in fracture toughness upon CNF incorporation to the resin. While 0.75 wt% CNF incorporation did not cause any change in the fracture toughness of the pristine resin, other amounts reduced its fracture toughness.
- The tendency in the tensile strength of the nanoclay incorporated nanocomposites was very different from the tendency in their fracture toughness. The tensile strength of 0.75 wt% and 1.00 wt% nanoclay incorporated nanocomposites were ~26% and ~30% lower compared to that of the pristine resin.
- Tensile strength of 0.35 wt% fCNT incorporated nanocomposite was slightly higher than that of the pristine resin. Therefore, fCNT incorporation by 0.35 wt% has been chosen as the most optimal nanoparticle type and amount combination. Consequently, 0.35 wt% fCNT incorporated nanocomposite has been used as the matrix of the glass fiber reinforced composites for the subsequent parts of the study.

Mode I and mode II interlaminar fracture toughness and tensile tests were performed on GFRP and GFRP with nanocomposite matrix.

- When the G_{Ic} values were compared, it was seen that fCNT incoporation to the matrix provided ~8% increase compared to the GFRP composite with pristine epoxy matrix. This was attributed to the bridging effect of CNTs preventing crack opening under tension.
- G_{IIc} was improved by ~35% for the GFRP with nanocomposite matrix.
- On the other hand, it was observed that tensile strength decreased by ~15% for the GFRP with nanocomposite matrix. The decrease was attributed to fCNT agglomerates considered as composite defects.

GFRP composites with nanocomposite matrix having ply drop-off regions were tensile tested.

- ~3% decrease in ultimate tensile strength and ~10% decrease in delamination strength were observed in GFRP composites with fCNT incorporated nanocomposite matrix.
- By using fCNT incorporated epoxy resin as the matrix of the GFRP composite, ~6% increase in W_f and ~9% increase in failure strain was observed.
- Observed deterioration in tensile properties may be acceptable considering the advantages of the fCNT incorporation in fracture behavior in terms of enhanced energy absorption and post-delamination load bearing capability.

REFERENCES

[1] S. L. Donaldson, T. Jared Stonecash, and S. Sihn, “Transverse Cracks at Ply Drops in Fiberglass Laminates,” *Int. J. Mater. Eng.*, vol. 2, no. 6, pp. 112–117, 2013.

[2] J. Qureshi, “A Review of Fibre Reinforced Polymer Bridges,” *Fibers*, vol. 11, no. 5, pp. 4–6, 2023.

[3] L. Mishnaevsky, K. Branner, H. N. Petersen, J. Beauson, M. McGugan, and B. F. Sørensen, “Materials for wind turbine blades: An overview,” *Materials (Basel).*, vol. 10, no. 11, pp. 1–24, 2017.

[4] S. U. Khan and J. K. Kim, “Impact and delamination failure of multiscale carbon nanotube-fiber reinforced polymer composites: A review,” *Int. J. Aeronaut. Sp. Sci.*, vol. 12, no. 2, pp. 115–133, 2011.

[5] A. Mukherjee and B. Varughese, “Design guidelines for ply drop-off in laminated composite structures,” *Compos. Part B Eng.*, vol. 32, no. 2, pp. 153–164, 2001.

[6] P. Agastra and J. F. Mandell, “Testing and simulation of damage growth at ply drops in wind turbine blade laminates,” *Int. SAMPE Symp. Exhib.*, 2010.

[7] J. F. Mandell, D. D. Samborsky, P. Agastra, A. T. Sears, and T. J. Wilson, “Analysis of SNL / MSU / DOE Fatigue Database Trends for Wind Turbine Blade Materials,” no. SAND2010-7052, pp. 1–198, 2010.

[8] L. Mishnaevsky, “Root Causes and Mechanisms of Failure of Wind Turbine Blades: Overview,” *Materials (Basel).*, vol. 15, no. 9, 2022.

[9] L. Thomas and M. Ramachandra, “Advanced materials for wind turbine blade- A Review,” *Mater. Today Proc.*, vol. 5, no. 1, pp. 2635–2640, 2018.

[10] M. Jureczko, M. Pawlak, and A. Mężyk, “Optimisation of wind turbine

blades," *J. Mater. Process. Technol.*, vol. 167, no. 2–3, pp. 463–471, 2005.

[11] "53-Composite Materials for Wind Turbine Blades.pdf." .

[12] T. Osborne, "An introduction to resin infusion," *Reinf. Plast.*, vol. 58, no. 1, pp. 25–29, 2014.

[13] D. S. Cairns, I. F. Mandell, M. E. Scott, and J. Z. Maccagnano, "Design considerations for ply drops in composite wind turbine blades," *35th Aerosp. Sci. Meet. Exhib.*, no. January, 1997.

[14] B. Varughese and A. Mukherjee, "A ply drop-off element for analysis of tapered laminated composites," *Compos. Struct.*, vol. 39, no. 1–2, pp. 123–144, 1997.

[15] S. Helmy and S. V. Hoa, "Tensile fatigue behavior of tapered glass fiber reinforced epoxy composites containing nanoclay," *Compos. Sci. Technol.*, vol. 102, pp. 10–19, 2014.

[16] J. P. Jensen and K. Skelton, "Wind turbine blade recycling: Experiences, challenges and possibilities in a circular economy," *Renew. Sustain. Energy Rev.*, vol. 97, no. October 2017, pp. 165–176, 2018.

[17] N. Jahan, A.-T. Narteh, M. Hosur, M. Rahman, and S. Jeelani, "Effect of Carboxyl Functionalized MWCNTs on the Cure Behavior of Epoxy Resin," *Open J. Compos. Mater.*, vol. 03, no. 02, pp. 40–47, 2013.

[18] A. K. Chakraborty, T. Plyhm, M. Barbezat, A. Necola, and G. P. Terrasi, "Carbon nanotube (CNT)-epoxy nanocomposites: A systematic investigation of CNT dispersion," *J. Nanoparticle Res.*, vol. 13, no. 12, pp. 6493–6506, 2011.

[19] F. H. Gojny, M. H. G. Wichmann, U. Köpke, B. Fiedler, and K. Schulte, "Carbon nanotube-reinforced epoxy-composites: Enhanced stiffness and fracture toughness at low nanotube content," *Compos. Sci. Technol.*, vol. 64, no. 15 SPEC. ISS., pp. 2363–2371, 2004.

[20] P. C. Ma, N. A. Siddiqui, G. Marom, and J. K. Kim, “Dispersion and functionalization of carbon nanotubes for polymer-based nanocomposites: A review,” *Compos. Part A Appl. Sci. Manuf.*, vol. 41, no. 10, pp. 1345–1367, 2010.

[21] B. Ribeiro, E. C. Botelho, M. L. Costa, and C. F. Bandeira, “Carbon nanotube buckypaper reinforced polymer composites: A review,” *Polimeros*, vol. 27, no. 3, pp. 247–255, 2017.

[22] D. Qian, G. J. Wagner, W. K. Liu, M. F. Yu, and R. S. Ruoff, “Mechanics of carbon nanotubes,” *Appl. Mech. Rev.*, vol. 55, no. 6, pp. 495–532, 2002.

[23] K. Balasubramanian and M. Burghard, “Chemically functionalized carbon nanotubes,” *Small*, vol. 1, no. 2, pp. 180–192, 2005.

[24] S. Ashoori, M. Abdideh, and A. Alavi, “3D geostatistical modelling and uncertainty analysis of clay minerals distribution in reservoir rocks,” *Geocarto Int.*, vol. 31, no. 3, pp. 241–255, 2016.

[25] J. W. Gilman, “Flammability and thermal stability studies of polymer layered-silicate (clay) nanocomposites,” *Appl. Clay Sci.*, vol. 15, no. 1–2, pp. 31–49, 1999.

[26] N. A. Siddiqui, R. S. C. Woo, J. K. Kim, C. C. K. Leung, and A. Munir, “Mode I interlaminar fracture behavior and mechanical properties of CFRPs with nanoclay-filled epoxy matrix,” *Compos. Part A Appl. Sci. Manuf.*, vol. 38, no. 2, pp. 449–460, 2007.

[27] L. Alves, E. Ferraz, and J. A. F. Gamelas, “Composites of nanofibrillated cellulose with clay minerals: A review,” *Adv. Colloid Interface Sci.*, vol. 272, 2019.

[28] N. Saba, F. Mohammad, M. Pervaiz, M. Jawaid, O. Y. Alothman, and M. Sain, “Mechanical, morphological and structural properties of cellulose nanofibers reinforced epoxy composites,” *Int. J. Biol. Macromol.*, vol. 97,

pp. 190–200, 2017.

[29] T. H. Hsieh, A. J. Kinloch, A. C. Taylor, and I. A. Kinloch, “The effect of carbon nanotubes on the fracture toughness and fatigue performance of a thermosetting epoxy polym,” *J. Mater. Sci.*, vol. 46, no. 23, pp. 7525–7535, 2011.

[30] Y. Zhou, F. Pervin, L. Lewis, and S. Jeelani, “Fabrication and characterization of carbon/epoxy composites mixed with multi-walled carbon nanotubes,” *Mater. Sci. Eng. A*, vol. 475, no. 1–2, pp. 157–165, 2008.

[31] B. Suresha, C. A. Varun, N. M. Indushekhara, H. R. Vishwanath, and Venkatesh, “Effect of Nano Filler Reinforcement on Mechanical Properties of Epoxy Composites,” *IOP Conf. Ser. Mater. Sci. Eng.*, vol. 574, no. 1, 2019.

[32] X. Zhang *et al.*, “Design of glass fiber reinforced plastics modified with CNT and pre-stretching fabric for potential sports instruments,” *Mater. Des.*, vol. 92, pp. 621–631, 2016.

[33] K. Yildiz, İ. Gürkan, F. Turgut, F. Cebeci, and H. Cebeci, “Fracture toughness enhancement of fuzzy CNT-glass fiber reinforced composites with a combined reinforcing strategy,” *Composites Communications*, vol. 21. 2020.

[34] American Society for Testing and Materials, “ASTM D638-14, Standard Practice for Preparation of Metallographic Specimens,” *ASTM Int.*, vol. 82, no. C, pp. 1–15, 2016.

[35] American Society for Testing and Materials, “ASTM D5045-14, Standard Test Methods for Plane-Strain Fracture Toughness and Strain Energy Release Rate of Plastic Materials,” *Annu. B. ASTM Stand.*, vol. 99, no. Reapproved, pp. 1–9, 1996.

[36] D. I. N. En, “DIN EN 6033: Aerospace series. Carbon fibre reinforced plastics. Test method. Determination of interlaminar fracture toughness energy. Mode I. GIC.”

[37] D. I. N. En, “DIN EN 6034: Aerospace series. Carbon fibre reinforced plastics. Test method. Determination of interlaminar fracture toughness energy. Mode II. GIC.”

[38] ASTM International, “ASTM D3039/D3039M-14 Standard Test Method for Tensile Properties of Polymer Matrix Composite Materials,” *Stand. Test Method Tensile Prop. Polym. Matrix Compos. Mater.*, vol. 03, 2008.

[39] A. Montazeri and M. Chitsazzadeh, “Effect of sonication parameters on the mechanical properties of multi-walled carbon nanotube/epoxy composites,” *Mater. Des.*, vol. 56, pp. 500–508, 2014.

[40] Y. Y. Huang and E. M. Terentjev, “Dispersion of carbon nanotubes: Mixing, sonication, stabilization, and composite properties,” *Polymers (Basel).*, vol. 4, no. 1, pp. 275–295, 2012.

[41] L. C. Tang *et al.*, “Fracture toughness and electrical conductivity of epoxy composites filled with carbon nanotubes and spherical particles,” *Compos. Part A Appl. Sci. Manuf.*, vol. 45, pp. 95–101, 2013.

[42] J. Cha, G. H. Jun, J. K. Park, J. C. Kim, H. J. Ryu, and S. H. Hong, “Improvement of modulus, strength and fracture toughness of CNT/Epoxy nanocomposites through the functionalization of carbon nanotubes,” *Compos. Part B Eng.*, vol. 129, pp. 169–179, 2017.

[43] P. Karapappas, A. Vavouliotis, P. Tsotra, V. Kostopoulos, and A. Paipetis, “Enhanced fracture properties of carbon reinforced composites by the addition of multi-wall carbon nanotubes,” *J. Compos. Mater.*, vol. 43, no. 9, pp. 977–985, 2009.

[44] P. Ma, F. Zhang, Z. Gao, G. Jiang, and Y. Zhu, “Transverse impact

behaviors of glass warp-knitted fabric/foam sandwich composites through carbon nanotubes incorporation," *Compos. Part B Eng.*, vol. 56, pp. 847–856, 2014.

[45] C. H. Chen, R. R. Chang, and P. H. Jeng, "On the fiber-bridging of cracks in fiber-reinforced composites," *Mech. Mater.*, vol. 20, no. 2, pp. 165–181, 1995.

APPENDICES

A. Pristine Resin Mechanical Test Results

Sample	K (MPam$^{1/2}$)	G (J/m^2)	σ_u (MPa)	E (GPa)
1	0.622	112.483	77.76	2.94
2	0.754	111.499	79.15	3.09
3	0.737	165.872	74.36	3.08
4	0.748	147.218	77.66	3.02
5	0.718	105.889	78.62	3.10
6			79.05	3.03
Avg	0.716	128.592	77.77	3.04
StD	0.054	26.476	1.78	0.06

B. Viscosity Test Results

0.35 wt% CNT	Sample	Pristine	Hand-Mixed	100 W				150 W			
Mixing Time (min)		**0**	**2**	**30**	**60**	**90**	**120**	**30**	**60**	**90**	**120**
cp (6 rpm)	1	1148	1164	1226	1295	1312	1448	1297	1290	1332	1494
cp (10 rpm)	2	1146	1164	1227	1293	1311	1449	1299	1287	1332	1494
cp (12 rpm)	3	1152	1162	1227	1297	1315	1447	1295	1292	1332	1492
avg (cp)		1148.7	1163.3	1226.7	1295.0	1312.7	1448.0	1297.0	1289.7	1332.0	1493.3
StD		3.06	1.15	0.58	2.00	2.08	1.00	2.00	2.52	0.00	1.15

		CNT				CNF			
0.35 wt%	**Sample**	**200 W**				**200 W**			
Mixing Time (min)		**30**	**60**	**90**	**120**	**30**	**60**	**90**	**120**
cp (6 rpm)	1	1218	1358	1350	2052	1170	1197	1266	1269
cp (10 rpm)	2	1215	1359	1350	2055	1172	1200	1267	1267
cp (12 rpm)	3	1220	1357	1350	2052	1179	1201	1267	1267
avg (cp)		1217.7	1358.0	1350.0	2053.0	1173.7	1199.3	1266.7	1267.7
StD		2.52	1.00	0.00	1.73	1.41	2.12	0.71	1.41

C. Fracture Toughness Results of Nanoparticle Incorporated Polymer Nanocomposites

	100W			150W			200W		
60 min	Sample	K ($MPam^{1/2}$)	G (J/m^2)	Sample	K ($MPam^{1/2}$)	G (J/m^2)	Sample	K ($MPam^{1/2}$)	G (J/m^2)
	1	0.818	111.08	1	0.940	159.33	1	0.797	144.13
	2	0.976	233.50	2	0.824	157.26	2	0.819	134.60
	3	0.844	127.00	3	0.937	244.85	3	0.705	151.87
	4	0.596	114.37	4	0.810	155.97	4		
	5	0.836	99.77	5	1.043	188.19	5		
	6	0.870	128.66	6			6		
	7	0.753	142.57	7			7		
	8	0.805	142.67	8			8		
	9	0.930	177.98	9			9		
	10	0.893	153.95	10			10		
	Avg	0.832	143.16	Avg	0.911	181.12	Avg	0.774	143.53
	StD	0.105	39.02	StD	0.096	38.04	StD	0.060	8.65
	100W			150W			200W		
120 min	Sample	K ($MPam^{1/2}$)	G (J/m^2)	Sample	K ($MPam^{1/2}$)	G (J/m^2)	Sample	K ($MPam^{1/2}$)	G (J/m^2)
	1	0.799	207.14	1	0.832	178.12	1	0.827	206.12
	2	0.629	159.22	2	0.795	138.17	2	0.813	215.30
	3	0.918	200.54	3	0.878	240.58	3	0.874	172.70
	4	1.368	368.76	4	1.436	361.73	4		
	5	0.767	145.80	5	1.057	251.11	5		
	6	1.144	253.87	6			6		
	7	0.893	141.08	7			7		
	8	0.833	150.60	8			8		
	9	0.831	172.37	9			9		
	Avg	0.909	199.93	Avg	1.000	233.94	Avg	0.838	198.04
	StD	0.220	73.07	StD	0.264	85.08	StD	0.032	22.42

	0.35 wt%			0.75 wt%			1.00 wt%		
fCNT	Sample	K ($MPam^{1/2}$)	G (J/m^2)	Sample	K ($MPam^{1/2}$)	G (J/m^2)	Sample	K ($MPam^{1/2}$)	G (J/m^2)
	1	0.940	159.33	1	0.899	192.19	1	0.722	106.97
	2	0.824	157.26	2	0.721	164.46	2	0.704	120.41
	3	0.937	244.85	3	0.598	141.96	3	0.862	123.34
	4	0.810	155.97	4	0.775	164.01	4	0.833	100.42
	5	1.043	188.19	5	0.731	130.08	5	0.751	82.02
	6			6	0.677	157.71	6	0.748	88.25
	7			7			7	0.727	155.79
	Avg	0.911	181.12	Avg	0.734	158.40	Avg	0.764	111.03
	StD	0.096	38.04	StD	0.101	21.37	StD	0.060	24.94

	0.35 wt%			0.75 wt%			1.00 wt%		
	Sample	K ($MPam^{1/2}$)	G (J/m^2)	Sample	K ($MPam^{1/2}$)	G (J/m^2)	Sample	K ($MPam^{1/2}$)	G (J/m^2)
Nanoclay	1	0.907	154.55	1	0.955	195.95	1	0.888	191.47
	2	0.951	199.67	2	0.845	208.34	2	1.023	156.60
	3	0.984	160.55	3	0.895	189.71	3	0.973	155.96
	4	0.816	111.29	4	0.903	218.10	4	0.956	229.60
	5	0.865	140.54	5	0.933	147.77	5		
	6	0.789	174.17	6	0.794	193.77	6		
	7	0.775	152.56	7	0.827	201.19	7		
	Avg	0.870	156.19	Avg	0.879	193.55	Avg	0.960	183.41
	StD	0.081	27.42	StD	0.059	22.35	StD	0.056	34.98

	0.35 wt%			0.75 wt%			1.00 wt%		
	Sample	K ($MPam^{1/2}$)	G (J/m^2)	Sample	K ($MPam^{1/2}$)	G (J/m^2)	Sample	K ($MPam^{1/2}$)	G (J/m^2)
CNF	1	0.633	107.11	1	0.688	111.61	1	0.682	86.83
	2	0.653	101.64	2	0.808	145.73	2	0.738	80.88
	3	0.690	123.76	3	0.615	150.19	3	0.702	88.63
	4	0.930	149.13	4	0.547	122.14	4	0.710	108.42
	5			5	0.788	120.23	5	0.724	75.92
	6			6	0.751	130.35	6	0.799	80.90
	Avg	0.727	120.41	Avg	0.700	130.04	Avg	0.726	86.93
	StD	0.138	21.33	StD	0.103	15.17	StD	0.041	11.48

D. Tensile Strength Results of Nanoparticle Incorporated Polymer Nanocomposites

	100W			150W			200W		
	Sample	σu (MPa)	E (GPa)	Sample	σu (MPa)	E (GPa)	Sample	σu (MPa)	E (GPa)
60 min	1	62.25	3.23	1	77.06	3.02	1	57.74	3.20
	2	62.53	3.24	2	77.77	3.08	2	70.98	3.05
	3	69.78	3.11	3	78.65	3.13	3	73.97	2.99
	4			4	79.38	3.12	4	66.92	3.06
	5			5	77.45	3.06	5		
	Avg	64.85	3.19	Avg	78.06	3.08	Avg	67.40	3.07
	StD	4.27	0.07	StD	0.94	0.05	StD	7.06	0.09
	100W			150W			200W		
	Sample	σu (MPa)	E (GPa)	Sample	σu (MPa)	E (GPa)	Sample	σu (MPa)	E (GPa)
120 min	1		3.08	1	73.25	2.96	1	64.08	3.09
	2	63.33	2.98	2	74.94	3.02	2	57.80	3.07
	3	77.01	3.11	3	75.65	3.03	3	72.10	3.07
	4	77.79	3.13	4	75.85	3.04	4	62.03	3.14
	Avg	72.71	3.07	Avg	74.92	3.01	Avg	64.00	3.09
	StD	8.13	0.07	StD	1.18	0.04	StD	6.00	0.03

	0.35 wt%		
	Sample	σ_u (MPa)	E (GPa)
CNT	1	77.06	3.016
	2	77.77	3.083
	3	78.65	3.13
	4	79.38	3.12
	5	77.45	3.06
	Avg	78.06	3.08
	StD	0.94	0.05

E. Fracture Toughness Results of GFRP Composites

Specimens	a (mm)	w (mm)	A (N.mm)	GIc (J/m^2)
DCB-1	103.52	25.11	1682	647
DCB-2	107.50	24.98	1432	533
DCB-3	103.73	25.08	1859	715
DCB-4	104.72	25.16	1810	687
DCB-5	103.46	25.16	1941	746
GFRP			AVG	666
			STD	82
			CV%	12

Specimens	w (mm)	P (N)	d (mm)	a (mm)	L (mm)	GIIc (J/m^2)
ENF-1	25.11	279.30	6.03	35	100	977
ENF-2	24.98	270.90	6.46	35	100	1020
ENF-3	25.08	268.65	6.22	35	100	970
ENF-4	25.16	260.40	6.13	35	100	923
ENF-5	25.16	286.60	6.21	35	100	1031
GFRP					AVG	984
					STD	43
					CV%	4

F. Tensile Test Results of GFRP Composites

Sample	w (mm)	t (mm)	A	Pmax	σ_u (MPa)
PURE-1	25.23	1.82	46.00	38030.34	827
PURE-2	25.31	1.80	45.55	36605.66	804
PURE-3	24.96	1.75	43.77	38573.09	881
PURE-4	25.16	1.82	45.79	30284.43	661
PURE-5	24.98	1.97	49.29	31802.20	645
				AVG	764
				STD	105
				CV%	14

G. Fracture Toughness Results of GFRP Composite with Nanocomposite Matrix

Specimens	a (mm)	w (mm)	A (N.mm)	GIc (J/m^2)
DCB-1	109.61	25.25	2363	854
DCB-2	106.33	25.22	1779	663
DCB-3	107.00	24.95	1725	646
DCB-4	104.58	24.88	1690	650
DCB-5	105.78	25.04	2089	789
CNT + GFRP			AVG	721
			STD	95
			CV%	13

Specimens	w (mm)	P (N)	d (mm)	a (mm)	L (mm)	GIIc (J/m^2)
ENF-2	25.22	352.10	5.89	35	100	1196
ENF-3	24.95	414.30	6.18	35	100	1494
ENF-4	24.88	363.45	7.08	35	100	1506
ENF-5	25.04	364.15	5.28	35	100	1118
CNT + GFRP					AVG	1328
					STD	201
					CV%	15

H. Tensile Test Results of GFRP Composite with Nanocomposite Matrix

Sample	w (mm)	t (mm)	A	Pmax	σ_u (MPa)
CNT-1	25.06	1.99	49.88	32854.38	659
CNT-2	25.06	1.94	48.53	32687.26	674
CNT-3	25.00	2.00	49.92	31345.04	628
CNT-4	24.77	2.01	49.78	32947.18	662
CNT-5	24.98	1.95	48.79	30782.82	631
				AVG	651
				STD	20
				CV%	3